UC San Diego
UC San Diego Electronic Theses and Dissertations

Title
Analysis of Holliday junction-binding compounds

Permalink
https://escholarship.org/uc/item/4w7709nn

Author
Rideout, Marc Christoffer

Publication Date
2011

Peer reviewed|Thesis/dissertation

UNIVERSITY OF CALIFORNIA, SAN DIEGO

SAN DIEGO STATE UNIVERSITY

Analysis of Holliday Junction-Binding Compounds

A dissertation submitted in partial satisfaction of the

requirements for the degree Doctor of Philosophy

in

Biology

by

Marc Christoffer Rideout

Committee in charge:

University of California, San Diego

       Professor E. Peter Geiduschek
       Professor Partho Ghosh

San Diego State University

       Professor Anca M. Segall, Chair
       Professor Alex B. Burgin
       Professor John J. Love
       Professor Douglas B. Grotjahn

2011

The dissertation of Marc Christoffer Rideout is acceptable in quality and form for publication of microfilm and electronically by:

_____

_____

_____

_____

_____
Chair

University of California San Diego

San Diego State University

2011

DEDICATIONS

This work is dedicated, first and foremost, to my father, Bronson Rideout.

No one has supported my education in a more consistent and quietly determined

manner. Without that influence, I could not possibly have made it to this point.

Rick Halsey and Bill Howell, for inspiring a love of biology early.

Alex and Anca, for demonstrating the dedication and enthuiasim necessary to

survive in this field.

Amy, for providing advice that eventually proved invaluable.

Ilham and the rest of my Moroccan family for love, support, and making sure I never

feel alone.

My mother, who would have loved to see me here.

TABLE OF CONTENTS

LIST OF ABBREVIATIONS

SSR   Site specific recombination

HJ   Holliday junction

NMR   Nuclear Magnetic Resonance

WRWYCR Peptide composed of L-amino acids

wrwycr   Peptide composed of d-amino acids

IC_{50} Inhibitory concentration (50% inhibition)

HR   Homologous recombination

DSB   Double stranded break

LC-MS   Liquid chromatography-Mass spectrometry

MTT   Tetrazole dye used to assay eukaryotic metabolism

MIC   Minimum inhibitory concentration

STm   *Salmonella enterica* serovar Typhimurium

TUNEL   Terminal deoxyribonucleotide transferase-mediated dUTP nick end

      labeling

LB   Luria Bertani media

MHB   Meuller-Hinton Broth media

PM	Peritoneal macrophages
EMSA	Electrophoretic mobility shift assay
2AP	2-aminopurine
HPLC	High pressure liquid chromatography
ACN	Acetonitrile
F_c	Fraction Complex

LIST OF FIGURES

LIST OF APPENDIX FIGURES

LIST OF TABLES

ACKNOWLEDGEMENTS

I would like to acknowledge Professor Anca M. Segall for guidance, support, creative solutions to problems and for managing our friendship in a manner that never conflicted with her role as a mentor.

Many thanks go to the people at the Torrey Pines Institute for Molecular Studies for scientific help, and in particular Clemencia "Chacha" Pinilla, for always taking time to help me understand their technology.

I am grateful to the members of the the Opella lab (UCSD) and the Love lab (SDSU) for help with the NMR experiemnts. Additionally, Professor Karin Crowhurst (CSU. Northridge), and especially Dr. Fabian Fillip (Opella lab) for their time spent teaching me how to process NMR data.

Specifal thanks to Jeff Boldt and Ilham Naili for scientific contributions.

Last, thanks to all the members of the Segall lab, past and present, for support, scientific contributions and lots of laughs.

Portions of Chapter 2 have been accepted for publication to the journal, "Molecular Diversity" as: Marc C. Rideout, Jeffrey L. Boldt, Gabriel Vahi-Ferguson, Peter Salamon, Adel Nefzi, John M. Ostresh, Marc Giulianotti, Clemencia Pinilla, and Anca M. Segall, 2011. Potent antimicrobial small molecules screened as inhibitors of tyrosine recombinases and Holliday junction-resolving enzymes. The screening of small molecule libraries and much of the crude compound characterizations were performed by Jeff Boldt as indicated in the pertinent figure legends.

Chapter 3 is being prepared for submission as: Marc C. Rideout, Ilham Naili, Jeffrey L. Boldt, America Flores-Fujimoto, Sukanya Patra and Anca M Segall, 2011. wrwyrggrywrw, a single-chain analog of peptide wrwycr, binds Holliday junctions, inhbits bacterial DNA repair enzymes, and has antibacterial activity. Portions of the *in vitro* assays were performed by Jeff Boldt and America Flores-Fujimoto, and the cell based assays were performed by Ilham Naili and Sukanya Patra as indicated in the pertinent figure legends.

VITA

Education

San Diego State University / University of California, San Diego

PhD, Biology

September, 2011

San Diego State University

BS, Cell and Molecular Biology

May, 2000

Teaching, mentorship and research experience

San Diego State University

Teaching Assistant for upper division biochemistry lab

September 2003 to May 2008

Mentorship experience:

Gabriel Vahi-Ferguson (June 2009 June 2011); Garrett York (June 2008 to June 2010); Tristan Nater (June 2006 to June 2007); Julie Hasse (September 2004 to June 2005)

Emerald Biostructures, Bainbridge Island, WA

Research Specialist

May 2001 to June 2003

San Diego State University, Principal investigator, Alex Burgin, PhD

Research Specialist and Lab Manager

May 2000 to May 2001

Publications

Accepted for publication: Marc C. Rideout, Jeffrey L. Boldt, Gabriel Vahi-Ferguson, Peter Salamon, Adel Nefzi, John M. Ostresh, Marc Giulianotti, Clemencia Pinilla, and Anca M. Segall. Potent antimicrobial small molecules screened as inhibitors of tyrosine recombinases and Holliday junction-resolving enzymes. Molecular Diversity, 2011.

Ranjit, D. K., M. C. Rideout, A. Nefzi, J. M. Ostresh, C. Pinilla and A. M. Segall (2010). "Small molecule functional analogs of peptides that inhibit lambda site-specific recombination and bind Holliday junctions." Bioorg Med Chem Lett **20**(15): 4531-4534.

Raymond, A. C., M. C. Rideout, B. Staker, K. Hjerrild and A. B. Burgin, Jr. (2004). "Analysis of human tyrosyl-DNA phosphodiesterase I catalytic residues." J Mol Biol **338**(5): 895-906.

Rideout, M. C., A. C. Raymond and A. B. Burgin, Jr. (2004). "Design and synthesis of fluorescent substrates for human tyrosyl-DNA phosphodiesterase I." Nucleic Acids Res **32**(15): 4657-4664.

Grotjahn, D. B., S. Van, D. Combs, D. A. Lev, C. Schneider, M. Rideout, C. Meyer, G. Hernandez and L. Mejorado (2002). "New flexible synthesis of pyrazoles with different, functionalized substituents at C3 and C5." J Org Chem **67**(26): 9200-9209.

Grotjahn, D. B., S. Van, D. Combs, D. A. Lev, C. Schneider, C. D. Incarvito, K. C. Lam, G. Rossi, A. L. Rheingold, M. Rideout, C. Meyer, G. Hernandez and L. Mejorado (2003). "Substituent control of hydrogen bonding in palladium(II)-pyrazole complexes." Inorg Chem **42**(10): 3347-3355

In preparation: Marc C. Rideout, Ilham Naili, Jeffrey L. Boldt, America Flores-Fujimoto, Sukanya Patra and Anca M Segall. wrwyrggrywrw, a single-chain analog of peptide wrwycr, binds Holliday junctions, inhibits bacterial DNA repair enzymes, and has antibacterial activity.

Presentations

May 2011 American Society for Microbiology, General Meeting, New Orleans, LA. "Potent Antimicrobial Small Moleculaes Screened as Inhibitors of Site-Specific Recombination and Holliday Junction-Resolving enzymes"

September 2008 Workshop on Site-Specific Recombination, Woods Hole, MA. "Peptides Inhibitors of Site-Specific Recombination"

April 2006-April 2011 San Diego State University Graduate Student Symposium, San Diego, CA. Various poster titles

May 2003-May 2011 San Diego Microbiology Group Annual Meeting, San Diego, CA. Various poster titles

Scholarships
Acheivment Rewards for College Scientists (ARCS) scholar, 2006 through 2011

ABSTRACT OF THE DISSERTATION

Analysis of Holliday junction-Binding Compounds

by

Marc Christoffer Rideout

Doctor of Philosophy in Biology

University of California, San Diego, 2011

San Diego State University, 2011

Professor Anca M. Segall, Chair

Holliday junctions (HJs) are critical intermediates in many recombination-dependent DNA repair pathways. Our lab has identified several hexameric peptides that target HJ intermediates formed in DNA recombination reactions. One of the most potent peptides, WRWYCR, is active as a homodimer and has shown bactericidal activity due in part to its ability to interfere with DNA repair proteins that act upon HJs. In order to increase the possibility of developing a therapeutic that targets DNA repair, we searched for small molecule inhibitors that were functional surrogates of the peptides. Initial screens of heterocyclic small molecule libraries resulted in the identification of several N-methyl aminocyclic thiourea inhibitors. Like the peptides, these inhibitors trapped HJs formed during recombination reactions *in vitro*, but were less potent than the peptides in biochemical assays and had little antibacterial activity. In this work we describe the development of functional analogs

based on either WRWYCR or the thiourea inhibitors. Our focus was on symmetry in an effort to mimic the symmetry of a WRWYCR homodimer and its target, the HJ. A set of 36 pyrrolidine bis-cyclic guanidine inhibitors were synthesized, and purified candidates were found to bind protein-free HJs and to interfere with the processing of HJs by DNA repair enzymes, *in vitro*. In addition, they are potent inhibitors of Gram-negative and especially Gram-positive bacterial growth, in contrast to the previously identified thiourea inhibitors. We also developed a single-chain linear analog of WRWYCR that does not require homedimer formation for activity. That analog, WRWYRGGRYWRW, binds to protein-free HJs and inhibits their resolution *in vitro*, in addition to causing DNA damage in bacteria and inhibiting bacterial growth. Finally, we implemented a peptide labeling strategy and demonstrated the effective isotope enrichment of several peptides using 2D and 3D nuclear magnetic resonance experiments. Together these inhibitors and the labeling strategy add to a "molecular toolbox" for studying the diverse set of reactions involving HJs. Additionally, these molecules are proof-of-principle of two classes of compounds each with novel activities which may in the future be developed into a new antibiotics that will expand the available choices for therapy against drug resistant bacteria.

Chapter 1. Introduction

Section 1.1. Holliday junctions

Holliday junctions (HJ) are branched DNA intermediates that form *in vivo* from the union of two duplex strands of DNA. These junctions were originally proposed by Robin Holliday in 1964 as a molecular mechanism to explain meiotic exchange and homologous recombination in fungi (Holliday 1964). Since then, HJs, as well as enzymes that process them have been found in most organisms from phage to humans. They are ubiquitous intermediates involved in strand exchange reactions that underlie diverse cellular processes including telomere maintenance in eukaryotes, chromosome segregation and the acquisition of antibiotic resistance in bacteria, viral life-cycles, and recombination-dependent DNA repair. Compounds that bind and interfere with the processing of HJs and other higher order DNA's are sought as potential chemotherapeutics for either bacteria and/or tumor cells and is the focus of this dissertation. In this introduction, I will focus first on describing some of the ways HJs are formed *in vivo*, with particular emphasis on DNA repair and why this repair intermediate makes a good chemotherapeutic target. I will then describe examples of compounds that bind to higher order DNA intermediates to outline a set of chemical characteristics that appear necessary for stable interactions with these substrates.

Section 1.2. DNA damage leads to HJ-dependent DNA repair in bacteria

DNA repair processes are invoked as a consequence of DNA damage which, for the purpose of this discussion, will be subdivided into two categories:

primary damage that modifies the DNA, and secondary damage that ensues following interaction with the primary damage (Figure 1-1). Damage is often direct modification of the DNA, such as deamination, oxidation, or alkylation of the nucleobases. These modifications usually occur at nucleophilic centers, such as the formation of O-6-methyl guanine, (reviewed in Krwawicz *et al.* 2007) and many are directly reversible by specialized enzymes for instance, O-6-methyl guanine transferase (Pegg 2000). In such cases, repair is often rapid and uncomplicated. Other modifications are more difficult to repair such as DNA intercalation, strand crosslinks, or hydrolysis leading to abasic sites or strand breaks. These modifications often require excision of both the damaged DNA and the surrounding region, followed by nucleotide replacement. Examples of these processes include the base excision repair (BER), nucleotide excision repair (NER), and mismatch repair (MR) pathways and each process must be highly coordinated and ideally fast enough to be completed before the replication forks arrive at the site of damage. Lesions under repair and those left un-repaired represent obstacles to DNA replisomes as well as other cellular processes. These obstacles can cause replication forks to either stall, or convert the primary DNA damage into a mismatch, a single stranded gap or double stranded break (DSB). While each of these outcomes is processed differently, all can lead to the formation of a HJ (Figure 1-1).
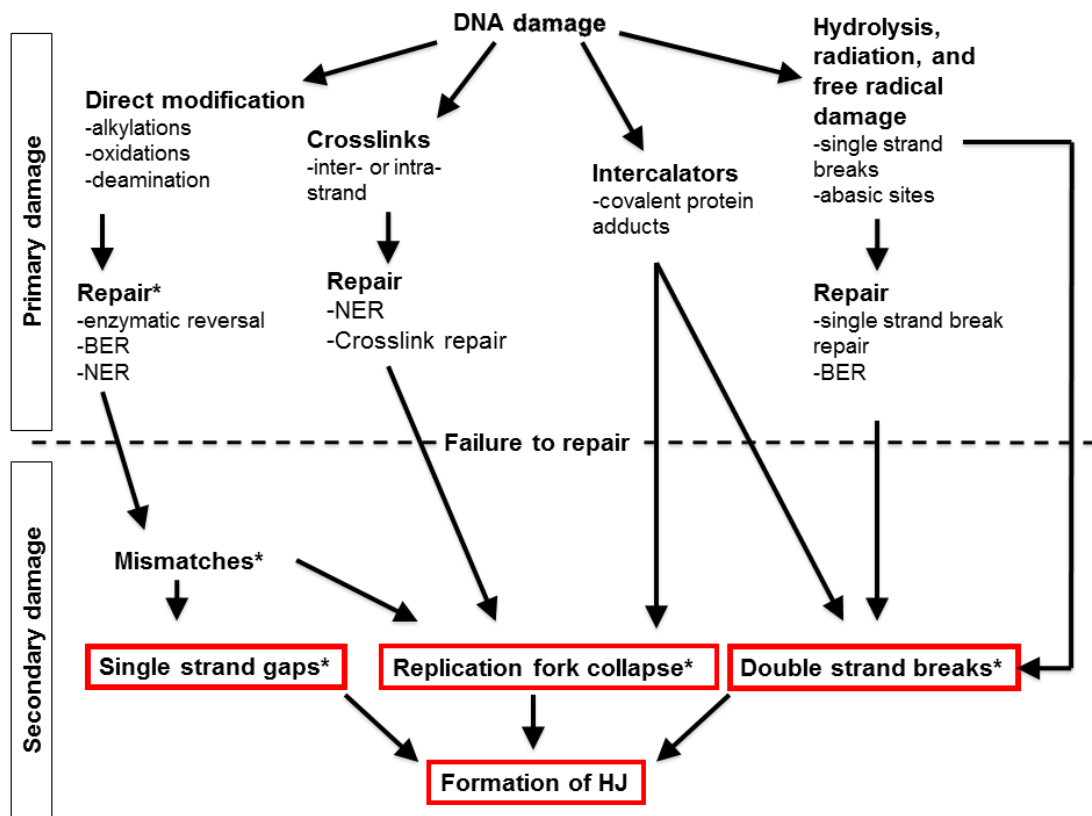
Figure 1-1. Primary and secondary DNA damage lead to HJ formation

Primary forms of DNA damage result in direct modification of the backbone, sugar ring, or bases. In many cases, this type of damage is directly reversible; in other cases, the damaged DNA is excised and replaced with unmodified DNA. "Failure to repair" the primary damage will result in more serious secondary damage such as gaps, DSBs, and can cause replication forks to collapse. Each of these types of secondary damage can, and in some cases must, be repaired through the formation of a HJ intermediate. * indicates repair pathways that do not involve the formation of a HJ (*e.g.,* mismatch repair, translesion sysnthsis, gap fill-in, NHEJ).

In *E. coli* the non-mutagenic repair of DSBs requires the RecBCD homologous recombination pathway (Figure 1-2, reviewed in (Singleton *et al.* 2004)). Briefly, the DSB-end is recognized by the RecBCD complex, which generates a single stranded 3' overhang. RecA coats the single strand forming a nucleoprotein filament that pairs with a homologous stretch of duplex of DNA on a sister chromatid. The homologous region of duplex DNA is "invaded," creating a single HJ and a structure known as a displacement loop (D-loop). DNA synthesis extends the 3' OH in the D-loop, and extension is followed by the creation of a second HJ. The resolution of both junctions is achieved via endonucleolytic cleavage by the RuvABC complex or possibly via branch migration via RecG helicase (Wardrope *et al.* 2009) to yield recombinant products.

Single stranded gaps form frequently in *E. coli* following DNA damage, and repair mostly relies on the formation of a RecA-dependent HJ (Heller *et al.* 2006). The gap is formed when a replication fork encounters DNA damage and is then re-primed on either strand downstream of the lesion; the resumption of DNA synthesis leaves a gap behind (Heller *et al.* 2006). The gap is coated with single stranded DNA binding protein (SSB) protecting the DNA and preventing the formation of secondary structures. The RecFOR complex of proteins displaces SSB and loads RecA protein, which catalyzes the formation of a HJ (Figure 1-2). DNA synthesis fills in the gap, and the junctions are resolved to create recombinant products in the same manner as for DSBs.
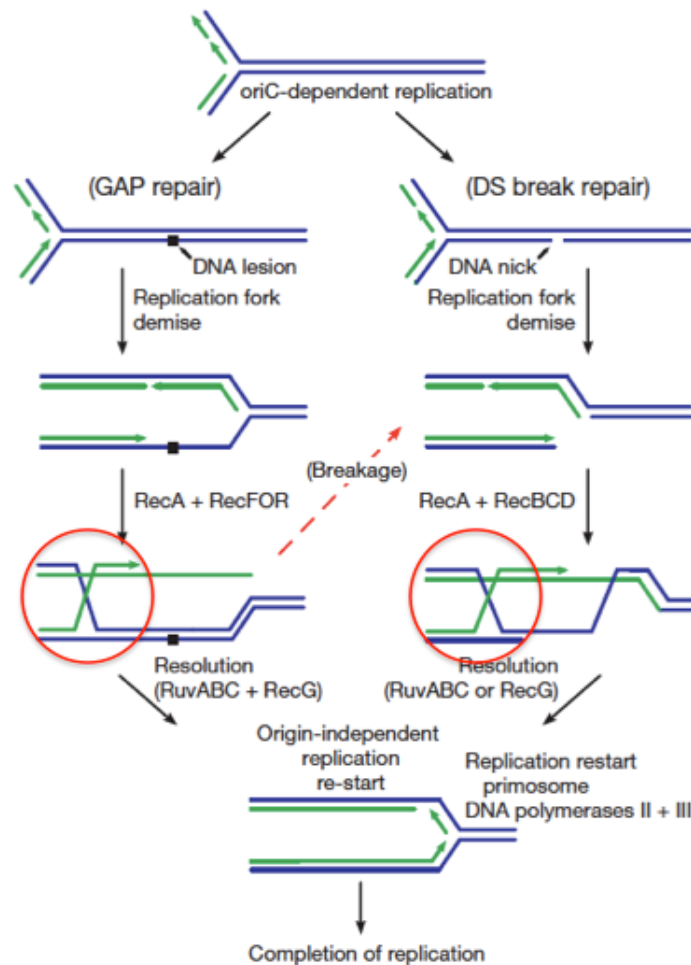
Figure 1-2. Repair of gaps and DSBs lead to the formation of HJs

Gaps and DSBs may form following replication fork collision with a lesion or break, respectively. Gap repair (left pathway) is started by RecFOR and RecA which catalyze the formation of a HJ (red circle). Strand synthesis (green arrow) is followed by resolution of the HJ, and the replication fork is restarted. DBS repair (right pathway) is mediated by RecBCD and RecA which also catalyze the formation of a HJ and a D-loop. DNA synthesis at the D-loop is followed by HJ resolution and restart of replication fork. Figure adapted from (McGlynn *et al.* 2002).

In addition to leaving gaps and DSBs, replication forks may stall or collapse if they encounter DNA lesions or active repair complexes and repair often involves the formation of a HJ (McGlynn *et al.* 2002). In *E. coli,* forks may be regressed by a helicase (*e.g.,* RuvAB, Rep, or possibly RecG (Michel *et al.* 2007)) such that the daughter strands pair with each other and form a HJ with a short arm (a "chicken foot" structure). Fork regression provides room repair of the lesion and if successful, the chicken foot is degraded and the fork is restarted with the help of origin-independent replication restart proteins (*e.g.,* PriA, B and C; Cox *et al.,* 2000). Alternatively, the chicken foot provides an elegant solution to permit DNA synthesis past the lesion, a process known as "template switching" (Figure 1-3). Following DNA synthesis, the fork is progressed (*i.e.,* driven forward) by a helicase and then restarted as above. Several other complex pathways exist that involve resolution of the HJ and recombination with template DNA ahead of the fork (reviewed in McGlynn *et al.* 2002).

While HJs are frequently formed in the DNA repair pathways described, other notable, non-HJ dependent mechanisms of repair are available, such as translesion DNA synthesis (which avoids gap formation, Georgescu *et al.* 2010) or non-homologous end joining (NHEJ) of double stranded breaks (Pitcher *et al.* 2007). However, the repair systems described above are highly conserved and nearly ubiquitous in all bacteria (Rocha *et al.* 2005) highlighting their importance and that of the HJ as a critical intermediate to genome maintenance and bacterial cell survival.
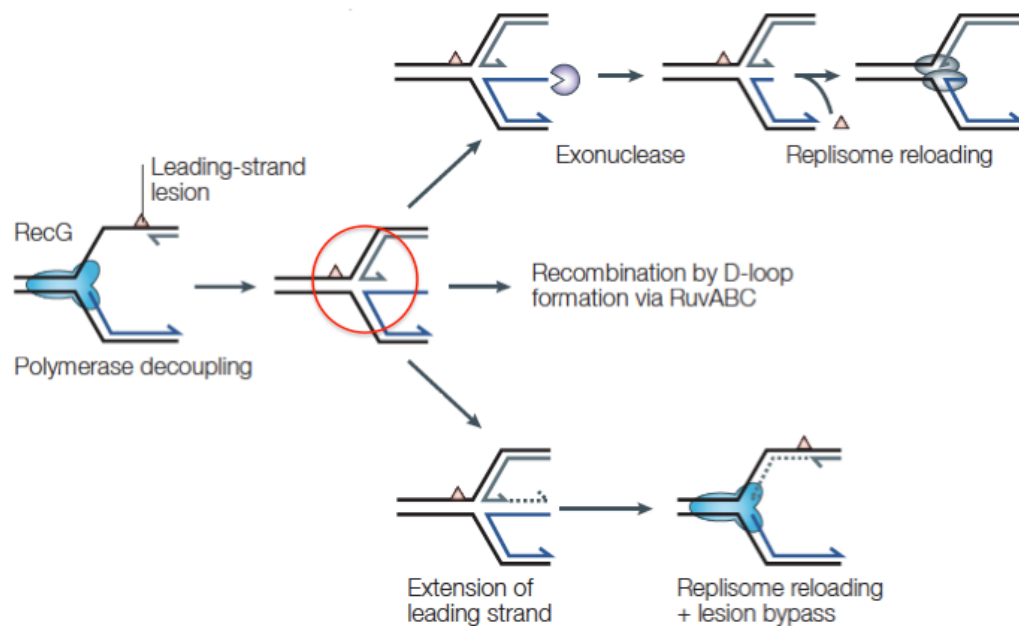
Figure 1-3. Replication fork repair involves the formation of a HJ

Replication forks that stall or collapse are bound by a helicase (*e.g.,* RecG) and regressed away from lesions (orange triangle). The newly synthesized leading and lagging strands pair and form a HJ ("chicken-foot", red circle) that may be processed in several ways. In the top pathway the lesion is removed, and the short arm of the HJ is degraded by an exonuclease allowing the replisome to be reloaded. In the bottom pathway (template switching), the lagging strand on the HJ can serve as a template for leading strand synthesis, which effectively bypasses the lesion; this is followed by reloading of the replisome. Finally, in the middle pathway, the chicken foot is processed (by a single stranded nuclease in combination RecBCD), or resolved (e.g. via RuvABC cleavage) creating a recombinagenic end that can form a D-loop with the template strands in front of the lesion. After the D-loop is processed the fork is restarted. Figure adapted from (McGlynn *et al.* 2002).

Section 1.3. HJ-formation in eukaryotes

DNA repair in eukaryotes is much more complex than in bacteria and the formation of HJs is much more tightly controled. In contrast to bacteria, eukaryotes have enormous tracts of redundant sequences and intronic regions which are hotspots for recombination. While genetic exchange is necessary, the potential for loss of genetic information resulting from homologous recombination (HR) is disasterous if not controlled (Lamarche et al, 2010). Control of HR is achieved in part by using repair pathways that do not involve genetic exchange or the formation of a HJ. For instance, eukaryotes rely on the potentially error-prone NHEJ as the prevalent means of DSB repair during G_1 phase (Lamarche *et al.* 2010). Eukaryotic DNA is also organized into heterochromatin which compacts the genetic material into the nucleus and this provides control over HR in the form of a physical barrier (Goodarzi *et al.* 2010). Heterochromatin is present in all stages of the cell cycle, however in S and G_2 phases heterochromatin is remodeled to allow for replication. This provides both access to the DNA, and equally important the presence of a sister chromatid with which to recombine (Cromie *et al.* 2001); thus DNA repair in eukaryotes is intimately involved with cell cycle control. In light of these differences, it is perhaps not surprising that true amino acid homologs of bacterial repair proteins are rare in eukaryotes. The notable exceptions are the major recombination proteins dedicated to HJ formation, RecA in bacteria, and RAD51 in eukaryotes (Shinohara *et al.* 1992; Ogawa *et al.* 1993; Wyman *et al.* 2004). A comparison of repair proteins with analogous biochemical activities in *H. Sapiens* and *E. coli* is shown in Table 1-1.

In *H. sapiens,* DBSs are recognized initially by the MRN complex which functions analogously to RecBCD by creating a 3'-OH overhang upon which the RAD51 protein is loaded (Lamarche *et al.* 2010). Loading of RAD51 is aided by RAD52 (analogous to RecFOR or RecB, (Cromie *et al.* 2001)), and the nucleoprotein filament that is formed can invade a homologous duplex to create a D-loop and a HJ. Following synthesis at the D-loop, the HJ must be resolved. The RAD51C-XRCC3 complex (Liu *et al.* 2007), MUS81, and the recently isolated GEN1 all resolve the junctions via endonucleolytic cleavage and produce recombinant products, though they do so via different mechanisms (Rass *et al.* 2010). Additionally, Bloom or Werner syndrome helicases (BLM or WRN, respectively) are known to unwind junctions, and BLM can act with TOPO III to resolve junctions in a cleavage-dependent, but non-recombinagenic manner (Petermann *et al.* 2010; Rass *et al.* 2010). Other pathways for HJ resolution exist and the extent of resolution options is indicative of the importance of junction resolution to genome maintenance. Not surprisingly mutations in the resolvases mentioned often have associated diseases in humans, many of which are various forms of cancer.

HJ formation is also tightly controlled in the repair of single stranded gaps and collapsed replication forks in eukaryotes. In fact, most gaps are filled in by XRCC1, polymerase β and DNA ligase III in a non-HJ dependent fashion. These proteins are recruited to both gaps and single stranded breaks by a DNA damage sensor and global regulator called PARP-1 (Megnin-Chanet *et al.* 2010). In contrast, HJs often form at stalled and collapsed eukaryotic replication forks. PARP-1 recruits factors that stabilize the fork from collapsing, and delay progression of the cell cycle allowing time for repair, such as the checkpoint proteins ATM, ATR, BRCA1 / 2,

P53, CHK1 / 2, ATK, (Bartek *et al.* 2004); however, it also recruits factors that promote and process HJs (MRE11, RAD51, BLM, WRN and others (Petermann *et al.* 2010)). Interestingly, while RAD51 is required for replication fork repair in *H. Sapiens* (Allen *et al.* 2011), RAD51 nucleoprotein foci are not formed at sites of impaired replication forks (Petermann *et al.* 2010). This again suggests control of HR and RAD51-dependent HJ intermediates (Petermann *et al.* 2010).

Table 1-1. Organism specific DNA repair proteins

Function	*E. coli*	*H. Sapiens*
Single strand binding protein	SSB	RP-A
Strand invasion protein	RecA	RAD51
Loading of strand invasion protein	RecFOR / RecB	RAD52 / BRCA1 / 2
DSB processing	RecBCD	MRE11 / RAD50 / NBS1 (MRN complex)
Gap processing	RecFOR	PARP-1 / XRCC1 / polymerase-β / DNA ligase III
Fork remodeling	RecG helicase	Blooms Syndrome helicase (BLM)
		Werners Syndrome helicase (WRN)
HJ resolvase	RuvABC	RAD51C / XRCC3
		MUS81 / GEN1
		BLM / TOPOIII
DNA Damage signaling	ssDNA + RecA	PARP-1
Checkpoint proteins	SulA?	ATM / ATR
		CHK1 / 2
		BRCA1 / 2

HJ are also formed in the maintanence of telomers at the ends of linear eukaryotic chromosomes. Considerable efforts are currently directed toward the study of telomeres and how cancer cells continually extent this region to avoid senescence. Approximately 85% of all cancer cells maintain active, detectible levels of telomerase which directly facilitates the extension (Figure 1-4A, and Biroccio *et al.* 2004), while the other 15% extend their telomeres through one of several related processes involving HR and the formation of a HJ; these processes are collectively known as Alternative Lengthening of Telomeres pathways (ALT, (Cesare *et al.* 2010; Nabetani *et al.* 2011). Telomere DNA is composed of nucleotide repeats; in humans the sequence is 5'-TTAGGG-3' and this provides a wealth of homology for recombination. The process is initiated by the formation of a structure called a "t-loop" (Figure 1-4B) similar to the D-loops formed in DSB repair. Many of the HR proteins that process HJs (MRN complex, RAD51 / RAD52, XRCC3, and WRN and BLM helicases) are involved in the formation, regulation, and replication of the t-loop DNA (Cesare *et al.* 2010; Lamarche *et al.* 2010; Nabetani *et al.* 2011). While the t-loop serves to protect the end of the chromosome from DSB repair pathways, it can also be primed for DNA synthesis, leading to extension of the telomere (de Lange 2004). Alternatively, newly replicated telomere DNA can invade a neighboring chromatid, again forming a D-loop, and initiating recombination dependent replication which also serves to lengthen the telomere (Figure 1-4C). In both telomerase-independent pathways resolution of the HJ formed at the loop is necessary to restore the telomere end.
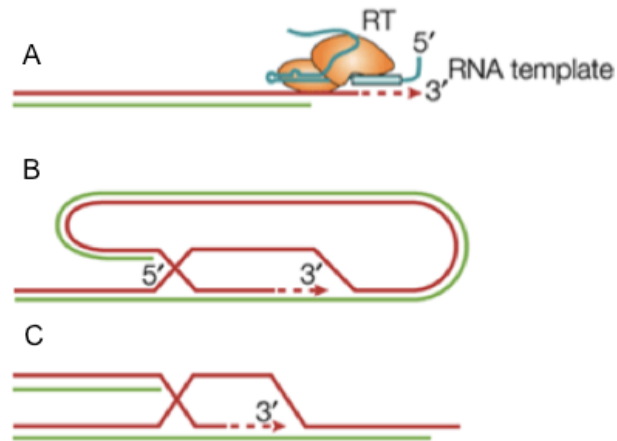
Figure 1-4.Formation of HJs in the extension of telomeres

In humans, telomere DNA is comprised of the repeat sequence 5' TTAGGG 3' (red and green lines). (A) In the majority of cancer cells, senescence is avoided by telomerase (orange blobs) a reverse transcriptase which extends telomere DNA from a nascent RNA template. (B and C) Cancer cells that do not produce telomerase, extend telomeres via recombination involving a HJ. The formation of a t-loop (shown in B) is similar to the D-loop that forms during DSB repair and are used to prime DNA synthesis and extend the telomere. Alternatively, a newly synthesized strand can invade the template and extend the telomere via recombination dependent replication. Adapted from (de Lange 2004)

Section 1.4. HJs as drug targets

Multi-drug resistant (MDR) pathogenic bacteria are currently considered one of the greatest challenges to the survival of humans as a species (Walker *et al.* 2009). Yet despite the increases in the number of MDR bacterial species and the cost associated (estimated at over 20 billion dollars annually in the US, (Roberts *et al.* 2009)) the number of new antibiotic drugs and those currently under investigation, has been steadily declining (Spellberg *et al.* 2011). Much of this is due to the prospect of developing a costly antimicrobial toward a target where resistance mechanisms are likely to be rapidly acquired (Taubes 2008; Leung *et al.* 2011). HJs are formed in multiple independent pathways and target site modification leading to resistance is unlikely to develop. HJs also hold promise as secondary targets to inhibit DNA repair in combination with traditional antibiotics. Evidence is growing that most traditional antibiotics (*i.e.,* inhibitors of the synthesis of proteins, peptidoglycan, RNA, DNA, or folic acid (reviewed in (Chopra *et al.* 2002)) all lead to DNA damage. This damage is mostly from the generation of hydroxyl radicals (Dwyer *et al.* 2007; Kohanski *et al.* 2007) and results in the upregulation of DNA repair pathways under the control of the SOS response. Downregulation of the SOS response or hydroxyl radical sensors has been shown to potentiate the effects of traditional antibiotics (Lu *et al.* 2009) and therefore critical intermediates in DNA repair, such as the HJ, may represent potential primary or secondary antibiotic targets.

As mentioned above, HJs also form in eukaryotic cells therefore a balance of toxic specificity is demanded for therapeutics that target HJs. Since these

compounds are DNA repair inhibitors, it is noteworthy that small molecules are currently in clinical trials that downregulate proteins in damage repair pathways (*e.g.,* PARP1, CHK2, ATM, ATR, (Maxmen 2010)). This strategy holds promise as a means of potentiating DNA damage causing chemotherapeutics (*e.g.,* cisplatin or topoisomerase poisons) in combination treatments. While side effects are likely for healthy eukaryotic cells, toxic specificity may exist for rapid dividing nature of cancer cells (or analogously, systemic bacterial infections), a characteristic exploited by many chemotherapeutics currently in use (*e.g.,* topoisomerase poisons). Additionally, telomerase-negative cancer cell types, including osteosarcoma, lung carcinoma, and malignant melanomas (Bryan *et al.*, 1997, Scheel *et al.*, 2001) that extend their telomeres via the ATL pathway are expected to be particular sensitive to drugs that target HJs.

Section 1.5. Ligands that interact with higher order DNA structures

The characteristics that govern ligand binding to higher order DNA structures are exemplified by ligands that bind to duplex DNA. Excluding covalent binding (*e.g.,* cisplatin), most DNA binding compounds target the major or minor grooves, or they form base stacking interactions by intercalating the double helix (Boer *et al.* 2009). Compounds exemplifying both types of interactions usually have heterocyclic ring systems, which are often aromatic, and capable of carrying a positive charge that interacts with the negatively charged DNA; however, the size and flexibility of the ligands vary depending on the type of interactions they establish with the DNA. For instance, groove binders have rotatable bonds that impart flexibility to follow the twist with the in the duplex (Strekowski *et al.* 2007). Flexibility also allows aromatic

rings to insert into the electronegative grooves forming strong Van der Waals interactions or hydrogen bonds with the bases. DNA binding dyes (DAPI, Hoechst), and polyamines such as distamycin (2) (shown in Figure 1-5) exemplify this class of ligands. In contrast, intercalating compounds are limited by the area between the base pairs with which they intercalate and therefore are usually much smaller. Additionally, in contrast to the flexibility necessary for groove binding, intercalators have fused aromatic rings systems that form a planar surface that facilitates the base stacking interactions. These hydrophobic π-π interactions between the ligand and the DNA are seen in a variety of ligands including propidium iodide, ethidium bromide, acridine, and ellipticine (1) shown in Figure 1-5.
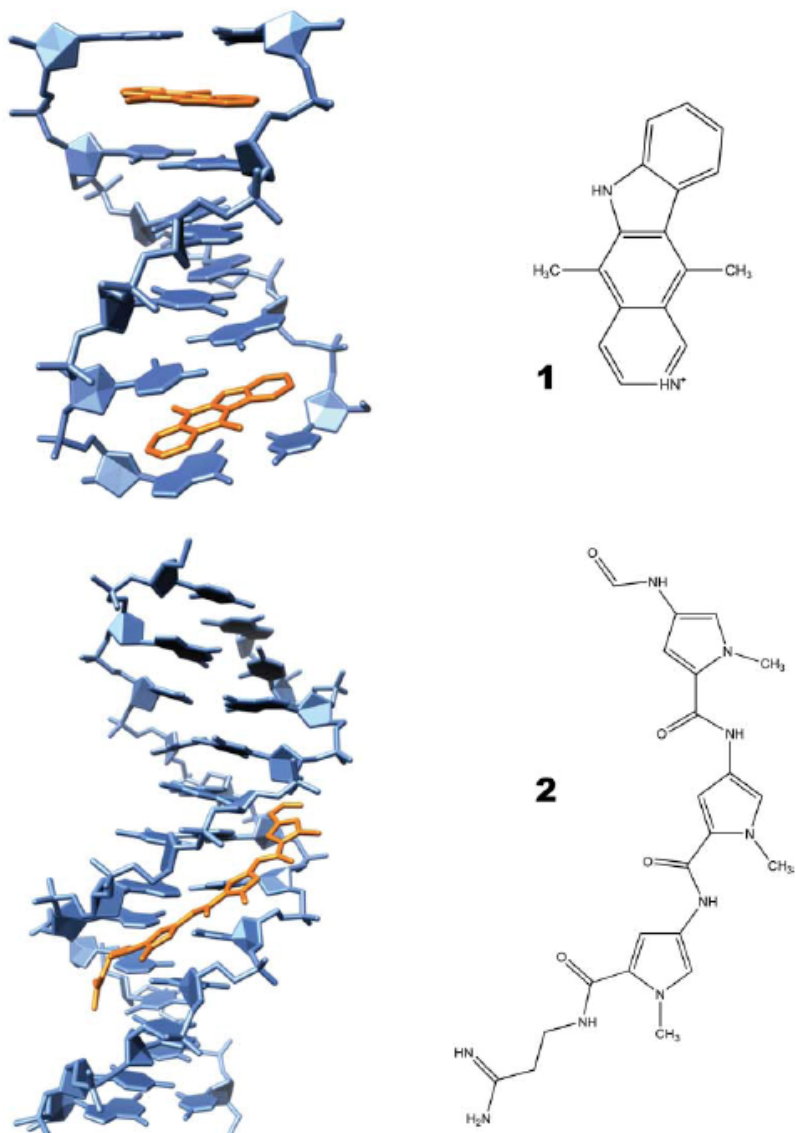
Figure 1-5. Duplex interacting molecules

Ellipticine (1) is an example of an intercalater with a fused aromatic ring system carrying a positive charge. Distamycin (2) is a example of a minor groove binder. X-ray structures for (1, (Canals *et al.* 2005)) and (2(Coll *et al.* 1987)) are shown on the left. Figure adapted from (Boer *et al.* 2009)

Examples of higher order DNA and RNA structures abound in biology (*e.g.,* ribozymes, riboswitches, DNA/RNA hybrids, i-motifs, G-quadruplexes, replication forks, HJs, etc.). Many of these higher order structures are branched such that the duplex strands that make up one arm are separated and repaired with strands from a neighboring arm. The nucleobases at the branch point have no stacking partners on one side and are therefore exposed to solvent at the center of the junction. Compounds that bind branched structures use a combination of flexibility and aromatic functionalities to span the branch point and form stacking interactions with the exposed bases. Two examples illustrate the different ways this can be achieved: a three-way DNA junction bound by a "supramolecule" (Figure 1-6; Oleksy *et al.* 2006)) and a four way junction bound by a bis-acridine (Figure 1-7; Brodgen *et al.* 2006). The ligand bound to the three-way junction is formed from three identical bis-pyridylimines that coordinate two Fe^{+2} atoms to form a positively charged, hydrophobic, triangle shaped "supramolecule" (Figure 1-6). The flexibility of the ligand allows coordination of the Fe^{+2} atoms, and establishes the shape of the "supramolecule" which allows it to insert into the triangular center of the three-way junction. The flexibility of the ligands also allows several of the aromatic rings to stack with the exposed bases at center of the junction that lie in different orientations with respect to the "supramolecule". Several other aromatic rings insert perpendicular to the major grooves presented to the center of the junction by the branching arms and this establishs a strong set of Van der Waals interactions. Finally, the interaction is stabilized by the two positively charged Fe^{+2} atoms that are coordinated by the phosphate backbone to establish strong ionic interactions.
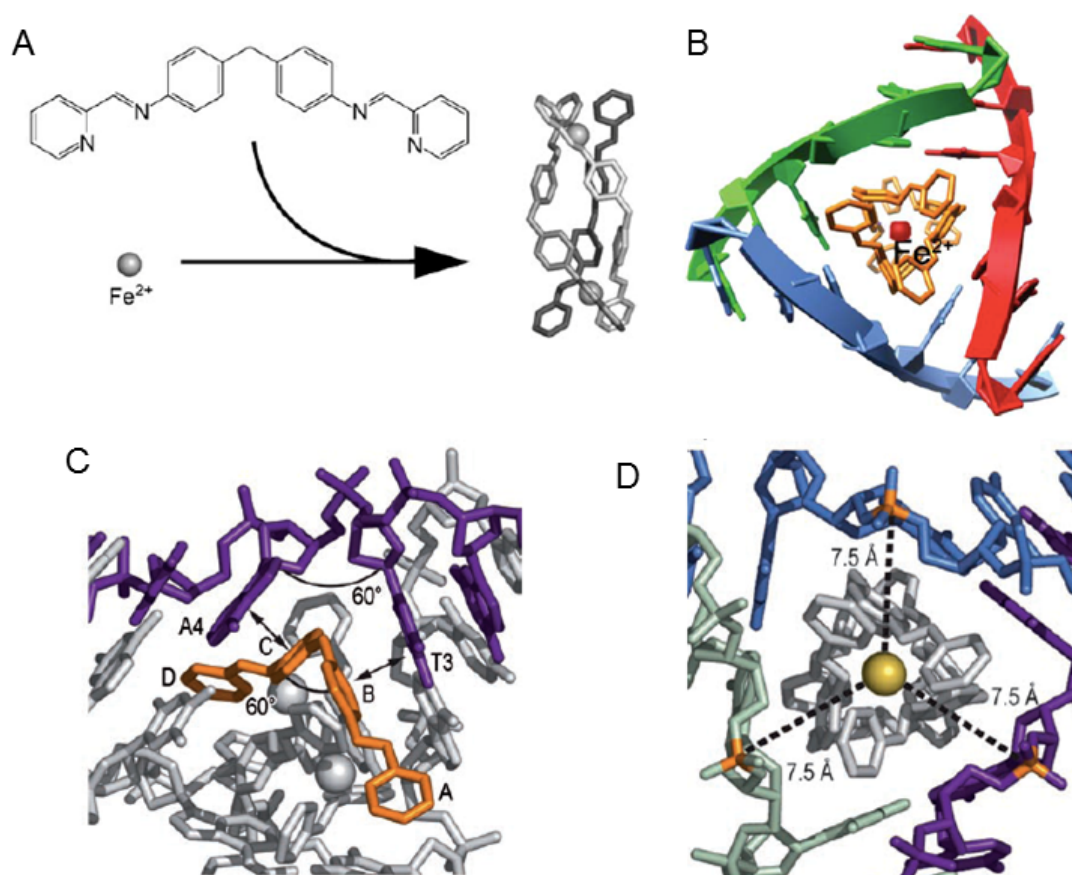
Figure 1-6. Ligand bound to a three-way junction

(A) Three bis-pyridylimine molecules bind two Fe^{+2} atoms to form the "supramolecule." (B) View of the "supramolecule" bound to the three-way junction (shown in ribbon form). (C) close up view of the center of the junction. The C and D rings indicated on the bis pyridylimine ligands (orange) are flexible enough to establish base stacking interactions with the A4 and T3 nucleobases (purple) exposed at the center of the junction. Additionally, the A and D rings of the bis pyridylimine insert perpendicular to the major grooves establishing Van der Waals interactions. (D) close-up looking down the center of the junction showing the overall shape of the supramolecule (grey) and coordination between the Fe^{+2} and selected phosphate groups (orange) on the backbone of the DNA. (A, B and D) are adapted from Oleksy *et al.* 2006, and (C) is adapted from (Boer *et al.* 2009).

In contrast to the three way junction, a single bis-acridine ligand is bound to the four-way junction shown in Figure 1-7. The ligand has four positively charged centers; two are present on aliphatic side-chains that lie in the minor grooves of HJ structure, and two are present in the fused aromatic acridine ring functionalities. Each acridine ring makes base stacking interactions similar to the manner in which they would intercalate duplex DNA. They also establish pseudo-base pairs with thymidine nucleobases displacing the normally hydrogen bonded adenosine. The two acridines are connected by a 6-carbon linker that allows a single ligand to span the center of the junction. Since the arms of the junction are tilted with respect to one another, the exposed nucleobases lie at different orientations. The 6-carbon linker allows the acridine rings on a single ligand to rotate and establish stacking interactions at different angles. Interestingly, a variety of linkers were experimented with, yet only the 6-carbon version produced crystals. This suggests that in addition to the flexibility, the distance between each aromatic ring system is a critical determinant for crystallization and potentially for HJ binding in general.

Both of these structures serve to illustrate characteristics of branched DNA binding. Aromatic rings are necessary for base stacking interactions, can be either single rings or fused systems. The ligands must carry positive charges, either in the form of protonated centers, or coordinated metal ions, that can facilitate interactions with the negatively charged DNA. Additionally, they must be flexible enough to allow stacking interactions to form with bases that are presented at various angles to the center of the junctions. Finally, it is noteworthy that most of the DNA binding ligands are not sequence specific. Such ligands recognize features of the DNA (*e.g.*, backbone, grooves, inter-base regions) and while the sequence of the DNA can

indirectly impact these features, the ligands themselves are usually too small to have the types of sequence recognition that proteins or macromolecular complexes exhibit. Thus, DNA binding ligands such as duplex intercalators (e.g., topoisomerase poisons) have severe toxicity since they bind indiscriminately. Since branched DNAs, such as HJs, form during distinct repair processes, they are predicted to be present less frequently than B-form double stranded DNA; therefore they may offer a measure of toxic selectivity not achievable with other DNA ligands.
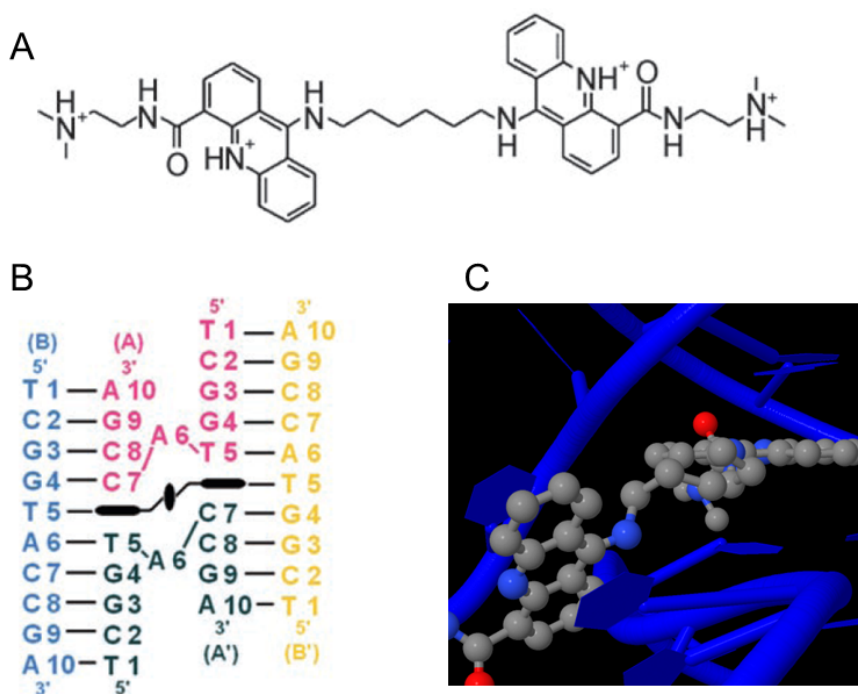
Figure 1-7. Bis-acridine bound to a HJ.

(A) The structure of the bis-acridine ligand. (B) Cartoon depiction of the binding of the bis-acridine ligand at the center of the HJ. The two acridine functionalities are shown as thick black horizontal lines and are connected by a 6 carbon aliphatic linker (thin black line). The crystallographic dyad is the thick vertical line in the center of the figure. The ligand makes pseudo-base pairing interactions with thymidine (T5) on both of the "B" strands (light blue and yellow), and base stacking interactions between T5 and C7 on the "A" strands (pink and dark blue). The displaced adenosine (A6) is disordered in the crystal structure. (C) Crystal structure of the center of the junction. DNA is in blue ribbon form, and the ligand is ball and stick form. Stacking interactions with one of the T5-C7 pairs is seen in the lower left corner. The other half of the ligand is rotated >60° to form base stacking interactions with the other T5-C7 pair on the opposite side of the junction. (A and B) are adapted from Brogden 2007. (C) was created using RasMol and PDB ID code 2GWA.

Chapter 2. Potent antimicrobial small molecules screened as inhibitors of tyrosine recombinases and Holliday junction-resolving enzymes

Section 2.1. Introduction

Site-specific recombination (SSR) catalyzed by phage λ Integrase (Int) requires the formation and subsequent resolution of a Holliday Junction intermediate (HJ) (Figure 2-1A). These enzymes are widespread, and include a subclass of bacterial-encoded enzymes, for example XerC and XerD of *E. coli* and RipX and CodV of *B. subtilis,* that help in the process of segregation of chromosomes to daughter cells. The mechanism and structure of these enzymes has been extensively studied (Azaro 2002). Previously, hexapeptide inhibitors that trapped recombinase-bound HJ intermediates and blocked recombination were isolated by screening and deconvoluting synthetic peptide combinatorial libraries (Cassell *et al.* 2000; Klemm *et al.* 2000; Boldt *et al.* 2004). Further analysis of the most potent peptide WRWYCR (Figure 2-1B) showed that its activity required the formation of a dodecapeptide via a disulfide bridge between the cysteines from each of two hexapeptides (Boldt *et al.* 2004). Peptides that do not readily dimerize were also identified in the screen (*e.g.,* WKHYNY, Figure 2-1C) but homodimers like WRWYCR and KWWCRW were more effective at trapping HJs *in vitro* and *in vivo* (Kepple *et al.* 2005; Kepple *et al.* 2008; Gunderson *et al.* 2009).
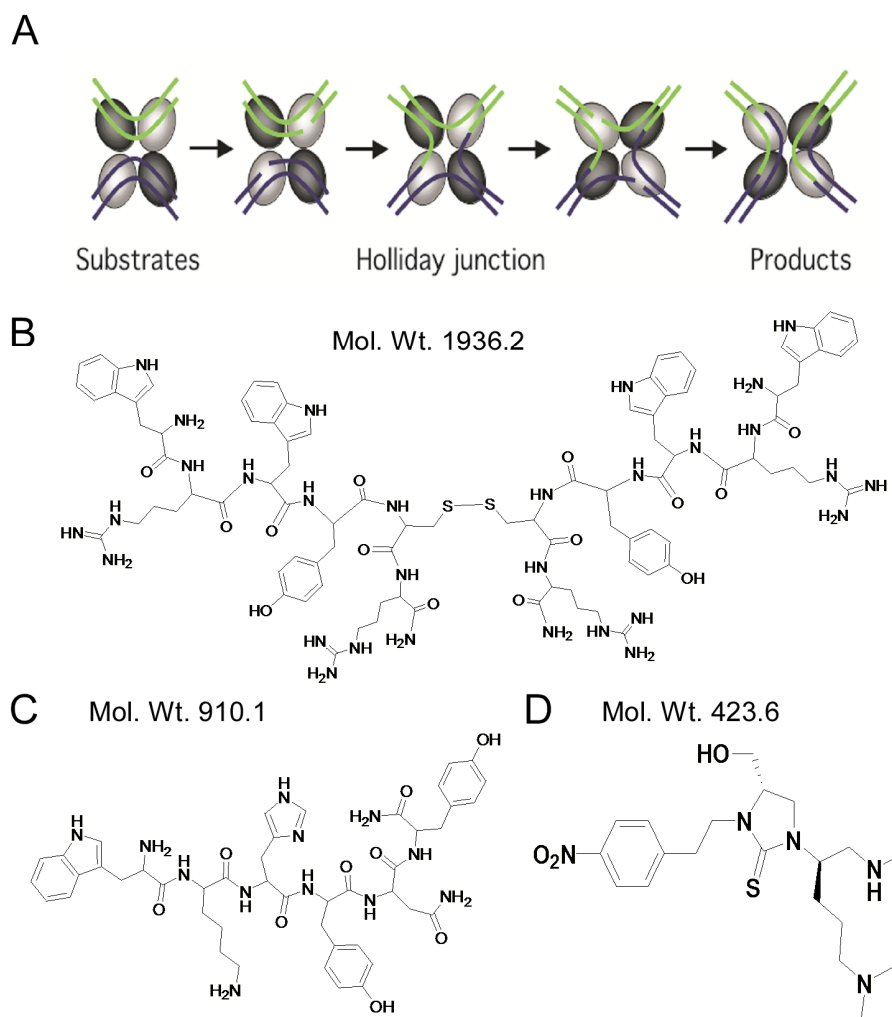
Figure 2-1. Inhibitors of Int-mediated recombination.

(A) Schematic of the tyrosine recombinase-mediated SSR pathway. Four Int monomers synapse the recombining DNA molecules; only the regions around the site of strand exchange are shown. Two Int monomers (shown as light grey ovals) each cleave opposing strands of DNA to form a covalent protein-DNA adduct at the 3' end, leaving a free 5' OH group. The strands ending in the 5' OH groups are exchanged and ligated, forming the Holliday junction (HJ) intermediate. In the absence of any inhibitors, the second pair of Int monomers cut, exchange and religate the second pair of DNA strands, resolving the HJ into recombinant products. The HJ is the primary target of the inhibitors, preventing cleavage of either pair of DNA strands. The requirement for the accessory proteins IHF and Xis (not shown) is dependent on the specific recombination pathway (Segall *et al.* 1996). (B) Structure of a WRWYCR dimer. (C) Structure of WKHYNY. (D) Structure of N-methyl aminocyclic thiourea, 1530-1.

The activity of WRWYCR and KWWCRW is not dependent upon interactions with any of the tyrosine recombinase proteins, which are very diverse in their primary amino acid sequence ((Boldt *et al.* 2004; Grindley *et al.* 2006; Gunderson *et al.* 2006)). WRWYCR and KWWCRW also inhibit DNA cleavage and HJ resolution by Vaccinia virus topoisomerase, the prototype of type IB topoisomerases (Klemm *et al.* 2000; Fujimoto *et al.* 2006). The mechanism and structure of the catalytic domains of tyrosine recombinases and type IB topoisomerases are highly related (Cheng *et al.* 1998; Champoux 2001). In addition, these peptides also inhibit structurally and mechanistically unrelated HJ processing enzymes like RecG helicase and RuvABC resolvase, whose only commonality with the tyrosine recombinases is their interactions with HJs (Kepple *et al.* 2005). The activities of the peptides are based on their ability to bind to the open or square planar conformation (Lilley 2008) of protein-free HJs, and with lesser affinity to other branched DNAs, including replication forks (Kepple *et al.* 2005).

HJs are central intermediates in several DNA repair pathways that are required during bacterial growth, and particularly in environments in which bacteria experience DNA damage, such as the immune system of mammalian hosts (Cano *et al.* 2002; Loughlin *et al.* 2003; Michel *et al.* 2007). WRWYCR, KWWCRW and their D-amino acid stereoisomers wrwycr and kwwcrw are broad spectrum antibacterials that have Minimal Inhibitory Concentrations (MIC) ranging from 32-64 μg/mL in Gram-negative bacteria and 4-32 μg/mL in Gram-positive bacteria (Gunderson *et al.* 2006). Whereas bacteria recover from treatment with even high doses of the L-amino acid isomers, they recover less or not at all from the D-amino acid peptides. The peptides are bactericidal and their effect is synergistic with other

DNA damaging agents, including UV, mitomycin C, H_2O_2, and norfloxacin in bacteria or etoposide in HeLa and U2OS cells (Gunderson *et al.* 2006) (Naili, I., Rostron, J. and Segall A., unpublished data; Su., L., Patra, S., and Segall, A., unpublished data). This led us to propose that the need for DNA repair creates HJ targets for the peptides, blocking further repair and/or DNA synthesis and causing the accumulation of fragmented DNA and ultimately cell death (Gunderson *et al.* 2006) (Xu, Y., Orchard, S., Naili, I., Contreras, A., and Segall A., unpublished data; Gunderson C., and Segall, A., unpublished data). Peptide wrwycr has antibacterial activity against *Salmonella enterica* serovar Typhimurium in murine macrophage cells, and treatment of *Salmonella*-invaded J774A.1 macrophages with wrwycr induces the SOS response in the intracellular bacteria (Su *et al.* 2010).

DNA repair intermediates such as HJs are largely unexploited antibacterial targets, and resistance is less likely to develop because HJs are generated in multiple independent ways (Michel *et al.* 2007). Indeed, we have been unable to isolate stable peptide-resistant mutants. In light of the emergence of multiple drug resistance in bacteria, we have been investigating the possibility of developing these inhibitors into therapeutic agents. Peptide-based drugs have some disadvantages. We have overcome a major disadvantage of the sensitivity of L-amino acid peptides to proteolysis by using the D-isomer version of the same peptides (Boldt *et al.* 2004; Gunderson *et al.* 2006; Gunderson *et al.* 2009). Other disadvantages of peptides are relatively high molecular weights, which lead to poor bioavailability and permeability across the intestinal and blood brain-barriers (Lipinski *et al.* 2001). Moreover, peptides have an excess of hydrogen bond donors and acceptors, often considered negative characteristics for potential therapeutics (Lipinski 2000).

In order to find non-peptide compounds with similar activities, we performed screens of small molecule libraries to isolate HJ-trapping surrogates. Like the peptide libraries, these are mixture-based libraries whose diversity is derived from functional groups (analogous to peptide R groups) on a unique scaffold (Houghten *et al.* 1999; Nefzi *et al.* 1999; Pinilla *et al.* 2003; Hensler *et al.* 2006). Our initial small molecule screen focused on libraries built on scaffolds with low molecular weight, and yielded a N-methyl aminocyclic thiourea that traps HJs formed during SSR reactions *in vitro* (1530-1, Figure 2-1D and (Ranjit *et al.* 2010)). This inhibitor binds specifically to protein-free HJs and inhibits HJ resolution by RecG. While showing that the same strategy that yielded potent peptide inhibitors could also yield non-peptide molecules with analogous activities, 1530-1 is less potent in *in vitro* reactions and showed only about 50% growth inhibition of a hyperpermeable *Salmonella* strain at 128 µg/mL (Ames *et al.*). A major difference between the most potent hexapeptide inhibitors and 1530-1 is a relatively low potential for forming dimers. In order to identify more potent compounds with antibacterial activity, we repeated the screen focusing specifically on libraries built on larger, more symmetric scaffolds in an effort to mimic the most potent peptide homodimers. Here we describe the identification of several pyrrolidine bis-cyclic guanidine inhibitors that inhibit phage lambda SSR and trap HJs. These compounds recognize protein-free HJs, inhibit HJ resolution by RecG helicase, and have antibacterial activity at least as potent as peptides wrwycr and kwwcrw.

Section 2.2. Results

2.2.1. Experimental strategy

The strategy used to identify individual compounds from the combinatorial libraries is outlined in (Figure 2-1). Underlined text refers to specific headings in the Results section where more detailed explanations can be found.

2.2.2. Scaffold Ranking

The ten mixture-based libraries screened (Figure A - 2) were selected to have some degree of two-fold symmetry in the scaffold compared to the lead molecule 1530-1. Each of the scaffolds has functionalities, or R groups, at 3 or 4 diversity positions depending on the scaffold. These functionalities are derived from coupling L - or D - amino acids at the first R group positions, and carboxylic acids at the last R group (R^3 or R^4, depending on the scaffold). The libraries are arranged in a positional scanning format (Pinilla *et al.* 1992) comprised of mixtures that can either be screened individually to identify potent R group functionalities, or pooled to test the potency of the library as a whole. For instance, the positional scanning TPI1346 library is composed of 120 mixtures (26 R^1 + 26 R^2 + 26 R^3 + 42 R^4 = 120) for a total diversity of 738,192 compounds (26 R^1 * 26 R^2 * 26 R^3 * 42 R^4 = 738,192). In mixture 1 (Figure A - 3) every compound contains the functionality S-methyl at position R^1 and a mixture of all other possible functionalities for this library at positions R^2-R^4, yielding a total of 28,392 compounds (1*26*26*42 = 28,392). Inclusion of this mixture into a given assay allows for assessment of the functionality S-methyl at position R^1 on this scaffold. Alternatively, the 26 R^1 mixtures can be

Scaffold ranking: Mixtures comprising the entire diversity of each
library (Figure A - 2)
were screened for inhibition of recombination (Figure 2-3)

Pyrrolidine bis-cyclic guanidine scaffold selected (Figure A - 3)
Total diversity = 738,392 compounds

Screening of positional scanning library: 120 mixtures screened
(recombination) to evaluate potent functionalities at the 4 diversity positions on the
pyrrolidine bis-cyclic guanidine scaffold (Figures A - 3 thru A - 6)

# of mixtures	R^1, R^2, and R^3 = 26 each	R^4 = 42
# of compounds/ mixture	R^1, R^2, and R^3 = 28,392	R^4 = 17,576
functionalities selected:	R^1 and R^2 = 2	R^3 and R^4 = 3

Synthesis of individual compounds (Figure 2-4)
2 x 2 x 3 x 3 = 36 compounds (Table 2-1)
Preliminary characterization:
- HJ binding & resolution (Figures A - 1 and A - 7)
- recombination (Figure A - 7)
- MIC (not shown)

Compound characterization:
Four compounds purified and characterized:
- recombination (Figure 2-6A)
- HJ binding affinity (Figure 2-6C and 2-7)
- HJ binding stability (Figure 2-8)
- DNA repair enzyme inhibition (Figure 2-6B)
- MICs (Gram +/- bacteria) (Table 2-5)
- Eukaryotic cytotoxicity (Figure 2-9)

Figure 2-2. Experimental strategy for inhibitor indentification.

Ten libraries were selected and screened in site-specific recombination (SSR) to determine the most potent scaffold. We next screened 120 defined mixtures representing the positional scanning to determine the most potent R-group functionalities on the scaffold; deconvolution involved the selection of the top functionalities to design 36 individual compounds, which were synthesized in parallel. After preliminary characterization, we selected four candidates for purification and further characterization in the assays listed. Figure A - 1 through A – 7 can be found in the Appendix.

pooled, to reconstitute the entire diversity of the library, and tested similarly; the same holds true for (R^2, R^3 or R^4 mixture pools). Comparisons with similar mixture pools from other libraries allows for selection of the best library.

We tested R^1 mixture pools for each of the ten libraries in the bent-L recombination pathway (see (Azaro 2002) for review) at 30 µg/mL. As seen in A, inclusion of these mixture pools leads to an increase in HJs and a concomitant decrease in recombinant products, depending on the potency of the library. We also compared these results with similar pools for the other R groups in each library (R^2, R^3 or R^4) and the results shown in Figure 2-3B are the average % recombination and the average % HJ accumulation for all the R group pools of a given library. The relatively small error bars shown reflect the fact that each of these mixture pools does indeed represent the complete diversity of the entire library and thus they give similar results. This concept has been developed into a "scaffold ranking strategy," described in detail in (Houghten *et al.* 2008).

The best-performing four libraries, TPI1276, TPI1319, TPI1345, and TPI1346, accumulated at least 25% of the input substrate as HJs (Figure 2-3B). Based on a dose titration from 0.25 to 150 µg/mL of each library (Figure 2-3C), we found that TPI1346 trapped the most HJs and had the lowest IC_{50} for HJ accumulation (0.6 µg/mL versus 2 µg/mL for the other three libraries). Library TPI1346 is synthesized on a pyrrolidine bis-cyclic guanidine scaffold (Figure A - 3) with four diversity positions divided among 120 mixtures, for a total diversity of 738,192 unique compounds.
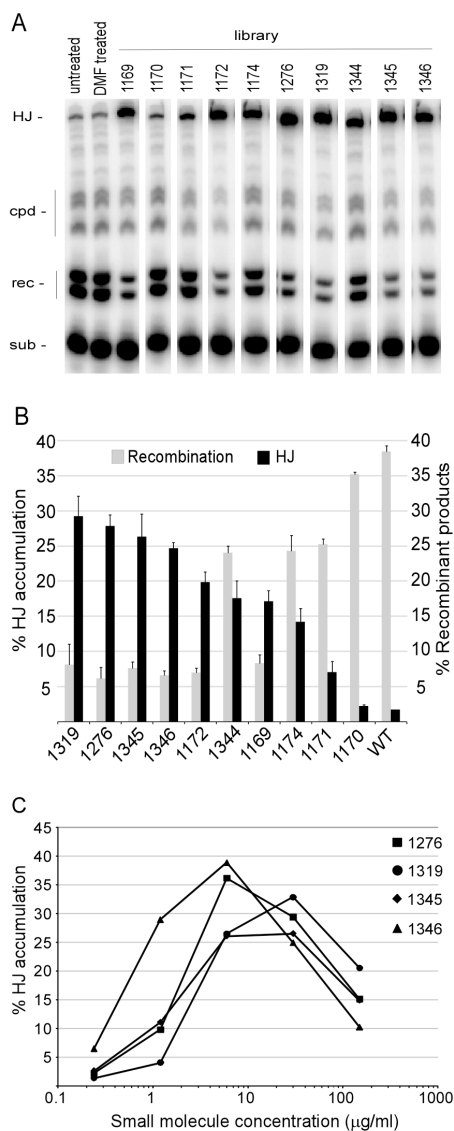
Figure 2-3. Scaffold ranking

(A) Representative lanes from several gels showing the effects of inclusion of various small R group pools on bent-L recombination. Sub, radiolabeled substrate that recombines with an unlabeled partner site to produce recombinant products, 'rec.' 'CPD', covalent protein-DNA complexes; 'HJ', Holliday junction. (B) Each mixture was tested at a concentration of 30 μg/mL and the average for all R group mixtures was determined. The error bars reflect the differences between R group pools within a given library. (C). Performance of the 4 most potent scaffolds evaluated by extent of HJ accumulation and IC_{50} values for recombination. High concentrations also inhibit the first cleavage event, reducing the HJ formed (refer to the mechanism of λ-SSR shown Figure 2-1A).Screening and deconvolution were performed by Jeff Boldt.

2.2.3. Screening of positional scanning libraries

The positional scanning mixtures in the TPI1346 library were screened in the excisive recombination pathway (Azaro 2002). The mixtures with defined functionalities at the first three diversity positions (R^1, R^2 and R^3) averaged 10-15% HJ accumulation at 1.0 μg/mL (Figure A - 4 through Figure A - 7). Mixtures with the following three functionalities exhibited a significant amount of HJ accumulation: the R and S isomers of 2-naphthylmethyl, and R-4-hydroxybenzyl. Although these mixtures accumulated a small fraction of substrates as HJs at 1.0 μg/mL, they outperformed all others at 0.5 μg/mL. This observation is also seen with high concentrations of peptides and is likely to reflect inhibition of the first DNA cleavage step in the recombination reaction, which reduces the% HJ formed (Boldt 2006). Mixtures with defined functionalities at the R4 position were tested at 1 μg/mL (Figure A - 7); on average, 9% of the starting substrates were accumulated as HJs. From these data, the defined functionalities 2-biphenyl-4-yl-ethyl and 3,4-dichlorophenylethyl were selected for incorporation at position R^4 (again, these functionalities outperformed all others at 0.5 μg/mL). Finally, the functionality 2-adamantan-1-yl-ethyl was included due its non-aromatic ring-like structure, in order to examine the effect of size/shape at this R position (Appendix). The functionalities selected for synthesis of individual compounds are marked with an asterisk in Figure A - 4 through Figure A - 7, and yielded the 36 possible individual combinations (R^1=2, R^2=2, R^3=3 and R^4=3, 2*2*3*3=36) which are shown in Table 2-1.

Table 2-1. R-group combinations for defined compound synthesis.

Position R^1 = R-2-naphthylmethy for compounds 1-18	Position R^1 = S-2-naphthylmethy for compounds 19-36	R^2	R^3	R^4
1609-1	1609-19	(R)-4-hydroxybenzyl	(R)-4-hydroxy benzyl	3,4-dichlorophenylethyl
1609-2	1609-20			2-adamantan-1-yl-ethyl
1609-3	1609-21			2-biphenyl-4-yl-ethyl
1609-4	1609-22		(S)-2-naphthyl methyl	3,4-dichlorophenylethyl
1609-5	1609-23			2-adamantan-1-yl-ethyl
1609-6	1609-24			2-biphenyl-4-yl-ethyl
1609-7	1609-25		(R)-2-naphthyl methyl	3,4-dichlorophenylethyl
1609-8	1609-26			2-adamantan-1-yl-ethyl
1609-9	1609-27			2-biphenyl-4-yl-ethyl
1609-10	1609-28	(S)-2-naphthylmethyl	(R)-4-hydroxy benzyl	3,4-dichlorophenylethyl
1609-11	1609-29			2-adamantan-1-yl-ethyl
1609-12	1609-30			2-biphenyl-4-yl-ethyl
1609-13	1609-31		(S)-2-naphthyl methyl	3,4-dichlorophenylethyl
1609-14	1609-32			2-adamantan-1-yl-ethyl
1609-15	1609-33			2-biphenyl-4-yl-ethyl
1609-16	1609-34		(R)-2-naphthyl methyl	3,4-dichlorophenylethyl
1609-17	1609-35			2-adamantan-1-yl-ethyl
1609-18	1609-36			2-biphenyl-4-yl-ethyl

2.2.4. Synthesis of individual compounds

The 36 compound were synthesized in parallel in 100 mg "tea-bags (Houghten 1985)" using methylbenzylhydramine (MBHA) resin as a support and as described in (Hensler *et al.* 2006). Briefly, resin was activated with a weak base (diisopyropylethylamine, DIPEA) and four Boc-protected amino acids (Figure A - 3) were sequentially coupled using diisopropylcarbodiimide (DIC) and N-hydroxybenxyotrizole (HOBt) as catalysts. In every case, proline was coupled second leaving a pyrrolidine ring as part of the final structures. The fifth coupling was always a carboxylic acid (Figure A - 3) yielding compound (1) in Figure 2-4. Every coupling was verified by a Ninhydrin assay to test for unreacted amines and an aliquot of the synthesis was verified by mass-spectrometry (MS) following the fifth coupling. Amide bonds were reduced with diborane to yield compound (2) and verified by (MS). Compounds were cyclized with cyanogen bromide and then cleaved from the support using hydrofluoric acid (HF) and anisole to yield (3). Compounds were extracted from the tea bags with 95% acetic acid, lyophilized and verified by MS. Yields for the 36 compounds were between 80 and 95 mg of crude compound. A small amount of each crude compound was resuspended in 10 - 50% (DMSO/water) and screened in the indicated biological assays without further purification.
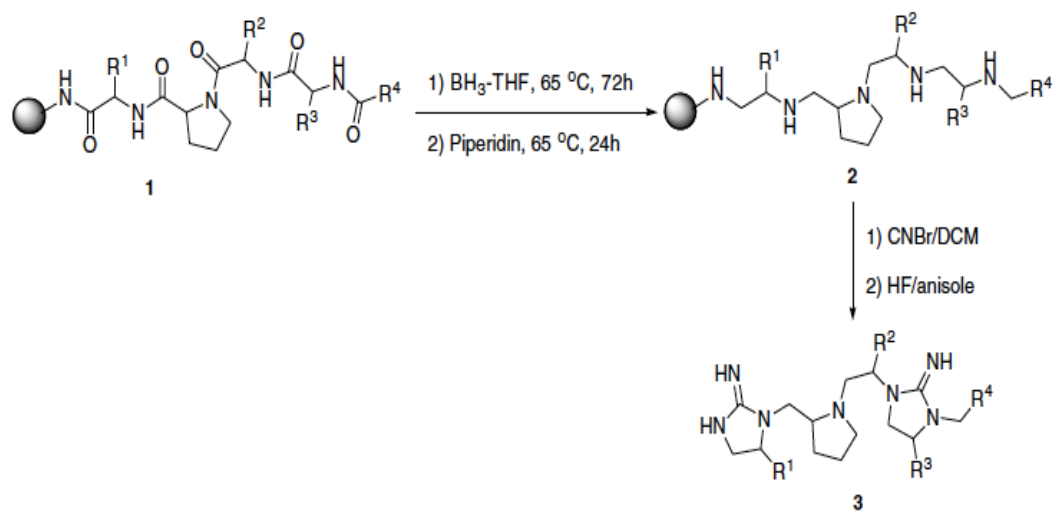
Figure 2-4. Synthesis scheme for the pyrrolidine bis-cyclic guanidines

The sequential coupling of Boc-protected amino acids followed by coupling of a carboxylic acid to MBHA resin (grey sphere) yields (1). Diborane reduction yields (2) which is followed by treatment with cyanogen bromide to cyclize the compounds. Compounds are cleaved from the resin using HF to yield (3). Figure adapted from (Hensler *et al.* 2006)

2.2.5. Crude compound screening

Individual compounds were designated 1609-1 through 1609-36. In order to select candidates for purification, these compounds were screened in the following assays: accumulation of HJs and inhibition of excision reactions (Figure A - 8), binding to protein-free HJ's (Figure A - 1), non-specific linear DNA binding (data not shown), inhibition of the HJ resolvase complex RuvABC (Figure A - 8), and inhibition of bacterial growth (data not shown). We also used these data to preliminarily assess the role of R group stereochemistry on selected parts of the scaffold (Appendix). The results of these assays were used to select four compounds for purification and characterization.

2.2.6. Purified compound characterization

Compounds 1609-1, 1609-3, 1609-10, and 1609-12 (Figure 2-5) were purified and their masses were confirmed by high-resolution mass spectrometry (Figure A - 9 through Figure A - 12).
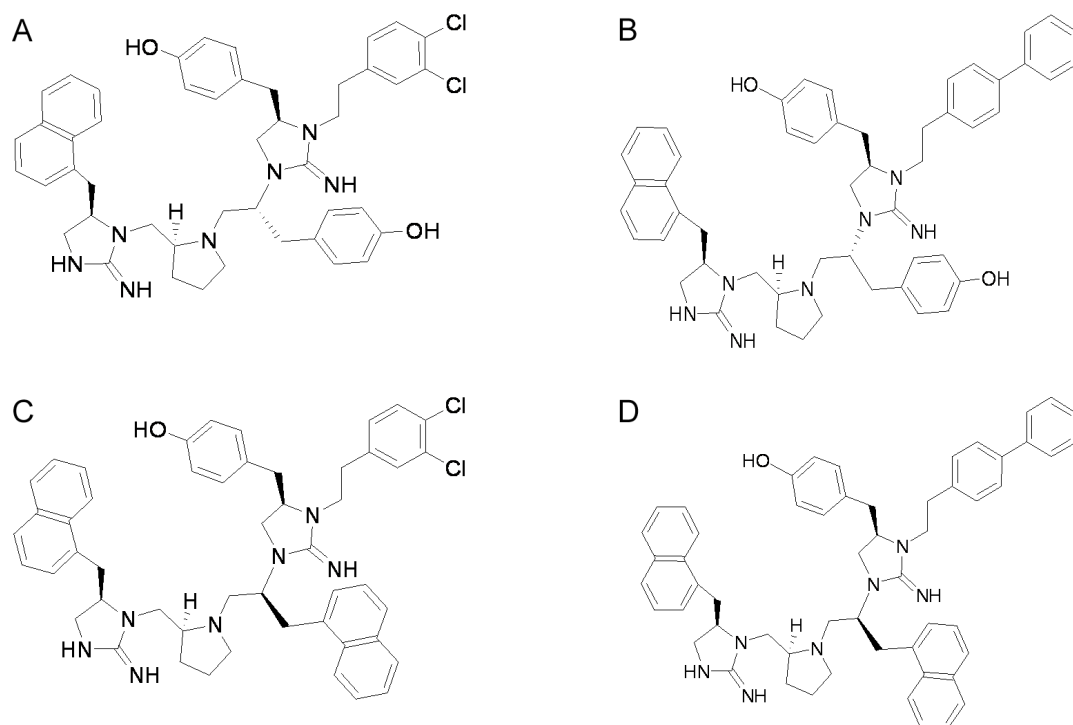
Figure 2-5. Compounds selected for purification

Shown are compounds (A) 1609-1 (M.W. 804.85), (B) 1609-3 (M.W. 812.05), (C) 1609-10 (M.W. 838.91), and (D) 1609-12 (M.W. 846.11).

The four compounds were titrated in excisive recombination reactions and shown to be inhibitory in a dose-dependent manner (Figure 2-6A). Inhibition of recombination was quantified at seven concentrations (0.25-8 µg/mL), and these data were used to estimate the IC_{50} values shown in Table 2-2. For comparison, the IC_{50} values of the peptides and the previously identified N-methyl aminocyclic thiourea (Ranjit *et al.* 2010) inhibitor 1530-1 are listed.

HJs arise in multiple pathways *in vivo*, and are acted upon by several proteins/complexes with distinct mechanisms and structures. To determine whether other HJ-processing enzymes are inhibited by the compounds, we tested their effect on the activity of the *E. coli* RecG protein. This monomeric helicase is conserved across almost all bacterial species and functions in recombination-dependent DNA repair by unwinding a variety of branched DNA substrates to prevent so-called pathologic replication (reviewed in (Rudolph *et al.* 2010). *In vitro,* the purified enzyme converts a HJ to two partial DNA duplexes in the presence of ATP and magnesium (Whitby *et al.* 1998; Kepple *et al.* 2005). We tested the ability of the four selected compounds to interfere with RecG helicase (Figure 2-6B) and found dose-dependent inhibition of unwinding activity. These titrations were used to estimate the IC_{50} values for each compound and the results are shown in Table 2-2.
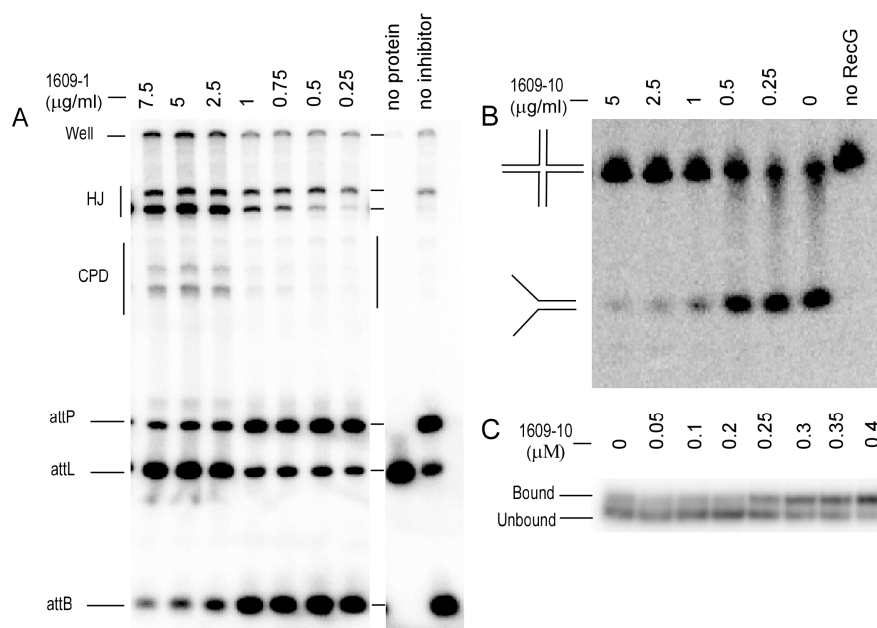
Figure 2-6. Small molecules interact with HJs

(A) Slices from a representative SDS-Tricine gel showing a dose titration of 1609-1 into an excision reaction. Recombination proteins (Int, IHF and Xis) recombine a radiolabeled substrate, *attL*, with an unlabeled partner site, *attR*, to form the recombinant products *attP* and *attB*. The HJ intermediate of this reaction is stabilized by 1609-1, blocking progression to products or regression to substrates (see Figure 1A). CPD, covalent protein-DNA complex; the lower HJ band is free HJ, while the upper HJ band is incompletely ligated, with Int still covalently attached. (**B**) An example of a HJ unwinding assay catalyzed by the RecG helicase. In the presence of HJ DNA, ATP and Mg^{+2}, RecG unwinds the HJ into two partial DNA duplex molecules, and this activity is inhibited by 1609-10 in a dose-dependent manner. IC_{50} values determined for 1609-1, -3, -10 and -12 for both excision and HJ unwinding were averaged from multiple titrations and are listed in Table 1. **(C)** 1609-10 binds to HJ. Radioactive end-labeled HJs run predominantly as a faster migrating unbound species in the absence of 1609-10. Treatment with increasing amounts of 1609-10 leads to a shift to a slower conformation. In some ionic conditions, we see a mixture of the two conformations (see text). The 1609-10-dependent transitions are not seen with DMSO alone. The estimated K_d for this binding reaction is ~ 300 nM which is approximately 0.25 µg/mL.

Table 2-2. Summary of *in vitro* activities of selected inhibitors.

Compound	Molecular weight[a]	Holliday junction binding (K_d)		DNA repair (µg/mL)	Recombination (µg/mL)	% DNA restriction by HindIII[b]	
		2-AP	EMSA	IC_{50} RecG	IC_{50} excision	1 µg/mL	10 µg/mL
WKHYNY	910.1	none[c]	no shift	91.01[d]	18.2[d]	NT	NT
WRWYCR	1936.2	14 nM[e]	12.5 nM[d]	0.16[d]	0.04[d]	100[f]	100[f]
1530-1	423.5	NT	11.8 µM[g]	0.36	10.5	100[g]	100[g]
1609-1	804.85	NT	NT	1.92	1.2	100	79
1609-3	812.05	NT	NT	1.18	1.2	100	54
1609-10	838.91	250 nM	300 nM	0.94	1.8	100	39
1609-12	846.11	NT	NT	0.75	0.7	100	11

[a] Molecular weight of active species; in the case of WRWYCR, this is a dimer.

[b] Numbers listed are the% activity at the indicated inhibitor concentration (corrected for DMSO effect) compared to untreated reactions.

[c] None = no binding detected in the 2-AP assay (Kepple *et al.* 2008); NT = not tested

[d,e,f,g] Numbers listed are from references (Boldt *et al.* 2004; Ranjit 2004; Kepple *et al.* 2005; Kepple *et al.* 2008) respectively.

[f] Reactions treated with 100 mg/mL compound, the maximum concentration tested, showed no inhibition of DNA restriction by the enzyme HindIII.

In order to address the specificity of these compounds for other DNA modification reactions, we assayed their effect on DNA cleavage by the HindIII restriction enzyme at the single recognition sequence in pUC19 plasmid DNA. Reactions were treated with each of the four selected compounds at a concentration near the IC_{50} values for recombination and HJ unwinding (1 µg/mL) and at a 10-fold higher concentration (10 µg/mL). Aliquots were removed from reactions at various time points, quenched with SDS and electrophoresed on agarose gels to quantify the extent of DNA restriction over time (Rideout, M., and Segall A, unpublished data). Restriction inhibition values in the presence of the DMSO solvent were subtracted from restriction inhibition values of reactions treated with each small molecule, to obtain the corrected reaction velocities. The data in Table 2-2 are listed as the corrected% DNA restriction/min compared to untreated reactions. As seen, none of the compounds affected DNA restriction by HindIII at 1 µg/mL, while some did inhibit, by as much as ~90%, at 10 µg/mL; this suggests that the 1609 compounds have less specificity for the HJ substrate than the peptides or compound 1530-1, but still prefer HJ substrates over B-form double-stranded DNA.

To further examine the nature of the interactions between the small molecules and the HJ we tested whether 1609-10 could recognize protein-free HJs in an electrophoretic mobility shift assay (EMSA). This assay measures the ability of the compound to bind to and change the conformation of a synthetic HJ (Figure 2-6C). In solution, HJs isomerize between "stacked-X" and "open square" conformations; in the former more compact conformation, the arms of the junction fold in such a way that the center of the junction is occluded, whereas in the open more extended conformation, the junction center is accessible to solvent (McKinney

et al. 2003; Lilley 2008). Under some conditions, junctions can take on either the open or the stacked form; in the leftmost lane of Figure 2-6C, the junction is seen as an unequal mixture of the two conformations. Adding 1609-10 changes the conformation of the junction into the open form in a dose-dependent manner; this band shift is similar to that seen with the peptides (Kepple *et al.* 2005) and 1530-1 (Ranjit *et al.* 2010).

The conformation change seen in Figure 2-6C likely results from 1609-10 binding at the center of the HJ. To test this hypothesis, we used a 2-AP fluorescence-quenching assay; this assay was used previously to determine the binding affinity of peptide WRWYCR to several branched DNA substrates, including HJs (Ghosh *et al.* 2005; Kepple *et al.* 2008). Briefly, synthetic HJs were assembled using oligonucleotides where a single adenine was substituted with its fluorescent analog 2-AP at the center of the HJ substrate. In dsDNA, the fluorescence of 2-AP is quenched by base stacking with flanking bases. The 2-AP residue at the center of the junction has no stacking neighbor on one side and thus displays about half the maximal fluorescence compared to that seen in single stranded DNA (Declais *et al.* 2000). This fluorescence may be quenched by the binding of an inhibitor at the center of the junction, as seen for the peptides (Kepple *et al.* 2008).

Earlier, we found that the position of the 2-AP reporter around the HJ branch point influenced the strength of the fluorescence signal (Kepple *et al.* 2008). Therefore, we measured binding to a HJ substituted with 2-AP at a single position that consistently gave a strong signal (position 4AP2, Figure A - 1). We performed three independent titrations with 15 to 20 concentrations of 1609-10 ranging from 0

to 900 nM. We performed similar titrations on a junction without the 2-AP substitution to correct for the background fluorescence of dsDNA (Fcorr = 2-AP substrate – noAP substrate at all small molecule concentrations). The three independent titrations are shown in Figure 2-7, and were used to model the binding equilibrium of 1609-10 and the HJ that is described below.

2.2.7. Model fitting of 2-AP fluorescence quenching data

We employed a mathematical modeling approach to explore the most likely mechanism of binding of the small molecule (ligand, L) to the HJ (receptor, R). We tried all possible mechanisms involving at most two L's per molecular species, and we did not distinguish between a dimerized small molecule binding as a single entity (analogous to a disulfide bridged homodimer of peptide WRWYCR) and two independent small molecules binding as discrete entities. We have no experimental evidence for small molecule dimerization, and as seen below, the energetics of dimer formation as judged by the equilibrium constant, were unfavorable. Despite this, two molecules bound to a junction will be designated as L_2 with the caveat that this designation does not imply the formation of a dimer. This gives the following list of possible species: L, L_2, R, RL, $R(L)_2$. Since equilibrium is assumed, only the species present matter, rather than the rates at which they are formed or disappear in solution. Furthermore, since L and R are known to be present, this leaves L_2, RL and $R(L)_2$ as the three species whose presence or absence is uncertain, giving the $8=2^3$ possibilities in the table below.

Table 2-3. Possible combinations of molecular species

Described in model (Table 2-4):	Species			Number
	L_2	RL	$R(L)_2$	
-	0	0	0	0 species
-	1	0	0	
A	0	1	0	1 species
B	0	0	1	
C	1	1	0	
D	1	0	1	2 species
E	0	1	1	
F	1	1	1	3 species

Of these eight models we excluded the first and the second, since neither involves binding between R and L. For each of the six cases remaining, equilibrium constants were determined by fitting predicted values to the observed values from the fluorescence experiments, described above. The fraction of HJ in a complex with 1609-10 (Fraction of Complex, or F_c) was calculated based on the following equation

$$F_{C_{observed}} = \frac{F_O - F_B}{F_O - F_S} \qquad (1)$$

where F_0 is the fluorescence of the receptor R with no ligand present; F_B is the fluorescence at a given concentration of ligand *[L_{tot}]* added; and F_S is the fluorescence at the experimentally determined point of saturation. We used a similar approach to model binding of WRWYCR to a HJ (Kepple *et al.* 2008) and in this case the fluorescence at saturation decreased to an asymptotic value. However, for

the binding of 1609-10 to the HJ the point of saturation was difficult to determine as the small molecules have some amount of intrinsic fluorescence at high concentrations (See Figure A - 13 for example of uncorrected titration). We attempted to adjust the saturation values to optimize the goodness of fit between predicted and experimental curves; however, in all cases the saturation values converged to zero, making this route untenable. Therefore the saturation values of F_S were taken as the minimum in the fluorescence quenching signal. The best of the six models was the consequent binding of two ligands to the receptor (Model E below). We illustrate our method of solution for these models with this best case. The equilibrium reactions are

$$R + L \overset{K_{eq1}}{\longleftrightarrow} RL$$
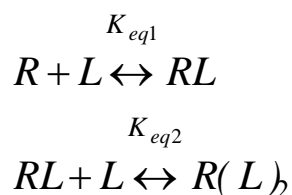
$$RL + L \overset{K_{eq2}}{\longleftrightarrow} R(L)_2$$

These give the two equilibrium conditions

$$\frac{RL}{R \cdot L} = K_{eq1} \qquad (2)$$

$$\frac{R(L)_2}{RL \cdot L} = K_{eq2} \qquad (3)$$

Two additional equations can be written based on the total amount of ligand and receptor in solution

$$[Lig_{total}] = L + RL + 2 \cdot R(L)_2 \qquad (4)$$

$$[R_{total}] = R + RL + R(L)_2 \qquad (5)$$

Using the experimental values of $[Lig_{total}]$, as well as $[R_{total}]$ = 100 nM and the assumed values of the two equilibrium constants, these four equations can be solved for the four unknowns: R, L, RL, and $R(L)_2$. The solution was arrived at by successive elimination of the first three variables, leaving the equation

$$[Lig_{total}] = L + \frac{0.1 \cdot K_{eq1} \cdot L}{1 + K_{eq1} \cdot L + K_{eq2} \cdot K_{eq1} \cdot L^2} + \frac{0.2 \cdot K_{eq2} \cdot K_{eq1} L^2}{1 + K_{eq1} \cdot L + K_{eq2} \cdot K_{eq1} \cdot L^2} \qquad (6)$$

which needs to be solved for L. To accomplish this we used a numerical method, as equation (6) cannot be solved in closed form without the use of the quartic formula. The predicted fraction of complex formed can then be calculated based on the concentrations using

$$F_c = \frac{RL + R(L)_2}{[R_{total}]} \qquad (7)$$

which assumes one ligand attached to the receptor is already sufficient to quench the signal. The alternative hypothesis that two ligands are required, leads to

$$F_c = \frac{R(L)_2}{[R_{total}]}. \qquad (8)$$

Equation 8 gave poorer fits to the data so all of the discussion below is based on equation 7. Predicted and observed values of F_c were compared, and the goodness of fit, as measured by the sum-squared error (SSE), was minimized using the "fminsearch" function in Matlab 11b to find the best values of the equilibrium constants. To correct for the differing number of adjustable parameters in the different models, the model selection was based on the corrected SSE known as the Akaike information criterion (AIC) (Akaike 1980). The best-fit model is identified as the one with the lowest SSE and the lowest AIC values.

The procedure described above was followed for all six of the models and the results are summarized in Table 2-4 and Figure 2-7. Each panel in Figure 2-7 shows the same three titrations (open symbols) and the best-fit curve for each model (solid red line). Table 2-4 shows the model equations and the best-fit equilibrium constants along with the SSE and AIC values for the models. While Model E was equivalent with Model F based only on the SSE values, the AIC selects Model E since it achieves its fit with fewer adjustable parameters. As mentioned previously, for models C, D, and F in which the possibility of initial formation of a ligand dimer was considered, the equilibrium constants for dimer formation were all very low. Finally, to explore the sensitivity of the estimated parameter values, we tried refitting the data while leaving off the last two datapoints before saturation for each of the titrations. The fit improved slightly, with Model E still outperforming the others while changing the equilibrium constants by a factor of two (not shown).

Table 2-4. Model equations showing best-fit values of the equilibrium constants along with SSE and the values of the AIC.

Model A	Model B
$K_{eq1}=8.2e{-}3$ $R+L \quad \leftrightarrow \quad RL$ SSE = 0.55 AIC = -29	$K_{eq1}=5.1e{-}5$ $R+2L \quad \leftrightarrow \quad R(L)_2$ SSE = 0.26 AIC = -70
Model C	**Model D**
$K_{eq1}=8.2e{-}3$ $R+L \quad \leftrightarrow \quad RL$ $K_{eq2}=2.5e{-}12$ $L+L \quad \leftrightarrow \quad L_2$ SSE = 0.55 AIC = -27	$K_{eq1}=5.2e6$ $R+L_2 \quad \leftrightarrow \quad R(L)_2$ $K_{eq2}=1.4e{-}1$ $L+L \quad \leftrightarrow \quad L_2$ SSE = 0.26 AIC = -68
Model E	**Model F**
$K_{eq1}=2.0e{-}3$ $R+L \quad \leftrightarrow \quad RL$ $K_{eq2}=2.6e{-}2$ $RL+L \quad \leftrightarrow \quad R(L)_2$ SSE = 0.23 AIC = -74	$K_{eq1}=2.0e{-}3$ $R+L \quad \leftrightarrow \quad RL$ $K_{eq2}=2.6e{-}2$ $RL+L \quad \leftrightarrow \quad R(L)_2$ $K_{eq3}=5.9e{-}101$ $L+L \quad \leftrightarrow \quad L_2$ SSE = 0.23 AIC = -72
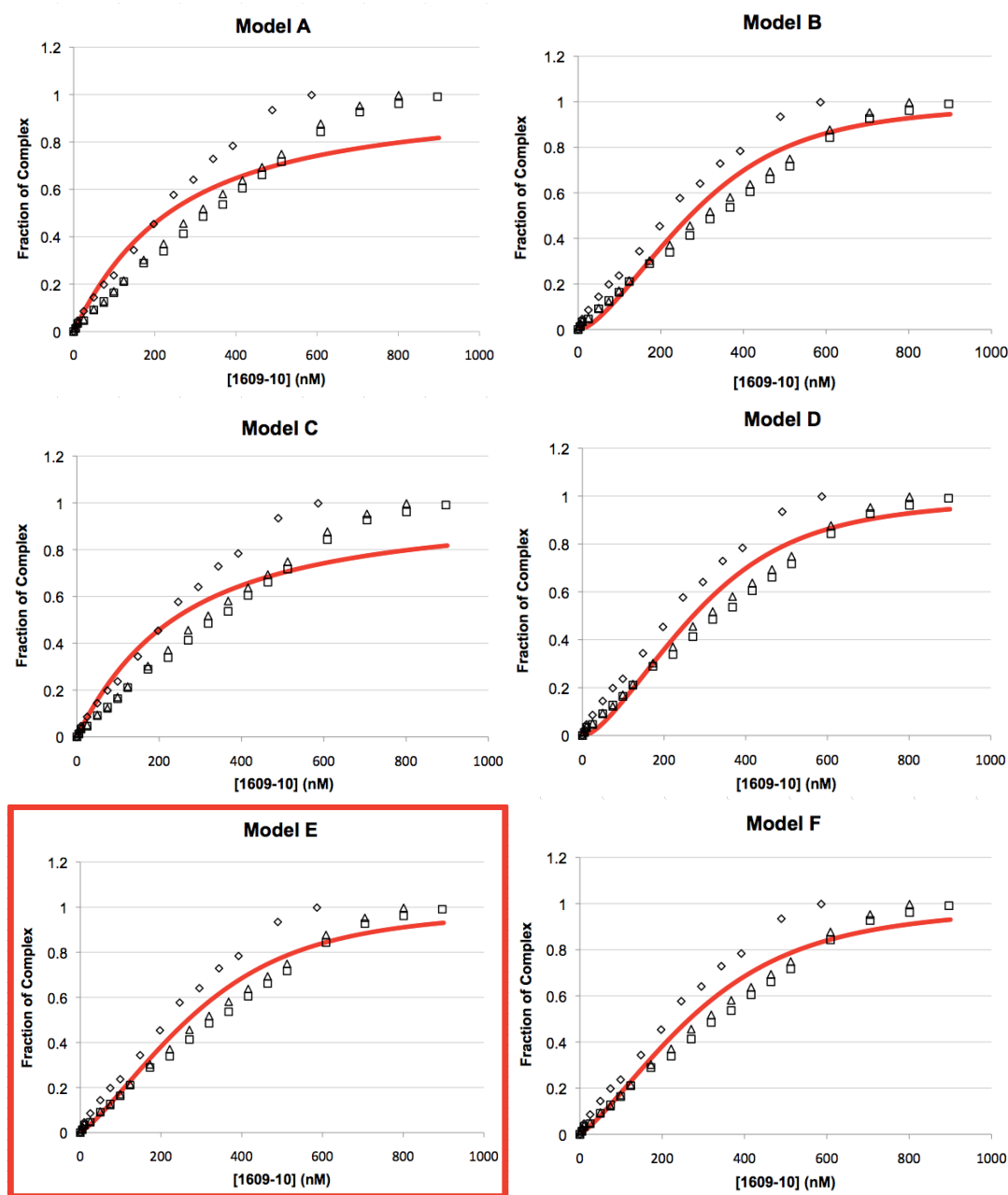
Figure 2-7.Comparison of experimental and predicted binding curves

Experimental binding curves from the three independent titrations of 1609-10 on the 2-AP HJ (HJ4AP2 (open symbols) are plotted as the fraction of receptor (HJ) complexed vs. [1609-10]. Note that these same three titrations appear in each model (A through F). The predicted binding curves based each model are shown as solid red lines. Based on the lowest SSE between the experimental and predicted curves, in addition to the lowest AIC value (Table 2-4), model E was selected as the best representative of binding. Model E is the subsequent binding of 2 molecules of 1609-10 to the HJ.

The modeling predicted that the dominant form of the HJ complex in solution contains at least two ligands and even at low concentrations of 1609-10 there is not much RL present. The apparent binding constant (K_d, defined as the [1609-10] which supports conversion of 50% substrate into a HJ-small molecule complex) is approximately 250 nM (Table 2-2). This binding constant is in good agreement with that derived from the gel-based EMSA shown in Figure 2-6C (K_d of ~300 nM (Table 2-2)). Together these data indicate that 1609-10 has significantly lower affinity for the HJ compared to peptides WRWYCR or KWWCRW; however, it has almost 50-fold greater affinity for the HJ than the previously identified small molecule, 1530-1.

Comparison of binding stability between 1609-10 and WRWYCR

Homodimers of WRWYCR and KWWCRW are predicted to carry a +4 charge at the pH of our binding assays, and are significantly more basic than the four 1609 compounds. This difference in charge may affect both the affinity of the compounds for the HJ and the stability of their interactions with the HJs. We chose to address this possibility in an assay where we could compare the stability of the compounds bound to an "open-square" HJ that was free from the influence of arm stacking isomerizations that dominate the protein-free HJs. To accomplish this, we assembled purified protein-free lambda excision HJs first with either WRWYCR or 1609-10, and then added Int, IHF and Xis which hold the junction in the "open-square" conformation. These reactions were incubated for 30 minutes to reach equilibrium, and then diluted 20-fold with recombination buffer containing 2 mg nonspecific DNA and a 28-fold molar excess of unlabeled HJ. If the inhibitor bound stably to the excision HJ substrate, like WRWYCR, this interaction should resist

dilution; however, if the interaction is weak and short-lived, the inhibitor should dissociate from the radioactively end-labeled junctions, rebinding most likely to the unlabeled junctions and allowing the stably bound recombination proteins to resolve the labeled HJ to products. Figure 2-8A is representative of several experiments testing different concentrations of 1609-10 or WRWYCR. For each experiment, undiluted reactions and reactions assembled in the final dilute volume provided an indication of the level of inhibition at a given volume and concentration of inhibitor. As seen from the 10 ml reaction controls, inhibitors are present in high enough concentrations to be effective during the initial 30 min incubation (compared to untreated with each inhibitor treatment). The 200 µl reactions show little HJ resolution, indicating that the recombination proteins are not present at high enough concentrations to perform efficient catalysis; therefore, the resolution seen in the 10→200 treatments is due to stably bound Int, Xis, and IHF. Regardless of the concentrations of inhibitors used, reactions treated with WRWYCR consistently showed 3-5 fold less HJ resolution (measured as% HJ resolution/min using a linear trendline) than reactions treated with 1609-10 (Figure 2-8B). This indicated that 1609-10 binds to HJs less stably than peptide WRWYCR.
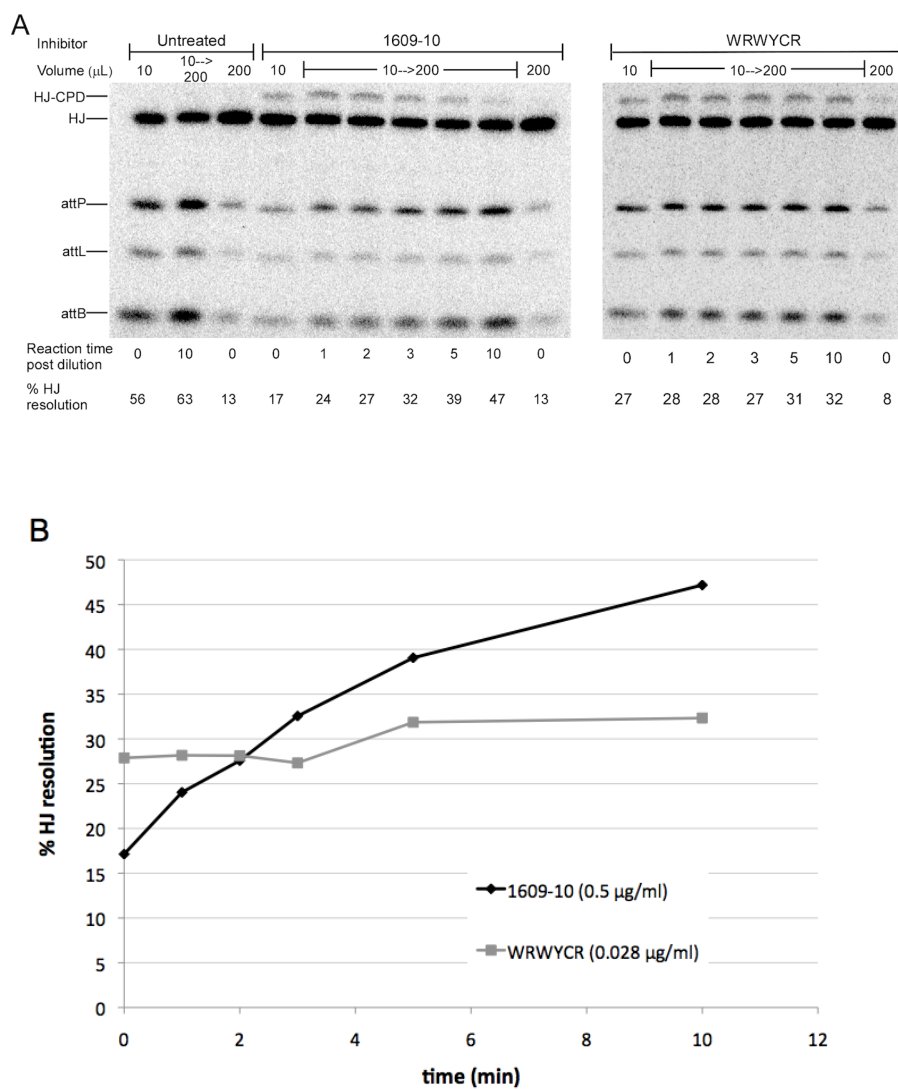
Figure 2-8. HJ resolution assay to address binding stability

(A) Excision HJs (20 pM) were incubated with recombination proteins in the presence or absence of inhibitors for 30 minutes. After initial incubation, reactions were either stopped with SDS (controls), or diluted 20-fold with 2 mg nonspecific DNA, and a 28-fold molar excess of unlabeled HJ over each inhibitor (shown as 10→200). Reactions were stopped at various time points, as shown, and loaded on SDS-Tris-Tricine gels to separate the HJ from the recombinant products (*attP, attL,* and *attB*). HJ-CPD refers to a sub-population of HJs with an Int molecule covalently bound to the DNA. (B) Graph of the% HJ resolution/min, beginning after dilution of the initial reaction.

2.2.8. Inhibition of bacterial growth

The ability of the four selected compounds to inhibit the growth of several bacteria was assayed using the standard broth microdilution MIC assay method (Ferraro 2000). The Gram-negative bacteria used were *E. coli* K12, *Salmonella enterica* serovar Typhimurium (STm), and a hyperpermeable STm *galE rfa* mutant with short LPS chains; the Gram-positive bacteria used were *B. subtilis* and methicillin-resistant *S. aureus* (MRSA). As seen in Table 2-5, the four selected compounds have a wide range of MIC values against the various bacteria tested, but were generally more potent against Gram-positive bacteria than against Gram-negative bacteria. This is probably due to the outer membrane LPS on Gram-negative bacteria, as indicated by the 2-16 fold greater sensitivity of the STm *galE rfa* mutant to the small molecules compared to STm LT2. It was notable that, unlike the previously identified small molecule 1530-1, selected 1609 compounds are also effective against the wild type LT2 strain. Moreover, the most potent of the 1609 compounds had lower MICs than the peptides against all of the bacteria tested.

2.2.9. Eukaryotic cell toxicity

Three compounds were tested for their effect on viability and metabolic activity of eukaryotic cells using an MTT assay. This assay relies on the activity of reductases in healthy mitochondria to convert MTT to a purple formazan, which can be measured spectroscopically (Mosmann 1983). As seen in Figure 2-9, the 1609 compounds do inhibit eukaryotic cells at 64 μg/mL by about 65%, but not at 16 μg/mL or lower.

Table 2-5. Minimal inhibitory concentrations (μg/mL) for selected compounds.[a]

Compound	Bacterial Strains				
	E. coli MG1655	*S. enterica* LT2	*S. enterica gal rfa*	*B. subtilis*	MRSA
1530-1	>100	>100	>100[b]	>100	>100
1609-1	8-16	16	2-8	2	2
1609-3	8-16	16-32	2-4	2	2
1609-10	16	16-32	2-4	2-4	2
1609-12	32-64	32-64	2-4	2	2
wrwycr	32-64	32-64	16-64	8-16	16
erythromycin	32-64	32-64	2-4	1	32-128

[a]Each MIC value is the average of at least 3 independent experiments; in this table (in contrast to Table 1) the MIC values were calculated using the MW of monomer wrwycr.
[b]At 100 μg/mL, the final OD_{600} of the *S. enterica* AMES strain was reduced by 50% compared to the wild-type *S. enterica* LT2 after 22 hours of incubation at 37°C.
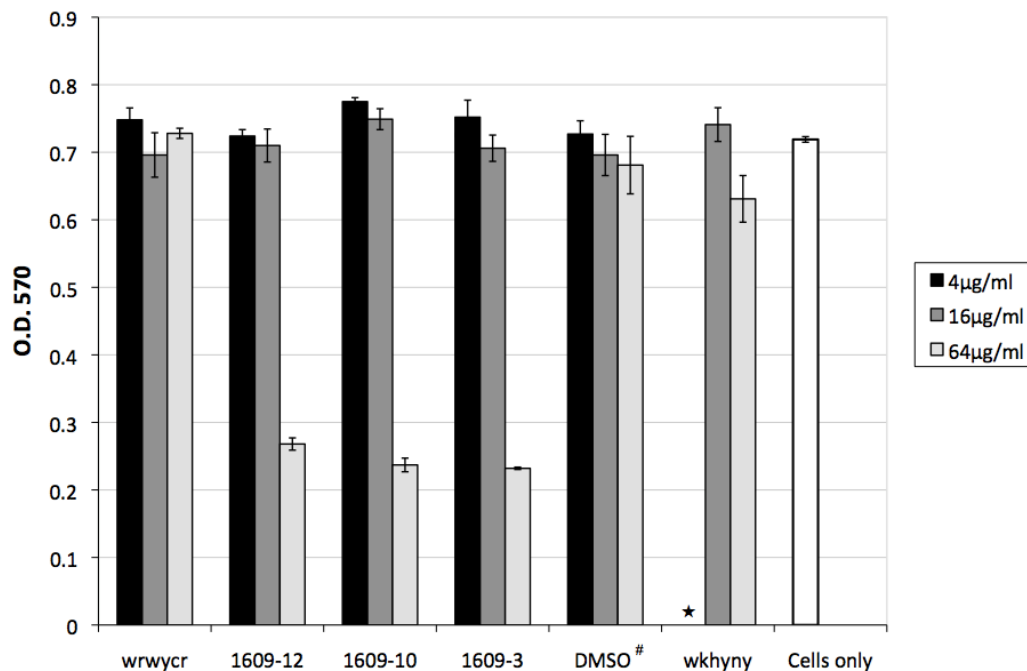
Figure 2-9. MTT reduction assay.

The effects of 1609-12, 1609-10 and 1609-3 were assayed for toxicity to BSC40 eukaryotic fibroblasts. Peptides wrwycr and wkhyny were also assayed, for comparison. Cells were grown in 96-well plates and treated with peptides or small molecules at the indicated concentrations for 24 hours. Following treatment, the cells were allowed up to 3h to convert MTT to formazan, as measured by the optical density at 570 nm; higher OD values reflect higher viability and metabolic activity. The average OD_{570} is shown from 3 independent experiments. ★ - 4µg/mL of wkhyny was not tested. DMSO[#] - The same DMSO solvent concentrations were used in these control reactions as were present in reactions treated with wrwycr. MTT assays were performed by Claudia Valejo.

Section 2.3. Discussion

The goal of this study was to identify small molecule surrogates of peptide inhibitors that bind to Holliday junction (HJ) intermediates of site-specific recombination (SSR) (Boldt *et al.* 2004), inhibit DNA repair proteins, and have antibacterial properties. The small molecule libraries we screened (Figure A - 2) were specifically chosen to have some measure of 2-fold symmetry about the scaffold, in an effort to mimic the active dimer form of the most potent hexapeptides (as example see WRWYCR, Figure 2-1B). Support for this reasoning comes from structure-activity relationship (SAR) studies of WRWYCR using alanine scan mutagenesis, which showed that some symmetry within the active peptide is important for interactions with HJs and for antimicrobial activity ((Kepple *et al.* 2005; Kepple *et al.* 2008), A. Flores-Fujimoto, and A. M. Segall, unpublished data). In fact, dimerization of WRWYCR is necessary for inhibition of recombinases and HJ-processing enzymes (Boldt *et al.* 2004; Kepple *et al.* 2005), as well as for bacterial growth inhibition (Gunderson *et al.* 2006). Further support comes from the crystal structure of a complex between Cre recombinase and the HJ intermediate trapped by peptide WKHYNY (Figure 2-1C), which strongly suggests that two monomer peptides per complex are necessary for binding and inhibition of enzyme activity (Ghosh *et al.* 2005). We presume that the need for symmetry stems from the fact that these inhibitors bind to a target with a pseudo two-fold axis of symmetry (McKinney *et al.* 2003), and thus we searched for small molecule scaffolds that could accommodate this characteristic.

The positional scanning data used to identify all inhibitors (Cassell *et al.* 2000; Klemm *et al.* 2000; Boldt *et al.* 2004; Fujimoto *et al.* 2006; Ranjit *et al.* 2010) showed that there are common functionalities that correlate well with efficacy, both *in vivo* and *in vitro*: specifically, the most potent molecules are those with aromatic functionalities, basic functionalities, and groups capable of forming hydrogen bonds. *In silico* molecular modeling, corroborated by fluorescence quenching studies, suggests that the aromatic functionalities on peptide WRWYCR are necessary for interactions with HJs and are likely to establish orthogonal and/or planar π-π interactions with solvent-accessible bases at the center of the HJ ((Kepple *et al.* 2008), R. Saha and A. M. Segall, unpublished data). The aromatic functionalities 2-naphthylmethyl and 4-hydroxybenzyl, identified as necessary for effective inhibition of SSR in the 1609 set of small molecules, are also likely to establish base stacking interactions with the HJ DNA. Aromatic functionalities are present at all three diversity positions in the most potent mixtures, suggesting that the nature of the functional group rather than its specific placement on the scaffold is the dominant aspect affecting compound activity. Further, this suggests that given an appropriately flexible scaffold, the functionalities may be able to adopt several effective conformations. Along these lines, macrocyclic peptide analogs that were specifically designed to be less flexible are only moderately effective at binding HJs and were ineffective at inhibiting bacterial growth (Bolla *et al.* 2003; Pan *et al.* 2006) despite having aromatic functionalities of a similar nature as linear peptides or the 1609 compounds. Aromatic functional groups also ranked high at position R^4 in terms of inhibition of SSR. We used this position to test whether shape and/or hydrophobicity of the functionality would more highly impact interactions with HJs by

incorporating the large hydrophobic but aliphatic functionality 2-adamantan-1-yl-ethyl derived from 1-adamantaneacetic acid (Figure A - 3). However, compounds containing this functionality performed poorly in most of our assays despite a high ranking in the positional scanning (Figure A - 7). This could be viewed as further support for the importance of aromatic functionalities in the inhibitors. Alternatively, this functionality may be potent only in combination with R-group functionalities that were present in the mixtures but were not selected for individual compound synthesis.

Positional scanning identified basic functionalities in all of the peptides and the 1530 set of small molecules (Ranjit *et al.* 2010). These groups are likely to be protonated at the pH of our *in vitro* reactions as well as inside cells, which may facilitate inhibitor binding to negatively charged DNA. These basic functionalities, usually derived from lysine, arginine, or following methylation and reduction of glutamine (1530-1, position R^1), were not present in small molecule library TPI1346, in order to avoid complications with the cyclization step used to generate the bis-cyclic guanidine groups. The SAR studies of peptide WRWYCR suggested that the arginine residues, particularly the one at the 6th position, are very important for SSR inhibition and protein-free HJ binding (A. Flores-Fujimoto, R. Saha, and A. Segall, unpublished data). While it is possible that the guanidine groups on the scaffold may be protonated, their charges may not be close enough to the DNA to make efficient ionic interactions. Thus, the decrease in the number of flexible, basic functionalities between WRWYCR and 1609-10 may have caused, at least in part, the observed decrease in the affinity and stability of binding interactions with HJ DNA.

Finally, the positional scanning data suggested that functional groups capable of forming strong hydrogen bonds contribute to the potency of these inhibitors with regard to inhibition of SSR and the other *in vitro* activities of these small molecules. Modeling of WRWYCR suggested that hydrogen bond interactions, especially those along the amide backbone, probably contribute to the stabilizing interactions between the peptide inhibitors and the HJ substrate (Kepple *et al.* 2008). While it is difficult to predict where hydrogen bonds will form, 1530-1 has far fewer electrophilic atoms capable of forming hydrogen bonds than the peptides, and the 1609 set of small molecules has only the phenolic groups of 4-hydroxybenzyl at positions R^2 and R^3. This functionality, derived from tyrosine, has performed well in all our screens and was also a determining factor in the activity seen with the macrocyclic peptide inhibitors (Pan *et al.* 2006). Thus, the absence of strong hydrogen bonding potential probably contributes to the decrease in stability/affinity of the 1609 compounds with HJ substrates and may also contribute to the increase in IC_{50} for SSR with respect to the peptides wrwycr and kwwcrw. While this increase is unfavorable, fewer hydrogen bond donor/acceptors are generally considered better in terms of therapeutic potential (Lipinski 2000; Lipinski *et al.* 2001) and the 1609 set of small molecules has far fewer of these electrophilic species than the peptides.

Our studies showed that binding to protein-free HJs is not necessarily indicative of inhibitory activity in our enzyme assays involving HJs. For instance, 1609-10 has nearly 50-fold greater affinity for protein-free HJs than 1530-1 (K_d = 0.25-0.3 μM versus 11.8 μM, respectively; Table 2-2); yet both inhibitors are equally potent at inhibiting RecG-mediated HJ unwinding and are within 10-fold of potency

compared with the active peptides. RecG interacts with HJ as a monomer, and has low processivity (Whitby *et al.* 1998; Slocum *et al.* 2007), factors which probably make it prone to being easily inhibited. In contrast, the compounds we have identified to date have a wide, 500-fold range of potencies at inhibiting excisive recombination, indicating that this reaction provides better discrimination of inhibitor efficacy. We note that, while 1530-1 inhibits excision reactions 5-fold more poorly compared to 1609-10, the former compound was identified using bent-L recombination assays and is about 5-fold more potent in those reactions than in excision reactions (Ranjit 2004). Differences in the architecture of the HJ intermediates in those recombination reactions may account for the different potencies seen (discussed in (Azaro, 2002)).

We used the 2-AP fluorescence quenching data to test several possible models of 1609-10 binding to a HJ. The best curve fit came from a linked-equilibria model where 1609-10 binds to a HJ first as monomer, but allows enough space for a 2nd molecule to bind consequently (Figure 2-7). Several of the models tested the possibility of a dimer of 1609-10 forming in solution, but in every case the equilibrium constant for dimer formation was so low that we deem this scenario unlikely. Furthermore, we have no evidence of dimer formation from HPLC analysis of 1609-10 solutions. Therefore the equilibrium state of this complex may be similar to that suggested by the crystal structure of the less-active monomeric peptide inhibitor WKHYNY bound to a HJ, where two molecules bind in discrete corners of the junction but are not physically connected to each other (Ghosh *et al.* 2005). We also tested models that predicted one molecule of 1609-10 binding and forming a saturated complex, but these also did not fit the data well, further supporting the

hypothesis that at least two molecules bind the HJ. These results imply that we may have isolated a more active surrogate of the monomer peptide that still does not make sufficient contacts to the HJ substrate to provide the affinity or the stable interactions characteristic of the dimerized peptide WRWYCR. With this in mind, we will include a sulfhydryl functionality in future small molecules to facilitate their dimerization, and test whether their potency increases concomitantly. A caveat is that our modeling analysis does not exclude the possibility that more than two molecules bind to the HJ either at the center or on the arms, in a non-specific manner. In fact, the 1609 set of compounds appear to be less specific for HJs than other inhibitors that we have identified to date. This is evident from their inhibition of DNA restriction enzymes (whose structure, mechanism of catalysis, and interaction with DNA differ fundamentally from those of the tyrosine recombinases) and further supported by band shifts of linear double stranded DNA conducted on the crude compounds where, at 10 µg/mL, the small molecules caused non-specific shifts of the DNA into the wells of the gel (Boldt 2006). Furthermore, our modeling studies also do not exclude the possibility of non-equivalent binding sites for these molecules, a scenario that seems likely since the DNA sequence is not identical on all corners of the junction center. Atomic level structural data will resolve these questions, and X-ray crystallography studies are in progress.

The 1609 compounds inhibited bacterial growth, particularly in the case of Gram-positive strains with MICs in the 2-4 mg/mL range, and surpassed the potency of the peptides even in Gram-negative bacteria. Experiments with a *Salmonella* hyperpermeable mutant indicated that the compounds have greater difficulty passing through the outer membrane of Gram-negative bacteria. The greater

antimicrobial activity of these compounds was surprising given that these compounds were less potent inhibitors of recombination. While the 1609 compounds clearly interact with HJs and interfere with HJ processing enzymes, it is possible either that they enter bacterial cells more readily than the peptides, and/or that they have additional targets *in vivo.* Further characterization of the effects of the bis-cyclic guanidine inhibitors on microbial physiology suggests that they induce envelope stress in bacteria, in addition to potentially interfering with DNA repair (S. Yitzhaki, J. Rostron, M. Rideout, R. N. Authement, S. Barlow, and A. Segall, data not shown). The 1609 compounds described are very hydrophobic, and we have obtained evidence that their toxicity may be due at least in part to some membrane perturbations. On-going compound syntheses aimed at optimizing the charged functionalities by including more polar groups may help alleviate this phenotype. Results from hemolysis studies showed that the presence of R-4-hydroxybenzyl at position R^3 is correlated with lower hemolysis (J. L. Boldt, I. Naili, and A. M. Segall, data not shown), whereas compounds containing either the R or S isomers of 2-naphthylmethyl at position R^3 were more hemolytic. This trend was not seen at position R^2 when 4-hydroxybenzyl was compared with 2-naphthylmethyl.

In summary, we have now identified a second class of small molecules with the ability to block SSR and HJ-processing enzymes *in vitro*; this set of molecules has much greater antimicrobial activity than 1530-1. While these compounds have good affinity toward HJs, they bind less stably to HJs than do the previously identified peptide inhibitors. These compounds are the most potent inhibitors of bacterial growth that we have isolated to date using the HJ-trapping assay, perhaps due to greater permeability. Our data suggest that modifications such as adding

symmetry and/or aromatic functionalities to the 1530 series of compounds might dramatically improve their efficacy. Conversely, adding basic functionalities to the 1609 compounds may increase the stability of HJ binding and perhaps decrease their toxicity. This new class of compounds may be a useful new addition to the current arsenal of antibiotics or disinfectants, particularly in an age of rising drug resistance.

Chapter 3. wrwyrggrywrw, a single-chain analog of peptide wrwycr, binds Holliday junctions, inhibits bacterial DNA repair enzymes, and has antibacterial activity

Section 3.1. Introduction

Holliday junctions (HJ) are 4-way branched DNA intermediates that form *in vivo* from the union of two duplex strands of DNA. These junctions arise as a result of two distinct recombination reactions: homologous (HR) or site-specific (SSR) recombination. HJs formed by HR are dependent on the RecA protein and are absolutely required for the nonmutagenic repair of double-stranded DNA breaks (Heitman *et al.* 1999; Meddows *et al.* 2004). Additionally, RecA-dependent HJs are intermediates in repair pathways that process single stranded gaps (Michel *et al.* 2007) and collapsed replication forks (McGlynn *et al.* 2002; Michel *et al.* 2007). HJ are also formed in SSR reactions that are catalyzed by tyrosine recombinases (Azaro 2002), and are important for the segregation of replicated chromosomes dimers (McGlynn *et al.* 2002) and the generation of antigenic variation associated with virulence caused by pillins and fimbria (reviewed in (Johnson 2002)). The HJs formed during both types of recombination reactions must be resolved in order to complete the biochemical process, and also to maintain genome integrity. This resolution is accomplished either by the site-specific recombinases themselves (reviewed in (Grindley *et al.* 2006)), or by structure selective nucleases in the case of HR (Declais *et al.* 2008). We have previously identified hexapeptide inhibitors, screened from combinatorial libraries, that are inhibitors of *in vitro* HJ resolution catalyzed by a variety of bacterial tyrosine recombinases (e.g. λ-Integrase (Cassell *et al.* 2000; Boldt *et al.* 2004), Cre (Ghosh *et al.* 2005), and XerC/D (Gunderson *et*

al. 2006)). *In vitro*, the peptides have been shown to bind stably and specifically to synthetic protein-free HJs, as well as other branched DNAs such as replication fork mimics (Kepple *et al.* 2005). It is through these interactions that they are able to inhibit the activity of DNA repair enzymes such as RuvABC resolvase and RecG helicase which act upon these branched DNA substrates (Kepple *et al.* 2005; Kepple *et al.* 2008). The peptides are potent antibacterial agents, trap HJs formed *in vivo* (Gunderson *et al.* 2009; Marcusson D., Medina-Cleghorn D., and Segall A., unpublished results), and their activity is consistent with a model where DNA repair is one of the targets of these compounds (Gunderson *et al.* 2006; Marcusson D., Medina-Cleghorn D., and Segall A., unpublished results). The most potent peptides identified to date, such as WRWYCR or KWWCRW, include cysteine residues, and the formation of a disulfide-bridged homodimer between two hexapeptides is a critical component for activity *in vitro* and *in vivo*. We hypothesized that single-chain linear analogs of WRWYCR or KWWCRW would retain characteristics of the homodimer while eliminating the need for dimer formation and stable maintenance of the disulfide bridge, in spite of the reducing environment of the bacterial cytoplasm (Stewart *et al.* 1998; Zheng *et al.* 1998). Here we describe the activity of peptide WRWYRGGRYWRW and its D-stereoisomer, wrwyrggrywrw (by convention, D-amino acid peptides are written in lower case), and show that they trap HJs formed in SSR (Rajeev *et al.* 2007), bind to protein-free HJ DNA and inhibit HJ resolution by RecG helicase and the RuvABC resolvasome *in vitro*. Treatment of bacteria with wrwyrggrywrw inhibits their growth and causes DNA damage. Peptide wrwyrggrywrw is particularly potent against Gram-positive bacteria, such as

methicillin resistant *Staphylococcus aureus* (MRSA), with potency equivalent or better than wrwycr.

Section 3.2. Results

3.2.1. Inhibition of site-specific recombination

The activity of WRWYCR is dependent upon the formation of a disulfide bridged homodimer (Boldt *et al.* 2004; Kepple *et al.* 2005; Gunderson *et al.* 2006). We hypothesized that single-chain linear analogs of WRWYCR could be designed that would retain the same characteristics as WRWYCR, but without the need for disulfide bond formation or maintenance. To investigate this hypothesis, we designed analogs of either 10 or 12 amino acids in length and screened them for the ability to inhibit the excisive site-specific recombination (SSR) pathway mediated by λ-Integrase (see Chapter 2, Figure 2-1). Initial testing indicated that a palindromic 12 amino acid analog, WRWYRGGRYWRW, had comparable activity to the parent peptide, WRWYCR (Table A - 1). We performed more extensive titrations of WRWYCR and WRWYRGGRYWRW in excision reactions, in the presence and absence of the reducing agent dithiothreitol (DTT, Figure 3-1A). Both peptides had equivalent IC_{50} values in the reactions conducted in the absence of DTT; however, WRWYRGGRYWRW maintained its activity in the presence of DTT, in contrast to WRWYCR (Figure 3-1B and (Table 3-1). Furthermore, the peptide concentrations necessary to trap the maximum amount of HJs in this reaction (40-50%) were approximately equivalent for the two peptides in the absence of DTT. This indicates a similar mechanism of action for both peptides.
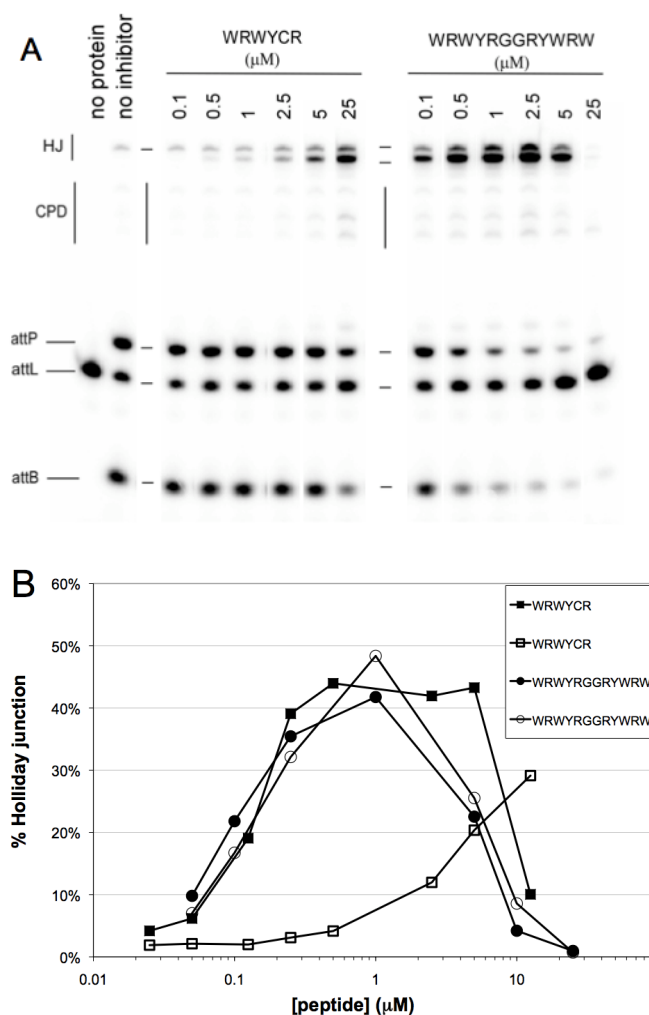
Figure 3-1. Inhibition of SSR under reduction conditions.

(A) Selected lanes from a representative Tricine-SDS gel showing the effects of peptides WRWYCR and WRWYRGGRYWRW on excisive recombination in the presence of 25 mM DTT. Recombination proteins (Int, IHF and Xis) recombine radiolabeled *attL* DNA, with an unlabeled partner site, attR, to form the recombinant products *att*P and *att*B. The HJ is the intermediate of this reaction and is stabilized by the peptides, which block progression to products or regression to substrates, albeit at different potencies in the presence of DTT. (B) Comparison of the ability of peptides WRWYCR (squares) and WRWYRGGRYWRW (circles) to accumulate HJs in excision recombination reactions in the presence (open symbols) or absence (solid symbols) of DTT. Treatment with DTT significantly reduces% accumulation of HJ intermediates by WRWYCR, but not by WRWYRGGRYWRW. High concentrations of either peptide inhibit the initial cleavage step of the reaction resulting in a decrease of HJs formed. Refer to Chapter 2, Figure 2-1A for description of SSR pathway. Excision titrations shown in Figure 3-1 were performed by Jeff Boldt.

3.2.2. Peptide-HJ interactions

We examined whether WRWYRGGRYWRW could interact with a HJ in the absence of recombination proteins by performing electrophoretic mobility shift assays (EMSA) on a radiolabeled protein-free HJ substrate (Figure 3-2). WRWYRGGRYWRW caused a change in the mobility of protein-free HJ DNA similar to shifts observed in previous experiments with WRWYCR (Kepple *et al.* 2005). This shift is likely due to a conformational change in the HJ from a faster migrating "stacked-X" to a slower migrating "open-square" conformation (reviewed in Lilley 2008). We also saw a "supershift" as well as the accumulation of DNA in the wells of the gel; however these shifts occurred at 10-fold higher concentrations than the apparent binding constant (Table 3-1). Furthermore, these shifts decreased with increasing amounts of unlabeled double-stranded competitor DNA indicating weaker, non-specific peptide/DNA interactions (Flores-Fujimoto A., and Segall A., unpublished data). In contrast, no specific shift or supershift was seen when double-stranded *attL* DNA was treated with increasing amounts of WRWYRGGRYWRW suggesting that the peptides prefer HJ DNA over linear B-form DNA (not shown). Titrations of all the single-chain linear peptides are shown in Figure A - 14.
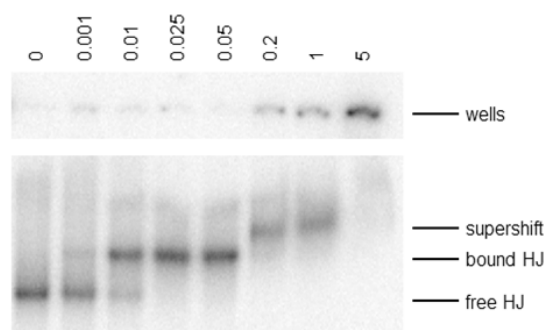
Figure 3-2. WRWYRGGRYWRW induced band shift of protein-free HJs

WRWYRGGRYWRW (concentrations in µM) causes a band shift of radioactively labeled HJ DNA. The shift seen is similar to that seen previously with WRWYCR and is likely the result of a conformational change in the HJ from a faster migrating "free HJ" species to a slower migrating "bound HJ." DNA present in the "supershift" and in the "wells" results from weaker non-specific interaction as these bands disappear with increasing concentrations of unlabeled, double-stranded linear DNA (not shown). The band shift shown was performed by America Flores-Fujimoto.

As an independent measure of peptide binding, we titrated WRWYCR and WRWYRGGRYWRW into reactions with a short HJ substrate (J1 has 8 base pair arms, see (Seeman *et al.* 1983)) that is unstable for electrophoresis in the absence of magnesium. Under these conditions, the junction can be stabilized for electrophoresis if it is treated with peptide (Figure A - 15). This indicates a specific and stable interaction with the HJ. The amount of HJ stabilized for electrophoresis in Figure A - 15 is given as a percentage of the total radioactive signal seen on the gel for each peptide treatment, shown graphically in Figure 3-3 (dashed lines). All values were normalized to a "no peptide" control. At all concentrations tested in the absence of DTT, WRWYCR stabilizes more of the HJ than WRWYRGGRYWRW. When titrations were conducted in the presence of 20 mM DTT, WRWYCR lost the ability to stabilize the junction but WRWYRGGRYWRW remained active (Figure 3-3

and Figure A - 15). Peptides WRWYAR and WKHYNY, do not bind protein-free HJs, and were also ineffective at stabilizing the HJ in this assay (Rideout, M., and Segall A, unpublished data). This assay also provides an indication of the non-specific binding activity of the peptides, relative to each other, seen as the decrease in total radioactive signal in each lane (solid lines, Figure 3-3). WRWYRGGRYWRW caused much greater loss of "total signal" than WRWYCR in a dose-dependent manner. In fact, the highest concentration of WRWYRGGRYWRW led to a loss of greater than 90% of the total DNA (compared with ~ 17% for WRWYCR). Measurements of residual radioactivity in the reaction tubes following sample loading did not account for the loss of signal (Rideout, M., and Segall A, unpublished data). The most likely scenario is that both peptides form aggregates and sequester the DNA at high concentrations, possibly even driving the aggregate toward the electrophoresis cathode; however WRWYRGGRYWRW does so to a much greater extent.
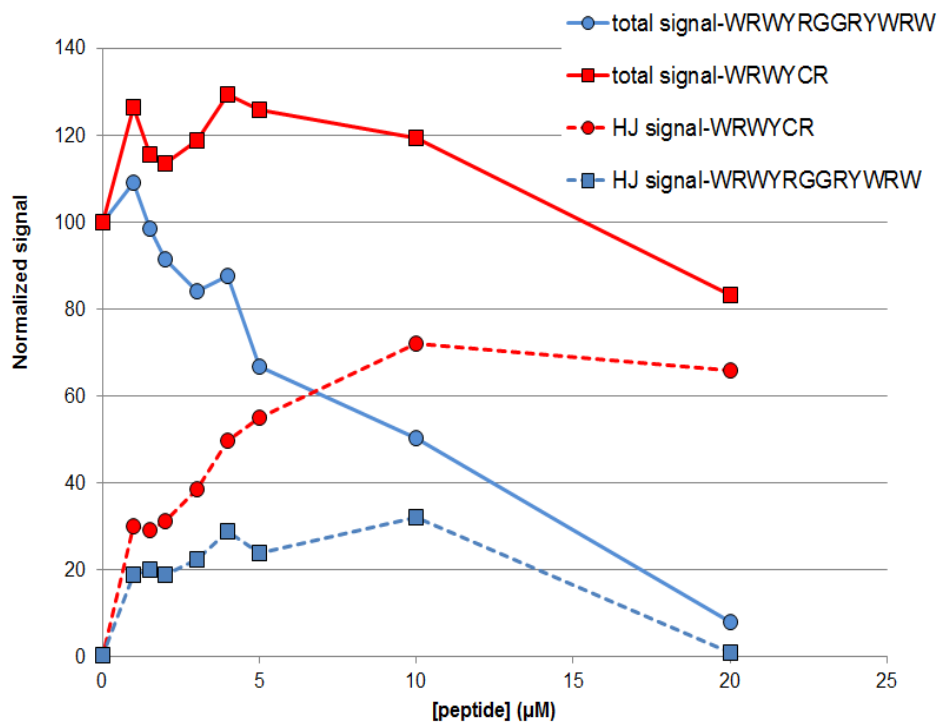
Figure 3-3. Quantification of peptide HJ stability assay.

Results from titrations of WRWYCR or WRWYRGGRYWRW into a binding assay with a short radioactive labeled HJ substrate in the absence of DTT. Junctions with 8 base pair arms are unstable for electrophoresis in the absence of magnesium, unless they are incubated with peptide (Figure A - 15). Squares, and circles indicate treatments with WRWYRGGRYWRW and WRWYCR, respectively. "HJ signal" (dashed line) indicates the amount HJ seen in each peptide treatment, and "total signal" (solid line) indicates the total amount of radioactivity detected in the gel with each peptide treatment. In both cases, the signals for each peptide treatment are normalized to the "no peptide" control. The amount of HJ that is stabilized increases with peptide treatment, in spite of the decreasing amounts of total signal, indicating that binding to the junction keeps the peptide in solution.

3.2.3. Interference with HJ-processing enzymes

Our band shifts suggest that WRWYRGGRYWRW recognizes and binds stably to protein-free HJs inducing a conformation change to the "open-square" form. We tested whether WRWYRGGRYWRW inhibits enzymes/complexes that process "open-square" HJs other than Int, namely the RecG helicase and the RuvABC resolvasome. RecG is an ATP-dependent DNA helicase and *in vivo* it binds to replication forks that have stalled or collapsed following an encounter with lesions or obstacles on the DNA template (McGlynn *et al.* 2002; Michel *et al.* 2007). RecG can *back the fork off* allowing for repair of the damaged DNA ahead of the fork. In addition, fork regression is also thought to be critical to the survival of the cell because it minimizes toxic, origin-independent replication formed at DNA repair intermediates (Rudolph *et al.* 2009; Rudolph *et al.* 2010). *In vitro*, the activity of RecG can be measured by its ability to unwind a HJ into a flayed duplex in the presence of Mg^{+2} and ATP (Whitby *et al.* 1998); we tested WRWYRGGRYWRW and wrwyrggrywrw to determine whether they could inhibit this activity (Figure 3-4). Both stereoisomers inhibit RecG unwinding by more than 70%, relative to DMSO treated controls, at 4-5 μM. Inhibition is dose-dependent, and while the D-stereoisomer was consistently more effective than the L-stereoisomer, neither was as effective as WRWYCR or wrwycr (Table 3-1, see discussion).

RecG acts as a monomer and has activity limited to branch migration of HJs and replication forks; in contrast, the RuvABC resolvasome is a multimeric complex of proteins that can both branch-migrate junctions and also resolve them by endonucleolytic cleavage. Like RecG, the RuvABC resolvasome plays a role in the

rescue of stalled replication forks. It is also important in processing HJs resulting from the repair of single strand gaps and double-strand breaks, both of which can arise as consequences of fork disruption. RuvA binds to HJs as either a tetramer or octamer, and holds the junction in the "open-square" conformation (Ariyoshi *et al.* 2000), allowing the 2 hexameric ring-helicases (RuvB) to drive branch migration (Parsons *et al.* 1992). The RuvAB subunit recruits a dimer of RuvC endonuclease which recognizes a preferred DNA sequence and cuts the junction DNA creating a pair of nicked duplex strands that can be re-ligated *in vivo* to reseal the DNA (Sharples *et al.* 1999). The cleavage activity of the RuvABC resolvasome has been reconstituted *in vitro* (Connolly *et al.* 1991), and we tested whether WRWYRGGRYWRW or wrwyrggrywrw could inhibit this process (Figure 3-5). The peptides inhibited the formation of cleavage products in a dose-dependent manner and were effective at lower concentrations than in the RecG assay (greater than 70% inhibition at 0.1 μM). It is interesting that both stereoisomers behaved similarly in this assay and both had IC_{50} values that were notably closer to the established values for WRWYCR and wrwycr in this assay (Table 3-1). This may indicate that the peptides have a different mechanism of inhibition in the RuvABC cleavage assay than in the RecG unwinding assay (see discussion).
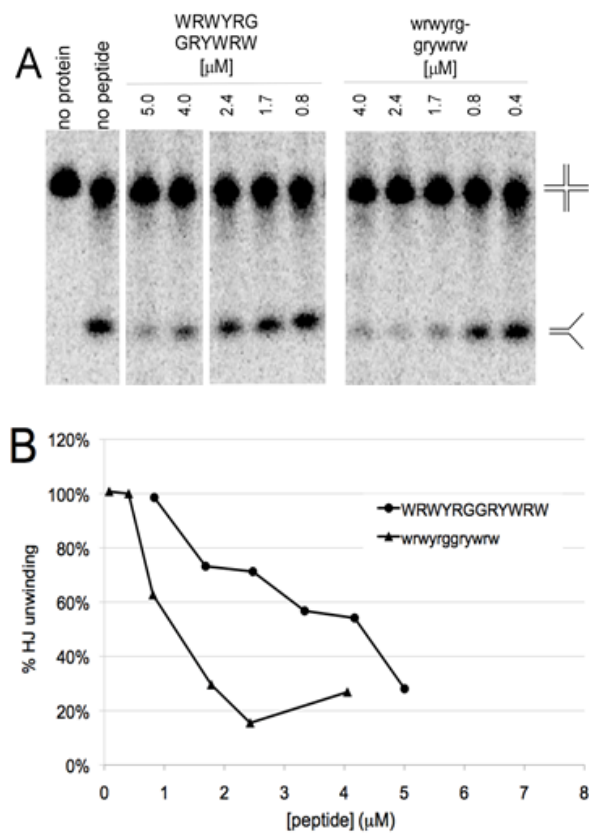
Figure 3-4. Inhibition of HJ processing by RecG helicase.

(A) RecG helicase will unwind a synthetic HJ *in vitro* in the presence of ATP and Mg^{+2} into a flayed duplex. Shown are selected lanes from denaturing polyacrylamide gels showing the dose-dependent inhibition of RecG unwinding activity due to treatment with peptides WRWYRGGRYWRW or wrwyrggrywrw. (B) Quantitation of gels in (A) normalized to a DMSO control.
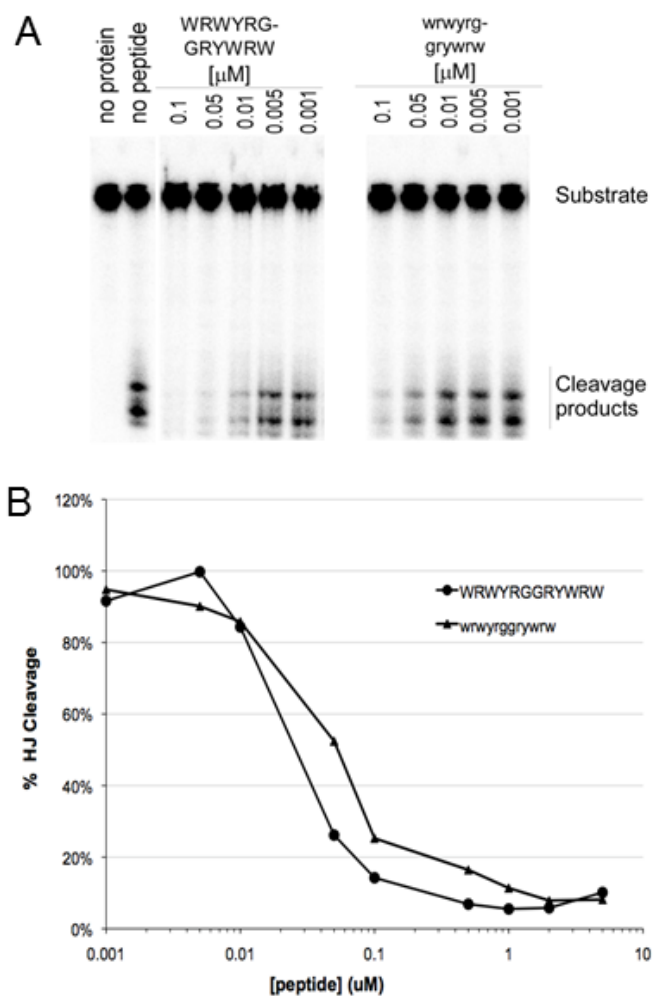
Figure 3-5. Inhibition of HJ cleavage by RuvABC.

(A) The endonuclease activity of the RuvABC resolvasome introduces cuts in synthetic HJs resulting in several double-stranded products depending upon the cleavage site. Products were separated on Tris-Tricine-SDS gels and the cleavage activity was inhibited by WRWYRGGRYWRW and wrwyrggrywrw. (B) quantitation of gels in (A) normalized to the DMSO control. The RuvABC cleavage assay shown was performed by Jeff Boldt.

Table 3-1. Summary of *in vitro* characteristics[a]

Assay	Site-specific recombination		Holliday junction interactions[b]		
	Excision (IC$_{50}$ in µM)		HJ binding (K$_d$ in µM)	HJ processing[c] (IC$_{50}$ in µM)	
Peptide	(-) DTT	(+) DTT	EMSA	RecG	RuvABC
WRWYCR[d]	0.021[e]	0.5	0.014[f]	0.12[f]	0.064[f]
WRWYRG-GRYWRW	0.025	0.055	0.025	2.53	0.045
wrwycr[d]	0.045[e]	NT	NT	0.25	0.2
wrwyrg-grywrw	NT	NT	NT	1.08	0.08

[a]All data shown are averages of 2 or more independent titrations over 8 concentrations
[b]All values reported for HJ interactions are (-) DTT
[c]Activity refers to HJ unwinding by RecG, and HJ cleavage by RuvABC
[d]Concentrations of WRWYCR and wrwycr are given in homodimer equivalents
[e,f]Published in (Boldt *et al.* 2004) and (Kepple *et al.* 2005), respectively, and shown here for comparison purposes.
The data shown in table 3-1 are contributions from Jeff Boldt and Marc Rideout

3.2.4. Antibacterial activity

The L - and D – isomers of WRWYCR are potent antibacterial compounds with minimal inhibitory concentrations (MIC) in the low µg/mL range (Gunderson *et al.* 2009). Given the similar *in vitro* characteristics of WRWYCR and WRWYRGGRYWRW (Table 3-1) we tested if the peptides had similar *in vivo* activities. While both stereoisomers of WRWYRGGRYWRW were tested, we focused on wrwyrggrywrw, since it is expected to resist degradation by proteolysis. We assayed the antibacterial activity with standard MIC determinations in microtiter plates in Mueller-Hinton broth (MHB) (Ferraro 2000), and found that wrwyrggrywrw was an effective inhibitor of bacterial growth, and like wrwycr, it had MICs in the low

µg/mL range (Table 3-2). For every bacterial strain tested, wrwyrggrywrw had equivalent or better MICs than wrwycr. In light of this, and the differences in the *in vitro* results shown in Table 3-1, wrwyrggrywrw may have additional targets *in vivo* than DNA repair or may cross the bacterial cell wall more efficiently (see Discussion). Several pathogenic clinical isolates were susceptible to peptide treatment, including a methicillin resistant *Staphylococcus aureus* (MRSA, strain ATCC 33591), in addition to the well-studied *Staphylococcus aureus* Newman strain, and a *Pseudomonas aeruginosa* small colony variant (SCV) (Haussler 2004). Both wrwyrggrywrw and wrwycr were more effective against Gram-positive bacteria than against Gram-negative bacteria and we have previously shown that lipopolysaccharide (LPS) chains in the outer membrane of Gram-negative bacteria may be a barrier to wrwycr entry into the cells (Gunderson *et al.,* 2006). To test this hypothesis for wrwyrggrywrw, we compared the MICs of a wild-type *Salmonella enterica* serovar Typhimurium LT2 (S.Tm) and a strain that carries mutations resulting in shortened LPS chains (a *galE rfa* strain, (Ames *et al.* 1973)). As seen in Table 3-2 the MIC was 2-4 fold lower in the AMES strain compared to wild-type S.Tm (LT2) strain confirming our hypothesis that the LPS of Gram-negative bacteria is a barrier to wrwyrggrywrw entry. The dodecamer peptides showed less difference in MIC between LT2 and the *galE rfa* mutant than the hexapeptides (whose concentrations are expressed in homodimer equivalents). This indicates that the LPS layer of wild-type S.Tm presents less of a barrier to the dodecamer peptides than it does to the hexamer peptides.

Table 3-2. Summary MIC (µg/mL) data for selected bacterial strains

Species	Gram-negative bacteria				Gram-positive bacteria			
	S. enterica Tm		*E. coli*	*P. aeruginosa*	*B. subtilis*	*S. aureus*		*S. pyogenes*
Strain	LT2	AMES	MG1655	small colony variant		MRSA	Newman	M49
Segall lab strain designation	G255	G455	G582	G1018	G510	G565	G748	G762
Peptide								
WRWYCR[a]	64[b]	16[b]	64[b]	NT	8[b]	32	NT	NT
WRWYRG-GRYWRW	32	16	32	NT	16	16	NT	NT
wrwycr[a]	64[b]	16[b]	32-64[b]	8	8[b]	32	128	8
wrwyrg-grywrw	8	4	16	8	4	16	32	4

[a]Concentrations of WRWYCR and wrwycr are given in homodimer equivalents.
[b]Published (Gunderson *et al.* 2006).
The data shown in Table 3-2 are contributions from Ilham Naili and Marc Rideout.

3.2.5. Analysis of *in vivo* DNA damage

Unresolved HJs in the context of a growing bacterium are expected to lead to DNA damage in the form of DNA breaks, a phenotype seen in both Gram-positive and Gram-negative bacteria treated with wrwycr (Gunderson *et al.* 2006). To investigate whether wrwyrggrywrw had similar effects, we measured DNA damage using a TUNEL assay, where exposed 3'-OH ends on single strand nicks, gaps, double-strand breaks, and regressed replication forks are labeled by terminal deoxynucleotidyl transferase (TdT) with fluorescein-conjugated dUTP (Rohwer *et al.* 2000; McGlynn *et al.* 2002). We treated MG1655 cells with wrwyrggrywrw, wrwycr for comparison, or DMSO at the highest concentration present in peptide treatments, and analyzed the results from the TUNEL assay by flow cytometery. Both wrwycr and wrwyrggrywrw caused a dose-dependent increase in TUNEL-positive cells (compared to DMSO treated cells, Figure 3-6); however, treatment at the MIC for MG1655 led to only a modest increase in TUNEL-positive cells (7.9% for wrwyrggrywrw at 8 μM, roughly equivalent to 16 μg/mL). At the highest concentration tested (32 μg/mL), wrwycr led to a higher percentage of TUNEL-positive cells compared to wrwyrggrywrw (75.6 ± 2.2% compared to 46.5 ± 4.3%, respectively). Several possibilities exist to explain these observations. First, it is likely that DNA damage takes time to accumulate and the 1.5-hour time point is not long enough to see the full consequences of the peptides at low concentrations. Second, the DNA damage that is seen may be the result of both direct effects on DNA repair and indirect effects on a secondary target. For instance, membrane stress has been indirectly linked to DNA damage (Kohanski *et. al.,* 2007, Kohanski *et. al.,* 2010). Thus, it is possible that indirect effects caused by wrwyrggrywrw that lead to DNA damage are not as severe

as those caused by wrwycr. Finally, WRWYRGGRYWRW displayed significant non-specific activity in the small HJ binding assay (Figure 3-3B) compared to WRWYCR at high concentrations (20 μM WRWYRGGRYWRW is equivalent to 36.5 μg/mL). Therefore, at high concentrations the amount of soluble wrwyrggrywrw may be lower compared with wrwycr. HPLC studies to address both the intercellular and extracellular concentrations of the peptides will be useful for addressing this issue. Additionally, a time course of DNA damage at low peptide concentrations concomitantly with a viability assay will help to determine if the former hypotheses are correct.
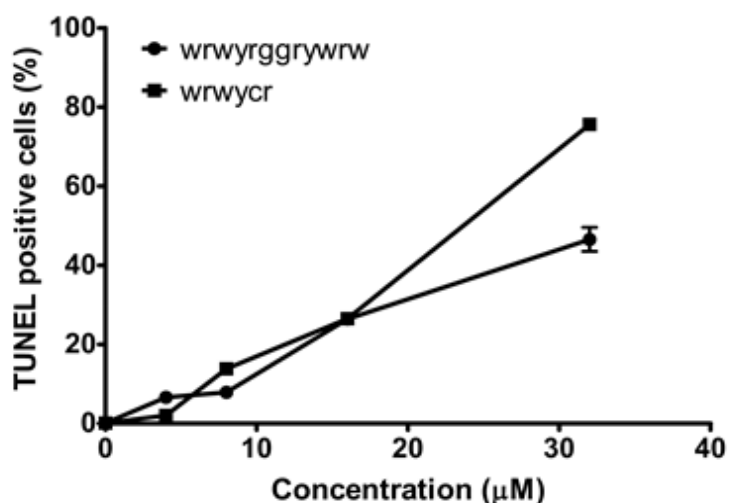
Figure 3-6. Peptide-induced DNA damage

E. coli cells were grown to an O.D. ~ 0.1 and then treated for 90 minutes with the indicated amounts of wrwyrggrywrw, wrwycr or DMSO equivalent to the highest concentration used in wrwycr treatment. Cells were then fixed, permeabilized, and treated with TUNEL reagents which conjugates fluorescein-labeled dUTP on to 3'-OH ends providing an indication of DNA damage (nicks, gaps, ds breaks, etc.) Cells were counter-stained with TOTO-3 and analyzed by flow cytometry. DMSO controls showed consistently fewer than 0.1% TUNEL-positive (not shown). The TUNEL assay shown was performed by Ilham Naili.

3.2.6. Cytotoxicity of wrwyrggrywrw in primary eukaryotic cells

As a preliminary measure of the toxicity toward eukaryotic cells we examined the hemolytic activity of wrwyrggrywrw and compared it with that of wrwycr. Red blood cells were incubated with peptides or the indicated controls for 1 hour and the supernatant of each treatment was analyzed for release of hemoglobin (Figure 3-7). For both peptides and all concentrations tested, the OD_{414} readings, reflective of the extent of hemoglobin release were lower than those observed with DMSO-treated red blood cells (OD_{414} of 0.25 ± 0.05), suggesting that the peptides themselves do not significantly affect red blood cell integrity. Although one of our treatments, 32µM wrwyrggrywrw, gave a higher absorbance reading than a water control (OD_{414} 0.23 ± 0.008 compared with 0.19 ± 0.03), none of the concentrations tested led to complete hemolysis when compared to red blood cells treated with 1% Triton-X 100. We conclude from our results that neither wrwyrggrywrw nor wrwycr are able to permeabilize red blood cells.
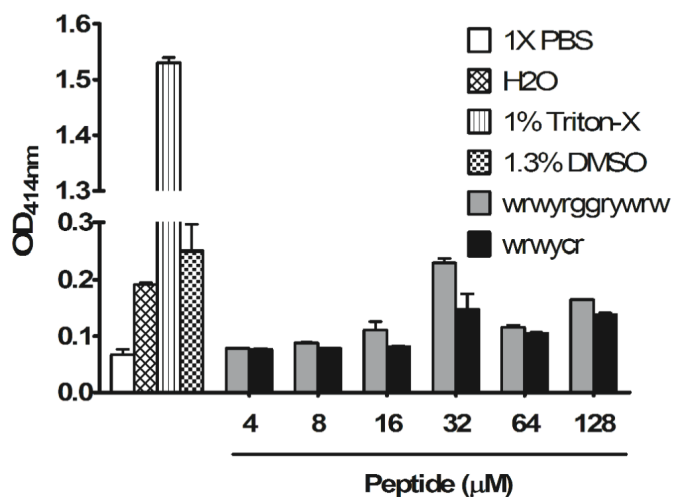
Figure 3-7. Hemolytic activity of peptides.

A solution of red blood cells (0.5% final concentration) was incubated with peptides or controls at the indicated concentrations for 1 hour at 37°C in 5% CO_2. The optical density of the supernatant was read at at OD_{414} nm to monitor the release of hemoglobin. A isotonic solution of "1X PBS" was used as a negative control provides an indication of no hemolysis. Nanopure "Water" was used as a control for osmotic hemolysis. "1% Triton X-100" was used as a control for complete hemolysis. wrwycr is given in terms of dimer equivalents. The hemolysis assay shown was performed by Ilham Naili.

To further address the toxicity toward primary eukaryotic cells, we preformed MTT assays on activated macrophages (PMs) isolated from the peritoneal cavities of BALB/c mice. This assay quantifies the conversion of 3-(4,5-dimethyl-2-thiazolyl)-2,5-diphenyl-2H-tetrazolium bromide (MTT) to a purple formazan derivative by active mitochondrial reductases (Mosmann 1983). Cells were treated with peptide or DMSO for 24 hours, and the absorbance at 575 nm was read as a measure of the metabolic activity (Figure 3-8A). We observed a dose-dependent decrease in OD_{575}, therefore in MTT reduction, with increasing amounts of peptide for either cell line. At lower peptide concentrations we saw significant variability in the results and an overall increase in the OD_{575} relative to DMSO treated cells. It is possible that the peptide stimulates metabolism and therefore MTT reduction. Alternatively, it is possible that treatment with low concentrations of peptide increases the permeability of the MTT compound and that at higher concentrations, the decrease in viability overwhelms this effect.

We also investigated whether a colorectal cancer cell line was susceptible to peptide treatment. Unlike the PMs, HCT116 cells are rapidly dividing, and should rely more heavily on DNA repair than the activated macrophages which we hypothesized might lead to greater sensitivity to peptide treatment. As with the PMs, we saw a dose-dependent decrease in OD_{575} with increasing wrwyrggrywrw treatment indicating that this peptide also affected the metabolism of HCT116 cells. Despite treating 4 times fewer HCT 116 cells than PMs, high concentrations of peptide were more effective at inhibiting MTT reduction in PMs than in HCT 116 cells (compare the highest peptide treatment in each cell line with the DMSO controls). It is possible that HCT cells do not take up the peptide as efficiently as PMs, which may sample more of their environment than the colon-derived cells (discussion).
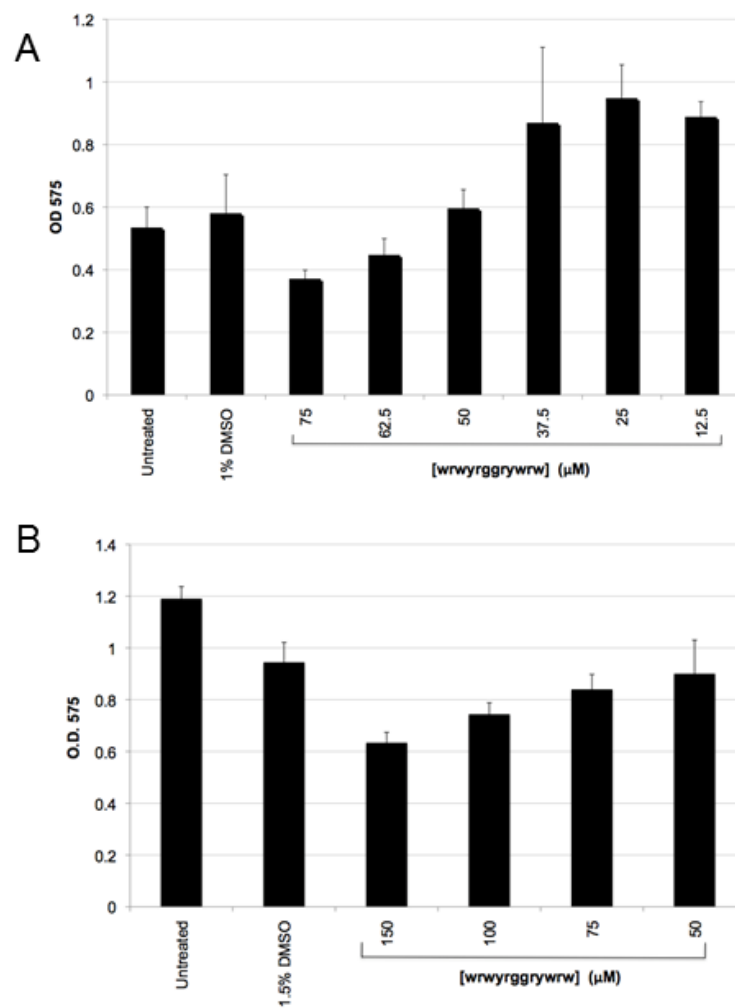
Figure 3-8. Effects of wrwyrggrywrw on eukaryotic cell metabolism.

MTT reduction assay on PMs (Panel A) or HCT116 cells (B). Approximately 40,000 PMs or 10,000 HCT116 cells were treated with the indicated peptide concentrations for 24 hours before being treated with MTT to assay metabolic activity by O.D. measurements at 575 nm. The MTT assays shown were performed by Ilham Naili and Sukanya Patra.

As an independent measure of viability we conducted a Live/Dead assay on the activated macrophages and the HCT 116 cells. This fluorescence-based assay monitors the ability of active cellular esterases to convert and retain calcein-AM (CAM) to a fluorescent product (the "live" stain). Additionally, the assay measures the uptake of a DNA binding-dye, ethidium homodimer (EH) that cannot cross into the cell unless the integrity of the membrane has been compromised; ethidium homodimer fluoresces only when bound to DNA (the "dead" stain). Thus, healthy active cells are EH-negative and CAM-positive, while dead cells are EH-positive and CAM-negative. Additionally, a subpopulation of cells that are "dying" may be positive for both dyes, indicating that there is some measure of membrane permeability and functional enzymatic activity. Approximately 40,000 PMs or 400,000 HCT116 cells were seeded and treated with wrwyrggrywrw or DMSO in media for a period of 24 hours and then the fluorescence was analyzed via flow cytometery. We saw a dose-dependent decrease in the number of live cells and a concomitant increase in dead cells with increasing peptide concentration (Figure 3-8A and Figure 3-8B). The IC_{50} of wrwyrggrywrw in this assay was approximately 40 μM (~ 73.1 μg/mL) for the PMs and about two fold higher (~85 μM = 155 μg/mL) for the HCT 116 cells. The HCT116 cells may be less sensitive than PMs in this assay, given the observation that a 10-fold greater cell number has only 2 fold-higher IC_{50}; this is contra the original hypothesis. Also, it is worth noting that the effects seen in both the MTT and Live/Dead assay occur at concentrations that are well below the MIC values established for most of the bacterial species that were tested (Table 3-2).
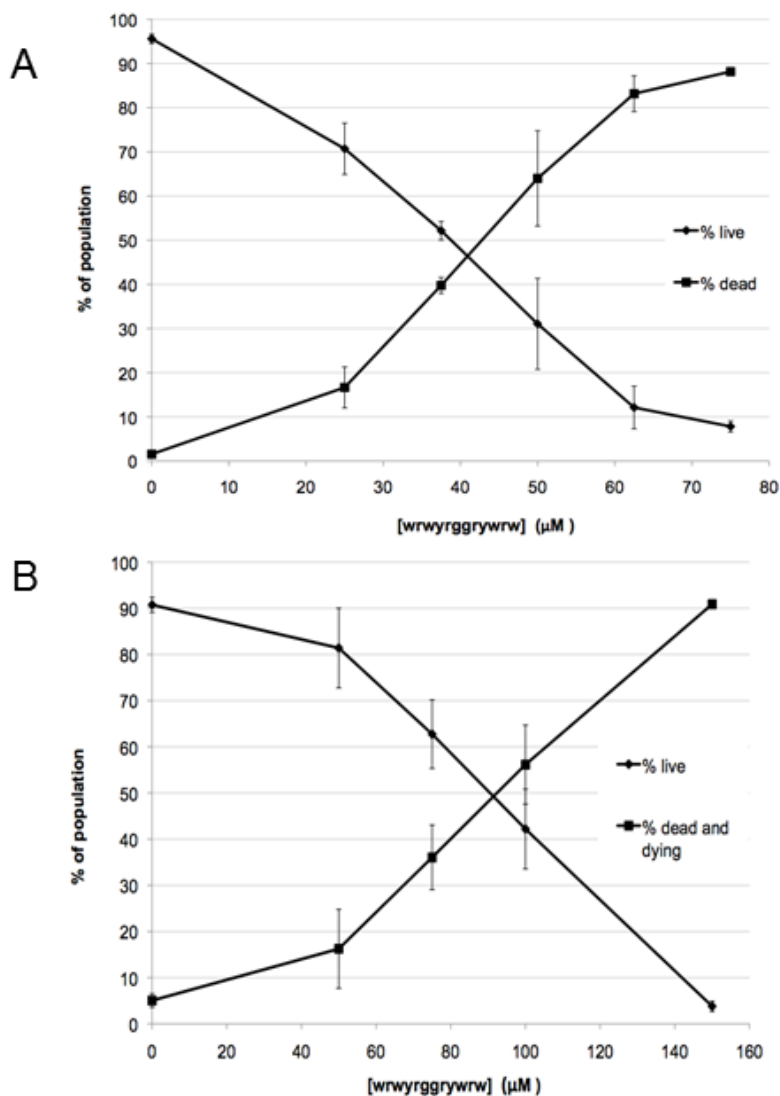
Figure 3-9. Effects of wrwyrggrywrw on eukaryotic cell viability.

Activated peritoneal macrophages (PM, Panel A) or human colorectal cancer cells, (HCT116, Panel B) were seeded at approximately 40,000 or 400,000 cells, respectively. Each cell type was treated with wrwyrggrywrw at the indicated concentrations, or DMSO as a control (the 0 [peptide]) for 24 hours, collected and stained for viability. Subpopulations of cells that stained stain positive for CAM (Live), or for EH (Dead), or both (Dying) were quantified by flow cytometery. Each point on the curve represents the average of three independent peptide treatments. Live/Dead assays shown were performed by Ilham Naili and Sukanya Patra

Section 3.3. Discussion

Our intent was to design single-chain linear peptide analogs that would mimic the action of the Holliday junction-trapping, bactericidal peptides, WRWYCR or KWWCRW. The hexapeptides require homodimer formation for maximum activity (Klemm *et al.* 2000; Boldt *et al.* 2004), and despite the fact that they are dissolved in an oxidizer (100% DMSO), the rate of dimerization is slow and often not complete (typically 85-95% dimerized as measured by HPLC). We reasoned that a single-chain linear analog would avoid this unwanted characteristic. Additionally, the peptides must survive the reducing environment of the bacterial cytoplasm in order to find their intended target, the HJ; thus analogs not dependent upon disulfide bond maintenance may confer an advantage in terms of *in vivo* activity. The analogs we designed were tested in recombination reactions (Table A - 1) as well as binding to protein free HJs (Figure A - 14). We found that decameric single-chain peptides containing only two basic amino acid residues were not effective SSR inhibitors nor did they bind well to protein free HJs. This may be due to lack of electrostatic interactions between the positively charged peptides and the negatively charged DNA resulting in weaker affinity, or weaker stability toward the DNA, a trend we have seen with two classes of small molecule inhibitors of SSR (Ranjit *et al.* 2010). Alternatively, it may be due to sub-optimal peptide length for HJ binding (*i.e.,* too long or too short). Peptides containing multiple cysteine residues did not confer added inhibitory characteristics, rather they had greater non-specific DNA interactions likely due to oligomerization, and possibly too many positive charges. A similar characteristic was seen with peptide inhibitors of HJ resolution by vaccinia virus topoisomerase that

contain multiple cysteine residues (Fujimoto *et al.* 2006). These data also suggest that there are both upper and lower limits to the length of peptide inhibitors that effectively trap HJs.

Among the potential candidates designed, peptide WRWYRGGRYWRW and its D-stereoisomer, wrwyrggrywrw were selected for extensive characterization. Both peptides had similar IC_{50} values, compared to WRWYCR, for recombination and HJ trapping in SSR in the absence of reducing agents (Figure 3-1A), suggesting a similar affinity for these reaction intermediates. In the presence of DTT however, WRWYRGGRYWRW remained potent while WRWYCR lost more than 90% of its potency (Figure 3-1A). The inclusion of peptide WRWYRGGRYWRW did not affect synaptic intermediates generated prior to the formation of the HJ (Boldt J., and Segall A., unpublished data) nor did it inhibit the initial cleavage reaction as evidenced by progression of the reaction to the HJ intermediate. This suggests that the mechanism of inhibition of SSR is similar for both peptide sequences.

Both WRWYCR and WRWYRGGRYWRW specifically recognized HJs in a protein-free context (Figure 3-2) but not linear B-form DNA (not shown), indicating affinity for branched DNA in general. Similar band shifts are seen with a variety of junctions, regardless of the sequence, arm length, or the ability to branch migrate (unpublished data). Indeed, if the peptides are to successfully trap HJs in the context of DNA repair, they must bind to HJs in a non-sequence specific manner. WRWYRGGRYWRW also quenches the fluorescence of a 2-AP junction in a dose dependent manner and with an apparent binding constant (K_d) similar to that predicted by the EMSA (~ 60 nM; York G., Rideout M., and Segall A., unpublished

data). The higher K_d indicates a slightly weaker affinity compared to WRWYCR (K_d = ~12-14 nM).

The use of short junctions (Figure 3-3 and Figure A - 15) provides a measure of the stability of the WRWYRGGRYWRW/HJ and WRWYCR/HJ complexes when electrophoresed in gels lacking Mg^{+2}. At the same time, this assay may provide an indication of the greater non-specific activity of WRWYRGGRYWRW compared to WRWYCR seen as a loss of radioactive DNA signal that enters the polyacrylamide gels with increasing amounts of peptide (Figure 3-3 and Figure A - 15). Interestingly, while the total signal decreases with increasing peptide treatment, the HJ signal does not (except at very high concentrations of WRWYRGGRYWRW) suggesting that binding to the HJ is able to solubilize the peptides to some extent. It is possible that the hydrophobicity of the tryptophan and tyrosine residues on WRWYRGGRYWRW could be minimized via base stacking interactions at the center of the junction, a hypothesis that was proposed for WRWYCR (Kepple *et al.* 2008).

In vivo, both HJ conformations have relevance and are recognized and processed by different HJ resolvases (Declais *et al.* 2008). RecG helicase and the RuvABC resolvasome both bind to "open-square" HJs and the *in vitro* activities of these proteins was inhibited by both isomers of WRWYRGGRYWRW (Figure 3-4 and Figure 3-5). WRWYRGGRYWRW is significantly less active against RecG than against RuvABC which may be due to the nature of the interactions between the components of the peptide/HJ/protein complex. The processivity of RecG is low (Whitby *et al.* 1998; Slocum *et al.* 2007) and we expect the peptide to be a competitive inhibitor, as was the case for WRWYCR (Kepple *et al.* 2005). If so, then

both the affinity and stability of WRWYRGGRYWRW for the HJ becomes the critical determinant for inhibition potency and, as discussed above, both are weaker than seen with WRWYCR. In contrast, inhibition of RuvABC may reflect a mechanistic inhibition, perhaps interfering with DNA phosphodiester backbone cleavage. The Cre-recombinase crystal structure with bound WKHYNY illustrated how the peptide could displace the scissile phosphate necessary for junction resolution, leaving the HJ intermediate trapped (Ghosh *et al.* 2005) and the same could be true for RuvABC. Inhibition of both HJ processing enzymes *in vivo* is likely to cause significant DNA repair problems and it has been shown previously that ΔRecG/RuvABC mutants are hypersensitive to DNA damage (Lloyd 1991; Ishioka *et al.* 1997; Sutherland *et al.* 2010). This could explain the enhanced bacterial cell killing seen when peptide treatments are combined with other DNA damaging agents such as mitomycin-C (Gunderson *et al.* 2006) norfloxacin (Naili I., Segall A., unpublished data) and H_2O_2 (Xu Y., Segall A., unpublished data) and could represent a powerful combination therapy.

WRWYRGGRYWRW is bactericidal, with MICs values in the low μg/mL range (Table 3-2), including for MRSA and small colony variants of *Pseudomonas*, two species of major concern in the clinical setting (Haussler 2004). In general, Gram-positive bacteria were more susceptible than Gram-negative bacteria with the exception of the *S.aureus* Newman strain. This same trend is seen with WRWYCR, and is likely attributable to the presence of the outer-membrane a hypothesis based on the greater susceptibility of the hyperpermeable *galE rfa* mutant strain compared to wild-type *Salmonella* LT2. Where comparisons are available, we see differences in the L- and D-stereoisomers, with the D-versions generally being 2-4 fold more

effective at bacterial growth inhibition. We also see that WRWYRGGRYWRW is generally 2-4 fold more effective than WRWYCR. Considering the differences seen in HJ affinity, stability, and RecG inhibition, it may be that WRWYRGGRYWRW has additional targets *in vivo*. Both WRWYCR and WRWYRGGRYWRW are cationic antimicrobial peptides, and in general these compounds have effects on the bacterial membranes. Peptide treatment of cells could lead to membrane stress, and possibly DNA damage through the generation of free radical species (Kohanski *et al.,* 2007, Kohanski *et al.,* 2010). However, treatment of cells with wrwyrggrywrw in anaerobic conditions leads to similar effects on viability, and induces greater than half of the DNA damage seen when treatments are conducted in aerobic conditions, thus membrane stress may not be the only explaintion (Rostron J., Segall A., unpublished results). The data from the TUNEL assay indicate both peptides induce DNA damage at lower concentrations, and at higher concentrations WRWYCR is more effective. Whether this damage is due to inhibition of DNA repair or generated in some other fashion is currently being investigated in our lab.

HJs are also formed by DNA repair processes in eukaryotic cells so it may be possible to exploit the toxicity in combination with chemotherapeutics that cause DNA damage (Su L., and Segall A., unpublished results; Patra S., and Segall A., unpublished results). The hemolysis assay provides a preliminary indication of non-specific toxicity toward eukaryotic cells and comparison with Triton X-100 control treatments suggest that the peptides are not actively permeabilizing the cells. While some of the treatments were comparable to osmotic lysis (water control, Figure 3-7), the DMSO control showed similar activity making it difficult to distinguish the effects of the peptides themselves. Noteably, the highest concentrations tested in this assay

(128 μM) corresponds to ~ 230 μg/mL peptide, which is approximately 15-fold lower than the MIC values for all of the Gram-positive and Gram-negative bacteria tested (Table 3-2). To further explore the toxicity in eukaryotic cells, we examined activated peritoneal macrophages and a colorectal carcinoma cell line (HCT116) in the MTT and Live/Dead assays. Since the cell types and cell numbers differ, direct comparisons are not possible; however, the peptides do show some toxicity towards both cell types. Nevertheless, in this assay as well the concentrations are above the MIC values for most of the bacteria tested. For instance, the IC_{50} for PMs in the Live/Dead was ~ 73 μg/mL and the IC_{50} for HCT116 cells was ~ 155 μg/mL. Interestingly, at the IC_{50} for the Live/Dead assay, HCT116 cells show ~ 50% reduction in metabolic activity (as measured by the MTT assay), in contrast to the PMs, which show no change at the corresponding IC_{50}. It is possible that the difference seen is attributed to the metabolic potential of the PMs. However, at low peptide concentrations the PMs had higher MTT activity than seen with untreated cells. This would suggest either an upregulation in metabolic activity, or perhaps increased permeabilization of the MTT reagent.

In summary, we have designed and characterized a single-chain linear analog of the HJ trapping, antibacterial peptide WRWYCR. WRWYRGGRYWRW is resistant to reducing conditions, and recognizes branched DNAs such as HJs, though it does so with weaker affinity and stability than WRWYCR. WRWYRGGRYWRW inhibits the activity of DNA repair enzymes, and induces DNA damage in bacteria; thus it is possible that the potency seen against both Gram-positive and Gram-negative bacteria is due partly to inhibition of DNA repair. Furthermore, the MIC values for tested bacteria are comparable, if not better, than WRWYCR and are below the range

of toxicity that we see with eukaryotic cells. Peptide sequence modifications are currently being tested to determine if the non-specific activities, and thus unwanted side-effects, can be minimized.

Chapter 4. Strategy for intrinsic labeling of peptides

Section 4.1. Introduction

The peptides described in this dissertation are structure-specific ligands of HJs. Peptide binding occurs regardless of the DNA sequence or the ability of the HJ to branch migrate or isomerize. The peptides prefer HJs over an excess of B-form duplex DNA suggesting that they are highly specific for branched forms of DNA. They inhibit the activity of a variety of unrelated HJ processing enzymes, and have potent antibacterial activity at least partly due to their interactions with HJs. The structure of a peptide bound to a HJ is a highly desirable goal. A structure would provide insight into the mechanism of inhibition and the characteristics necessary for binding. It would also provide information necessary to improve the inhibitors, perhaps making them even more stable or effective. Finally, the structure of a ligand in complex with a protein-free, open-square HJ would be the first of its kind and would likely be of general interest to the growing field of researchers targeting higher-order DNAs as potential therapeutics.

The only known structure of one of the peptide inhibitors is in complex with Cre-recombinase trapped on a HJ by peptide WKHYNY (Ghosh *et al.* 2005). In this structure, the center of junction contains peptide-dependent electron density, and WKHYNY could not be modeled to fit the density unambiguously. As an explanation for the disorder, the authors pointed out that the center of the HJ was sheltered from the crystal packing interactions by the recombinase proteins and therefore peptides at the center may have been free to adopt several different orientations. This may be the case for other peptides; WRWYRGGRYWRW has, thus far, not yielded

results in crystal trials (A. Segall, personal communication), and trials with WRWYCR or other homodimers were not possible due to the requirement for DTT in the Cre crystallizations. For these reasons, we felt that a protein-free structure might be more tractable.

Two possible approaches were postulated to solve the structure of a peptide in complex with a HJ: crystallography, and nuclear magnetic resonance (NMR). Both of these approaches have the benefit of small DNA substrates which would be readily and cheaply available as oligonucleotides, and both approaches would eliminate the need to purify large amounts of protein. However, NMR had the additional requirement of isotope-enriched peptides (*i.e.,* ^{13}C and ^{15}N). While such enrichments are costly to introduce synthetically, they can be incorporated *in vivo* in bacteria expressing the peptide. This requires bacterial growth in minimal media with the ^{13}C-glucose, and ^{15}N- ammonium sulfate as the sole carbon and nitrogen sources. Though the setup of a labeling strategy presented an immediate challenge to overcome, in the event that structural studies were unsuccessful the system could still be used to label peptides in other ways. For instance, radioactive isotopes such as ^{3}H, would be particularly useful for *in vivo* tracking. As such, initial efforts were directed toward solving the structure by NMR and this chapter describes the work to establish a peptide labeling strategy.

Section 4.2. Results

4.2.1. Overall Strategy

The expression of an antibacterial peptide inside of bacteria demanded that it be fused to a larger "carrier" protein in order to minimize its toxicity. Alternatively, precise separation of the carrier protein and the peptide was deemed equally important since a single residual amino acid left on the peptide would constitute a large% change from the original 6 amino acid sequence. To solve these problems, we used a ubiquitin fusion strategy previously employed to label peptides for NMR (Pilon *et al.* 1997; Kohno *et al.* 1998). Briefly, peptide sequences were cloned C-terminal to ubiquitin on a T7 expression vector. Cultures of *E. coli* bearing the vector were grown in minimal media with uniformly labeled ^{13}C-glucose and ^{15}N-ammonium sulfate as the sole carbon and nitrogen sources, respectively; thus any proteins produced by the bacteria should have these labels uniformly incorporated. A 6-histidine purification tag on the N-terminus of ubiquitin was used for purification of the fusion. Cleavage of the peptide was facilitated by the ubiquitin C-terminal hydrolase that recognizes an (RGG) amino acid motif which is conserved during the peptide cloning (UCH-L3, (Larsen *et al.* 1996). Cleavage after the last glycine yields the peptide with a native N-terminal amine that can then be purified by reversed phase HPLC.

4.2.2. Cloning of peptides WRWYCR, WKHYNY, and WRWYRGGRYWRW C-terminal to 6x His-tagged Ubiquitin.

Primers were designed to create double stranded inserts with cohesive ends to the restricted ubiquitin fusion vector. The DNA sequence of the insert was codon optimized for expression of peptide WRWYCR (MRP1F and MRP1R), and peptide WKHYNY (MRP4F and MRP4R, Section 6.3) in an *E. coli* host strain using the information found at (http://www.sci.sdsu.edu/~smaloy/MicrobialGenetics/topics/in-vitro-genetics/codon-usage.html). Oligonucleotides for the insert were first gel purified and then annealed together. The ubiquitin fusion vector was double digested with BamHI and KspI, gel purified, and then the annealed inserts were ligated into the vector using T4 DNA ligase. The plasmid containing the insert was electroporated into *E. coli* S17 cells for stable maintenance of the plasmid, and into an *E. coli* BL21 (DE3) expression strain (Strain G274).

The aforementioned protocol did not work for peptide WRWYRGGRYWRW, so we employed a primer extension strategy instead. The plasmid with the WRWYCR insert was used as a template and two primers (Primer 1 and 2, Figure 4-1) were designed to create an insert that amplified the region between the NdeI site upstream of the 6x His-tag, and the DNA coding for the first 4 amino acids of peptide WRWYCR. After PCR amplification, the products were denatured and cooled in the presence of Primer 3 which forms a 12 base pair overlap with the template and codes for the expression of the remainder of the peptide, namely RGGRYWRW. This was used as a template for fill-in PCR, creating a new insert that is flanked by NdeI and BamHI sites. The fill in product was purified, double

digested, and inserted into a double digested, gel purified ubiquitin fusion vector. The plasmid containing the insert was electroporated into *E. coli* S17 cells for stable maintenance of the plasmid (Strain 1259, Section 6.3), and into an *E. coli* BL21 (DE3) expression strain (Strain G 274, see Section 6.3)

4.2.3. Colony PCR screen peptide inserts C-terminal to 6x His-tag Ubiquitin protein

The strategies described above yielded large numbers of ampicillin resistant transformants; however many of them contained the vector with no insert. Attempts to decrease these "false-positive" results by treating with calf intestinal phosphatase and varying the ratio of insert to vector, led to only a modest decrease in transformants bearing the empty vector. In order to avoid sequencing large numbers of colonies, and additionally to develop a method for rapid detection of other peptide inserts for possible future work, we developed a colony PCR based screen. A primer was designed that annealed to the 6x His-tag region (Oligo 8, Section 6.3). Three other primers were designed that were complementary to the coding strand of the three peptide inserts (Oligos 9 – 11, Section 6.3). PCR reactions with the appropriate primers were inoculated with a small number of cells from potential transformants. The results of the PCR reaction were run on an agarose gel and yielded a product of approximately 280 base pairs (Figure 4-2). This product is strictly dependent upon the presence of the peptide insert, as the parental strain does not give the same size product. The vector was isolated from the PCR-positive clones and sequence verified.
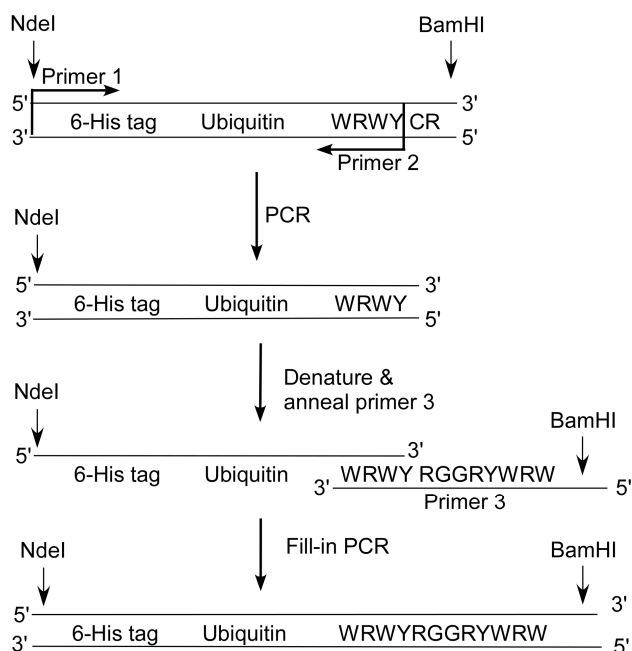
Figure 4-1. Primer extension cloning strategy for WRWYRGGRYWRW

The WRWYCR fusion is used as template for this strategy. The region between the 6-His tag and the DNA coding for "WRWY" is amplified using primers 1 and 2. Primer 3 is added to this product and the mixture is denatured and cooled allowing primer 3 to anneal to the coding strand of the PCR product. Fill-in PCR produces the insert containing the codon optimized DNA sequence coding for peptide WRWYRGGRYWRW.
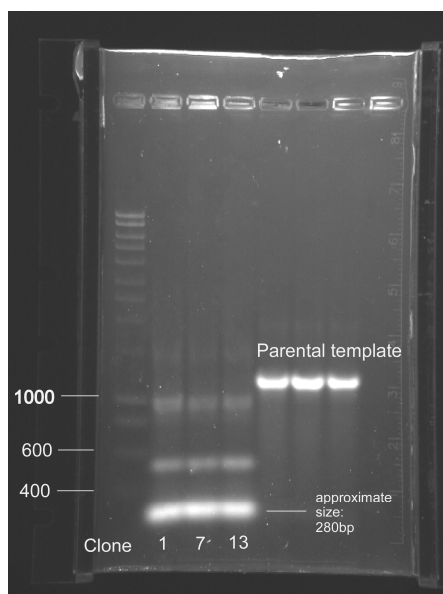
Figure 4-2. Colony based PCR screen

Template for the PCR is provided by inoculating the reaction with cells from a potential transformant. A primer that anneals to the 6-His tag region of the fusion vector is used in conjunction with a 2nd primer that anneals to the peptide coding region of the insert, and produces a PCR product of ~280bp. Primers can be designed for potentially any peptide insert, and thus this system can be used to rapidly screen for proper clones prior to sequencing.

4.2.4. Growth analysis and protein expression

To examine the effect of producing a potentially toxic peptide inside of bacterial cells, we measured growth rates of BL21 cells expressing either the ubiquitin-WRWYCR or ubiquitin-WKHYNY fusions. Growth curves were conducted in rich media in the presence or absence of the inducer for overexpression, IPTG. In addition, we checked protein levels in all sets of cultures to insure that the fusion was expressed. Cultures were treated with IPTG, or media (untreated control), and allowed to express protein for five hours. As seen in Figure 4-3A, neither the growth rate of the strains nor final OD_{600} at saturation is significantly altered compared to

the control cultures, indicating that the peptide fusions are not toxic. Bacterial cells from all three sets of uninduced and induced cultures were harvested and lysed via sonication. Normalized amounts of lysate were loaded on a 4-20% Tris-glycine SDS (TGS) polyacrylamide gel to view protein expression. As seen in figure 4-3B the fusion protein was expressed in the induced cultures and in approximately equal amounts between each set, suggesting that the production of this fusion containing either of the peptides, is not toxic to the cells (see discussion). Also notable is that the ubiquitin protein lacking the peptide fusion has a greater mobility through the gels than the fusions than ubiquitin fused to either peptide. This immediately suggested that cleavage of the peptide could be monitored by SDS-PAGE (discussed below).
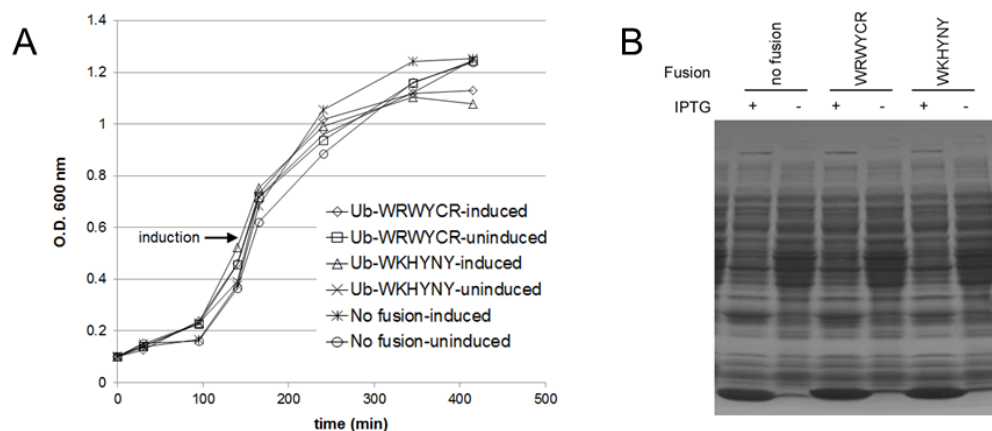
Figure 4-3. Growth rates and protein expression of peptide fusions

(A) 10 ml cultures of cells containing the indicated vectors were grown to an OD of ~0.5 and then induced with 0.5 mM IPTG, and allowed to grow for 5 hours. OD_{600} readings were taken to monitor growth rates as well as the final OD_{600} at saturation. (B) Cells were pelleted and resuspended in buffer to give equal amounts of cells/mL. Cells were then lysed, and the supernatant was run on a 4-20% TGS gel to determine the assay for expression amounts).

4.2.5. Ubiquitin-peptide fusion expression purification and cleavage

For peptide labeling, the strains harboring the ubiquitin-peptide fusions were grown in M9 minimal media with the indicated isotope enriched supplements and induced with IPTG. Successful fusion production generally correlated with saturating OD_{600} values of ~ 1.2. Good cell lysis was routinely achieved by a round of freeze-thaw followed by sonication at room temperature, without protease inhibitors, EDTA, or any reducing agents. This was due to the fact that the ubiquitin fusion was stable at room temperature, and due to the subsequent metal-ion purification and cysteine protease (UCH-L3) treatment. The major soluble protein in the lysate was the fusion, but a significant amount was also carried into the cell-debris pellet as inclusion bodies. While attempts to purify this isoluble material were successful, subsequent cleavage was poor, suggesting that the fusion was not properly refolded. The soluble material was purified by affinity chromatography over a Cobalt chelation column and eluted with imidazole using a segmented linear gradient that was developed to minimize contaminating proteins that also stick to the cobalt resin; generally fusion protein would elute between 200 and 250 mM imidazole (not shown). Fractions containing the fusions were determined by SDS-PAGE (not shown) but were not dialyzed to remove imidazole. We found that the removal of the imidazole, or the time required for dialysis, lead to precipitation of the fusion (not shown). Further, as shown below, the subsequent cleavage step did not seem to be inhibited by the presence of the imidazole. Fusion production was quantified using a Bradford protein assay (Table 4-1) and the quantity varied depending upon the fusion construct. The expression levels of the WRWYRGGRYWRW fusion, were much lower than the other two fusions though the cultures reached saturation as

monitored by OD_{600}, and growth curves showed no change after induction (not shown). Attempts to isolate the peptide by the methods described below were ineffective or produced yields too small to be useful; as a result, this peptide fusion was not pursued further. Several possible explanations for this fusion are addressed in the discussion.

Table 4-1. Ubiquitin-peptide fusion expression and purified peptide yields

Strain	EDT1184	EDT1193	EDT1458
Fusion peptide	WRWYCR	WKHYNY	WRWYRGGRYWRW
Fusion/Liter[a]	15 - 22.5 mg	17-20 mg	2-5 mg
Theoretical yield[b]	1.2-1.8 mg	1.2-1.9 mg	0.3-0.75 mg
Peptide produced[a]	0.03-0.32 mg	0.7-1.5 mg	Not detected

[a]Amounts of fusion and peptide shown are given as a range based on at least 3 independent trials
[b]Theoretical yield based on 100% cleavage and recovery of fusion peptide

The ubiquitin hydrolase (UCH-L3) was expressed and purified as in the same manner as the fusion, though always using a dedicated Cobalt-chelation column. We found that even minor amounts of this protease would lead to cleavage of the fusion if purifications were performed over the same column. The cleavage of the ubiquitin::peptide fusions were monitored on 4-20% TGS gel (Figure 4-4), or by RP-HPLC (not shown). Several ratios (hydrolase to fusion) were tested and we found that a 1:100 ratio, respectively, at 37° C overnight in undialyzed Cobalt column purification buffer was adequate for cleavage. It should be noted that in most cases the cleavage reaction was not complete (generally between 70-80% cut fusion).
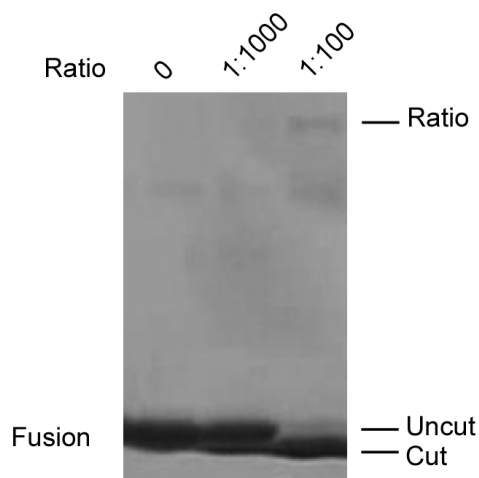
Figure 4-4. Cleavage of ubiquitin::peptide fusion.

Shown is the cleavage of ubiquitin::WRWYCR fusion overnight at 37° C with the indicated ratios of UCH-L3 to fusion. Cleavage reactions were run on a 4-20% TGS gel which can separate cut from uncut fusion.

4.2.6. WRWYCR purification

The strategy employed for peptides WRWYCR and WKHYNY were different as a result of the different behavior seen with each peptide once cleaved off the fusion. Each peptide purification strategy will be described separately.

Following cleavage of the ubiquitin::WRWYCR fusion, a fluffy white precipitate formed. This precipitate was collected resuspended in SDS-PAGE loading buffer, heated and then run on an SDS gel. As seen in Figure 4-5, the precipitate contained peptide WRWYCR along with other contaminants and a large amount of uncut fusion. Since the fusion is known to be soluble prior to cleavage, this suggests that the cut peptide may be interacting with uncut fusion, perhaps specifically with the WRWYCR still fused to the C-terminus of ubiquitin, and causing it to precipitate as well. Based on the amount of control WRWYCR that was loaded

on this gel, we estimated that this precipitate had somewhere between 0.01 and 0.1 mg of WRWYCR, representing between 3 and 30% of the total yield.

The insoluble material was resuspended in 6M Guanidium Hydrochloride (GHCl), and dialyzed to 2M GHCl for purification. Several different types of chromatography were attempted including, a size exclusion column, a cation exchange column (the pI of WRWYCR in pH 8 buffer is 9.5), and a high pressure C18 HPLC column. Each of these had significant backpressure issues that forced us to search for alternatives. The insoluble material, as well as the soluble fraction, were eventually purified over a low pressure disposable C18 column. We developed a linear segmented gradient with increasing amounts of acetonitrile to separate the peptide from the rest of the contaminating material (Figure 4-6). The fractionation was monitored by UV absorbance at 280 nm and the activity of fractionated material was monitored by including fractions or the appropriate controls into excision recombination reactions and as seen in the inset of Figure R2-5, active fractions elute specifically from one of the UV absorbing peaks, and trap HJ's in a manner consistent with our synthesized inhibitor (compare with WRWYCR control) and suggests that the peptide was dimerized.
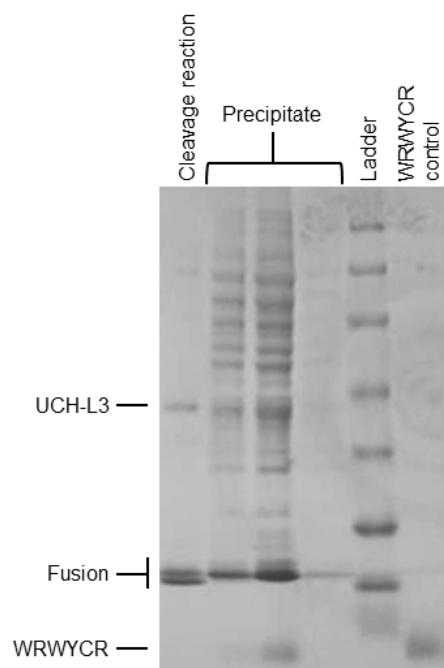
Figure 4-5. Insoluble material from cleavage reactions.

The precipitate formed after cleavage of WRWYCR from the ubiquitin fusion was collected, resuspended in SDS loading buffer and run on a 4-20% TGS gel. Three different dilutions of this resuspension are shown. This material contained WRWYCR, a significant amount of uncut fusion in addition to other contaminants (compare to cleavage reaction, where both cut and uncut fusion are visible). WRWYCR control indicates 0.1 mg of synthesized peptide and based on this control we estimated that the precipitated material contained approximately 30% of the theoretical yield of WRWYCR from this preparation.
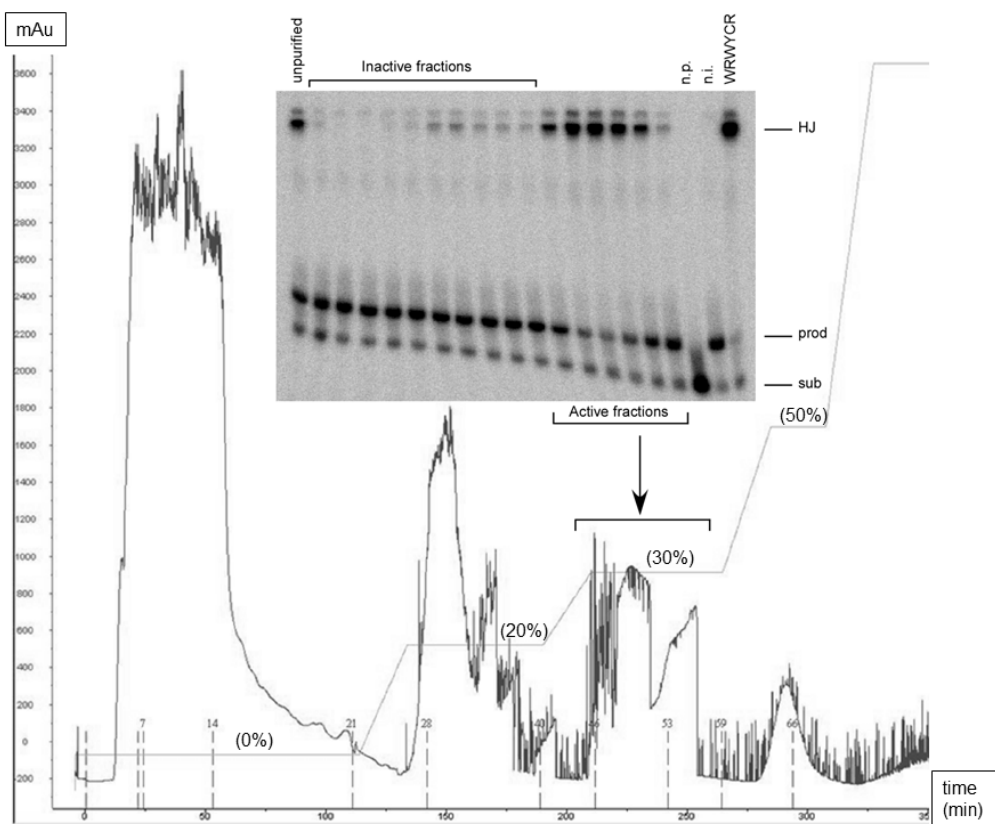
Figure 4-6. Low-pressure C18 purification of peptide WRWYCR.

Shown is the purification of the soluble fraction following ubiquitin::WRWYCR cleavage on a low pressure C18 column. A linear segmented gradient with increasing amounts of acetonitrile was used and a detailed description can be found in the materials and methods. Numbers in parenthesis indicate the acetonitrile concentrations where the various peaks eluted Fractions from the purification were tested in the excision reactions shown in the inset. "sub" refers to the radioactive end-labeled excision substrate; "prod", referes to one of two different size recombination products (one of which is below sub, and has run off this gel). "HJ" refers to the Holliday junction intermediate that is trapped by purified WRWYCR; "n.p." refers to a control reaction without recombinant proteins; "n.i." refers to an untreated reaction; "WRWYCR" refers to treatment with 0.5 μM comercially synthesized WRWYCR as a control. The insoluble material was purified separately, using a similar gradient with similar results.

4.2.7. Peptide purification –WKHYNY

In contrast to WRWYCR, cleavage of peptide WKHYNY from the ubiquitin fusion did not cause a precipitate to form. As a result, the entire supernatant was loaded over a separate low pressure C-18 column and eluted using a similar gradient of Acetonitrile (not shown). To test for activity, these fractions were included in a alternative λ-Int mediated recombination pathway, know as the "Bent-L". WKHYNY was originally isolated by screening combinatorial libraries for inhibition of the Bent-L pathway and is about 5 times more active in this pathway than in the excision pathway (Boldt *et al.* 2004).

4.2.8. Verification of purification and species by mass-spectrometry

Following purification and testing in the appropriate recombination reaction the active fractions were analyzed by liquid chromatography coupled to mass spectrometry (LC-MS) to gauge the extent of purification and detect the increase in molecular weight from isotope labeling. Media conditions for the isotope enrichment can be found in the Materials and Methods. Shown in Figure 4-7 are LC-MS results of individual fractions from the purification of an ^{15}N labeled WRWYCR preparation (A and B) and from a ^{13}C, ^{15}N labeled WKHYNY preparation (C and D). Panel A has a single fraction of WRWYCR that was greater than 90% pure. The molecular formula of WRWCYR with a C-terminal carboxyl group is $C_{46}H_{60}N_{14}O_8S_1$ corresponding to a molecular mass of 968.44. By labeling with ^{15}N, the molecular mass of this peptide is expected to increase to (968.44 + 14) = 983.44; this species is visible in panel B (983.35). In addition a species of 982.51 may represent the unprotonated C-terminal carboxyl (pKa of roughly ~1.8 to 2.0). A dimer of

WRWYCR would result in a species of $((983.443 - 2)_2 = 1964.886))$, and this species is also seen (1964.69) indicating that some amount of dimer has survived the ionization (see discussion). An unknown species of molecular weight 975.68 is also present though we are unsure of its identity. It should be noted that in this case only, the C18 column used for the purification was also used previously for unlabeled peptide purifications and this likely explains the observation of a species of 969.20 which would correspond to unlabeled WRWYCR (+) 1 hydrogen. Based on these data we concluded that the proper species had been synthesized and purified, though the presence of contaminating species, made the extent of purification questionable (see discussion). Based on the results of the LC, we pooled fractions that were greater than 90% purity, lyophilized them, and used them for preliminary NMR experiments described below.

WKHYNY has a molecular formula of $C_{45}H_{55}N_{11}O_{10}$ yielding a molecular mass of 909.41, which increases to $(909.41 + 45 + 11) = 965.41$ when uniformly labeled with ^{13}C, ^{15}N. As seen in panel C this fraction from the purification was also greater than 90% pure and it contained species of the correct mass (+) one proton (966.46), and the correct mass (+) one sodium atom (988.50). Additionally, there is a species of the correct mass (-) one proton (964.53), and as was the case with WRWYCR, this species is likely a unprotonated C-terminal carboxyl group. In case of WKHYNY, the pooled fractions were also lyophilized and used in the NMR experiments described below.
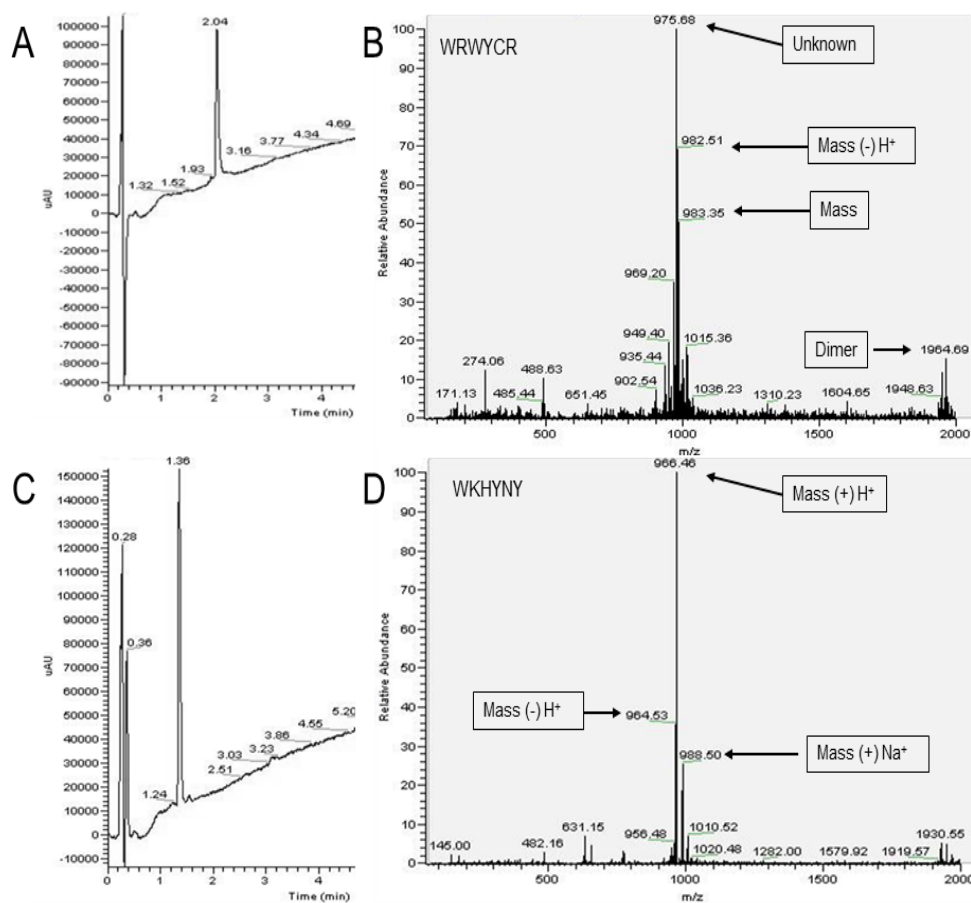
Figure 4-7. LC-MS from labeled peptide purifications.

(A) UV trace from a fraction from the C-18 column purification of WRWYCR. (B) ESI-Mass spectrometry of the peak shown in panel A. Species present include ^{15}N labeled peptide (983.35), ^{15}N labeled peptide (-) one proton (982.51), an unknown species (975.68) and some amount of dimerized WRWYCR (1964.69). (C) UV trace from a fraction from the C-18 column purification of WKHYNY. (D) ESI-Mass spectrometry of the peak shown in panel C. Species present include ^{15}N, ^{13}C labeled peptide (+) one proton (966.46) or (+) one sodium atom (988.50), and ^{15}N, ^{13}C labeled peptide (-) one proton (964.53).

4.2.9. Multidimensional NMR experiments

Two multidimensional experiments were conducted on the labeled peptides:

a ^{1}H -^{15}N Heteronuclear Single Quantum Coherence (HSQC, for both WRWYCR

and WKHYNY) and a ^{1}H-^{15}N-^{13}C HNCACB on the double labeled WKHYNY. Briefly,

as seen in Figure 4-8 (left) the HSQC involves the transfer of magnetization between ^{1}H nuclei and labeled ^{15}N nuclei. This establishes the chemical shifts of the amide nuclei, as well as the N-H bond on the indole ring of tryptophan and in some cases N-H bonds in arginine, asparagine, and glutamine. The HNCACB experiment (Figure 4-8, right) is similar to the HSQC with the additional transfer of magnetization to the α- and β- ^{13}C directly bonded to the amide nitrogen of each amino acid in the polypeptide chain. Additionally, transfer of magnetization to the α- and β-carbons on the n-1 amino acid takes place and is helpful in confirmation of the primary peptide sequence.
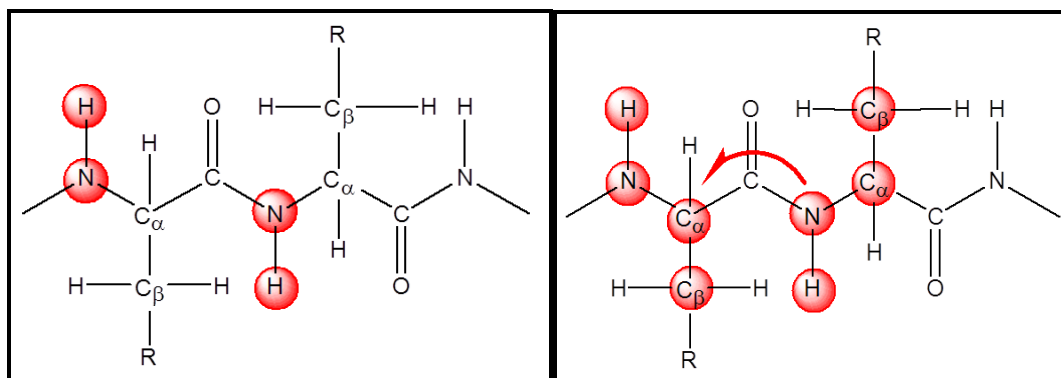
Figure 4-8. Description of multidimensional NMR experiments conducted.

(Left) ^{1}H-^{15}N HSQC. Magnetization is transferred from the hydrogen to the ^{15}N labeled nitrogen via a scalar (through-bond) coupling. The chemical shift is evolved in the ^{15}N dimension and then transferred back to the hydrogen for detection resulting in a 2-D spectrum. (Right) ^{1}H-^{15}N-^{13}C HNCACB. Similar to the HSQC, but magnetization is transferred via the amide bond to the α- and β-carbon of the amino acid residue, as well as that of the preceding residue (n-1). The chemical shift is evolved in all three dimensions producing a 3-D spectrum.

The results from the HSQC experiment on WRWYCR is presented in Figure 4-9. There are 5 amide bonds present that are predicted to have chemical shifts at approximately 8 ppm in the ^{1}H dimension (Ulrich *et al.* 2008); four of these are visible in the spectrum. The HSQC spectrum has two peaks upfield of the amide protons that likely correspond to the N-H bonds on the indole rings of the W1 and W3 residues (Ulrich *et al.* 2008). Finally the N-H bonds from the guanidine functionalities of the arginine side chains are likely to be the peaks seen between 6 and 7 ppm (Ulrich *et al.* 2008). Why are there not 2 sets of the aforementioned peaks corresponding to a dimer of WRWYCR? The activity of the peptide in recombination assays suggests that the peptide is dimerized. Furthermore, this spectrum was obtained in 100% DMSO-d$_6$, which would leave the peptide completely unfolded. It is reasonable to assume that the symmetry of the WRWYCR places the individual NMR active nuclei on either side of the dimer in similar magnetic environments and this would lead to overlap of the individual resonances. As mentioned, the magnetization in the HSQC experiment is evolved on both the nitrogen and hydrogen dimensions which allows for presentation as a 2-D spectra (shown in Figure 4-10). In this case the individual peaks in Figure 4-9 appear as "spots" in Figure 4-10.
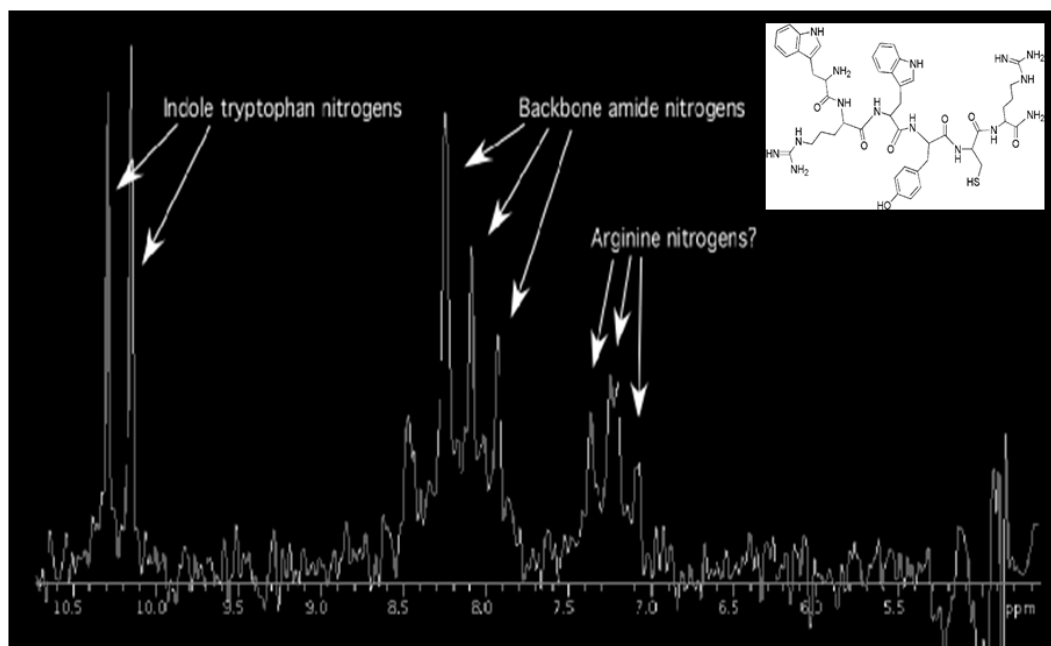
Figure 4-9. ^{1}H -^{15}N HSQC of WRWYCR

Shown is the ^{1}H - ^{15}N HSQC from WRWYCR. Peaks between 10.5 and 10 ppm correspond to the H-N bonds on the indole ring of each of the tryptophans. Between 8.5 and 7.5 ppm, 4 of the 5 H-N bonds on the amide backbone are visible. The peaks between 7.5 and 7 ppm may be from the side chains of the two arginine residues (the structure of a WRWYCR monomer is shown in inset). The spectrum was obtained in 100% DMSO-d$_6$ so the peaks seen are from two disulfide bridged hexamers that have nuclei with overlapping chemical shifts.
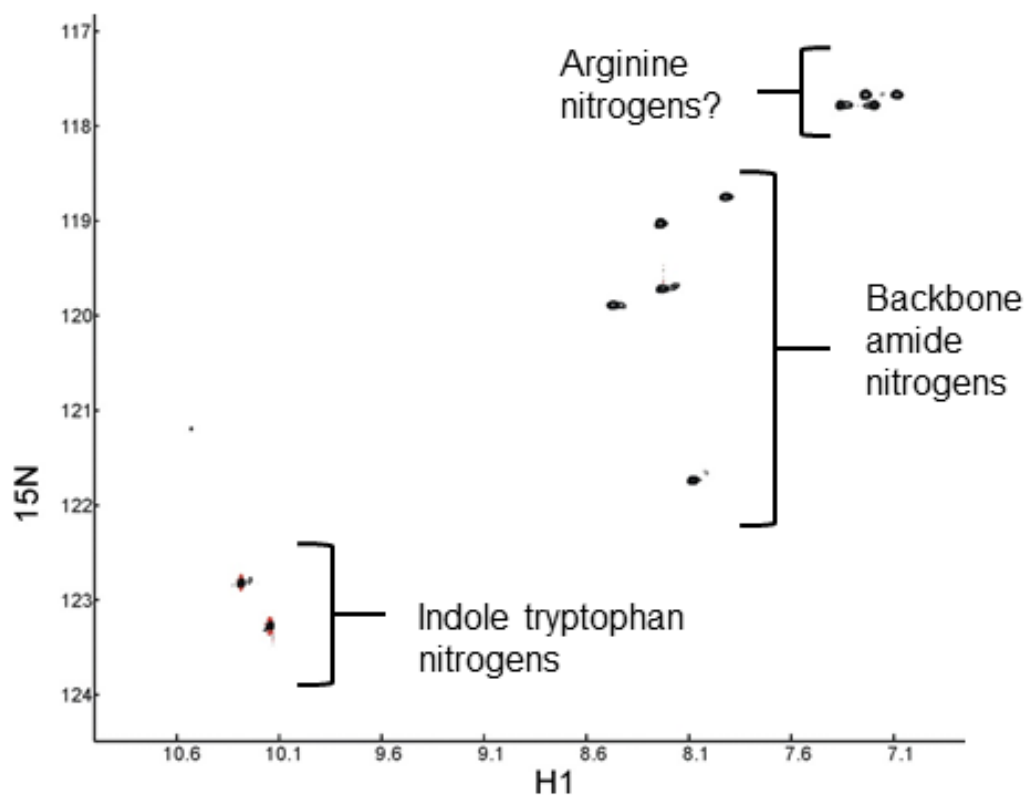
Figure 4-10. ^{1}H – ^{15}N HSQC on ^{15}N –labeled WRWYCR.

A 2-dimensional plot of the HSQC experiment seen in Figure 4-9. The ^{1}H dimension corresponds to that seen in Figure 4-9.

A ^{1}H-^{15}N HSQC was performed on WKHYNY, and the spectrum is shown in Figure 4-11. WKHYNY has only one tryptophan, in contrast to WRWYCR, and thus this spectrum has only one indole N-H peak (~11 ppm). Peaks corresponding to the 5 amide bonds are visible between 9 and 8 ppm. The two peaks between 8 and 7 ppm may be the result of the amide bond on the side chain of asparagine, and the primary amine of lysine. N-H bonds in the histidine ring generally do not produce a signal in the HSQC (Ulrich *et al.* 2008). Finally, it should be noted that while the spectra obtained for WRWYCR was referenced to an internal standard, the spectrum of WKHYNY was not. Therefore, the chemical shifts seen are not likely to be accurate.

In addition to the HSCQ, a triple resonance experiment was performed on ^{15}N-^{13}C labeled WKHYNY. As described (Figure 4-8), this experiment detects the transfer of magnetization from the amide bond down the amino acid side chain and yields a series of 2-D spectra several of which are shown in Figure 4-12. Each spectrum has identical ^{13}C chemical shifts plotted on the y-axis, and ^{1}H chemical shifts on the X-axis. The peaks and intensities seen in each 2-D spectra vary in the ^{15}N dimension (indicated as ^{15}N = 90 ppm, 91 ppm, etc). Shown are 14 of the 136 2-dimensional slices that were recorded in this experiment. Orange peaks (positive) correspond to α-carbons, blue peaks (negative) correspond to β carbon. Notably, some weak n-1 peaks can be seen (at approximately 30 ppm in the ^{13}C dimension from slices ^{15}N = 94 - 98 ppm). Also, it should be noted that the chemical shifts in this spectra are also unreferenced and therefore they are not likely to be accurate.
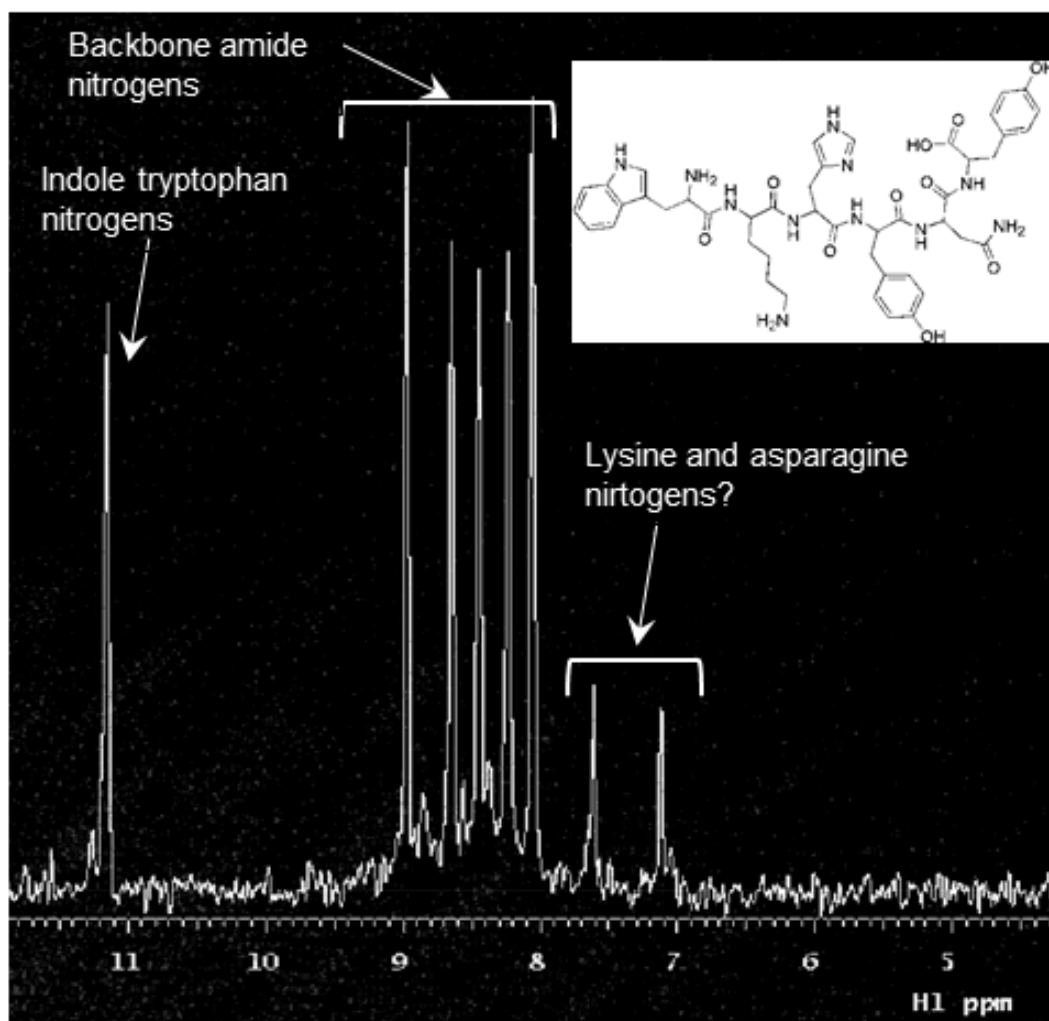
Figure 4-11. ^{1}H -^{15}N HSQC of WKHYHY.

Individual peaks correspond to ^{1}H atoms directly bonded to ^{15}N atoms. Notably, the peak at ~ 11 ppm likely corresponds to the H-N bond on the indole ring of tryptophan. The peaks between 9-8 ppm likely account for the 5 H-N bonds on the amide backbone. Peaks between 7 and 8 ppm may be from the primary amine of the lysine side chain and the amide bond of the asparagine side chain (the structure of WKHYNY is shown in inset). Note that this spectrum was not referenced to an internal standard and therefore the chemical shifts may not be accurate.
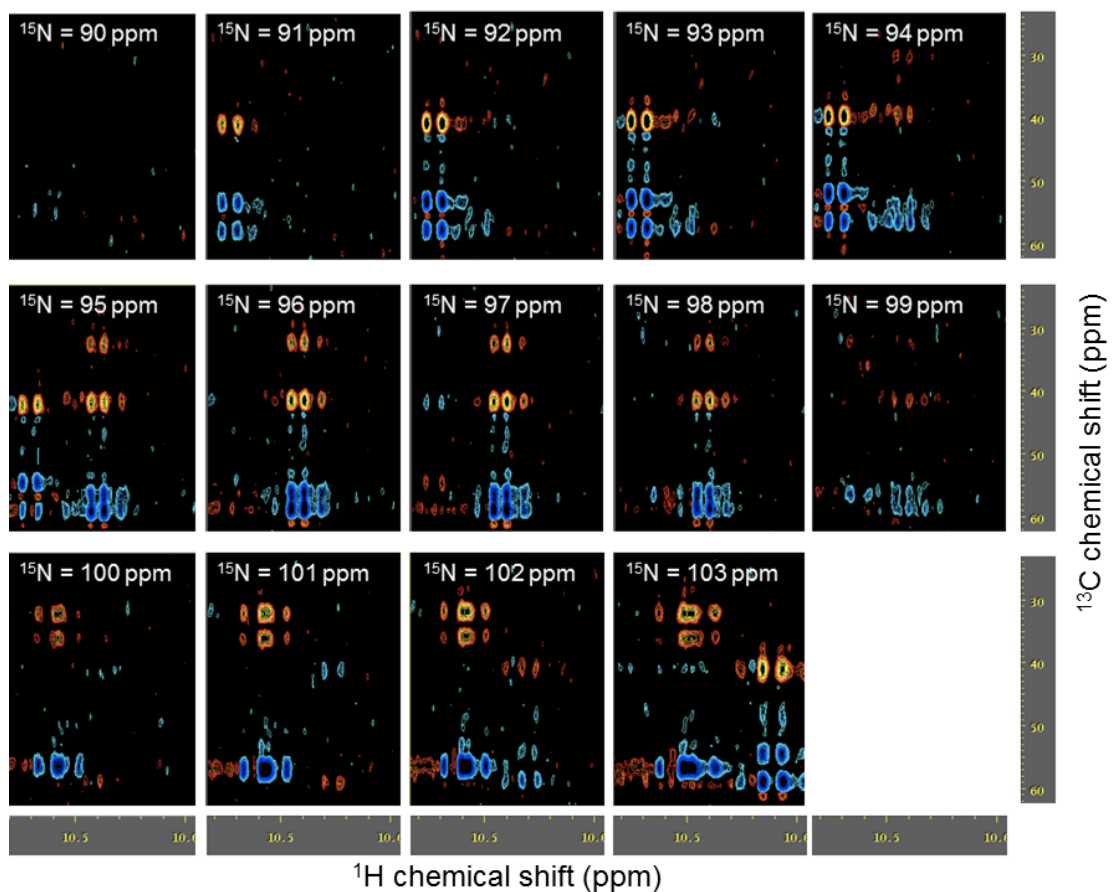
Figure 4-12. ^{1}H-^{15}N-^{13}C HNCACB experiment on double labeled WKHYNY.

Shown are 14 individual 2-dimensional spectra plotting ^{13}C chemical shift on the y-axis, and the ^{1}H chemical shift on the X-axis. Each slice corresponds to the indicated chemical shift in the nitrogen dimension (e.g. ^{15}N = 90 ppm, 91 ppm, etc.) Orange peaks (positive) correspond to α-carbons, blue peaks (negative) correspond to β carbon. Note also that the chemical shifts in these spectra are unreferenced and therefore they may not be accurate.

Section 4.3. Discussion

The experiments and strategy described here provide a cost-efficient, effective means to intrinsically label most peptide. Significant hurdles were overcome in the cloning stage of this project by using a primer extension strategy that could be useful for other peptides of similar sequences. Additionally, the colony PCR assay described would be useful in the event that a larger number of peptide sequences are intended for study. Verification via LC-MS and inhibition of recombination also provide means for rapidly validating labeled peptides. Finally, the labels need not be solely for use in NMR, as the incorporation of deuterium or tritium would prove functional for *in vivo* tracking. This is especially significant when one considers that the activity of a 6-amino acid peptide is likely be altered by incorporation of any extrinsic tag regardless of size.

Unfortunately, WRWYGRRYWRW was not a tractable construct in our hands. The fusion construct, promoter region and Shine-Dalgarno site were all verified (unpublished data) suggesting that a DNA sequence anomaly is not at fault for the expression problems. It was clear from induction experiments that some amount of this fusion was made (Table 4-1). Since induction did not lead to change in growth rate, nor did it affect the cell density at saturation, it is likely that the C-terminal peptide fusion is not interfering with HJ processing. Along these lines, we tried to induce expression in conjunction with mild UV exposure but did not see any additional sensitivity compared to uninduced controls (York G., Rideout M., Seagll A., unpublished data). The small HJ band shift experiments (Figure A - 15), suggest that this peptide is more hydrophobic than a dimer of WRWYCR, though we did not

find a significant amount of insoluble protein in the cell debris (not shown). It is also possible that this construct simply was not translated well, though we did not check the transcript levels. If translation and hydrophobicity are linked then cloning and expressing a potentially more soluble analogs of WRWYRGGRYWRW may yield better expression.

WRWYCR was also problematic. Several attempts were made to produce the double-labeled peptide fusion, and in each case the cleaved peptide was not recoverable. In some instances, C18 purified fractions had activity in recombination assays suggesting that the peptide was present. However, HPLC analysis of the active fractions revealed many smaller peaks, rather than a single peak such as that seen in Figure 4-7A. Attempts to further purify the active peaks were not successful. In one other instance, fusion production and hydrolase cleavage resulted in material with no activity. It is possible that in this preparation the peptide was not dimerized. Despite the fact that UCH-L3 is a cysteine protease, our cleavage reactions contained no reducing reagents to avoid problems with dimerization and most of the previous preparations had active peptide. Our preps also contain no protease inhibitors, and therefore it is possible that a non-specific protease survived the purification degraded the peptide following cleavage. A series of protease inhibitor cocktails should be tried to determine if they interfere with the activity of UCH-L3. If none can be found then an alternative possibility could be to heat inactivate any proteases prior to cleavage. Heat shock to 42°C has been shown to increase both the yield and purity of ubiquitin fusions (Pilon *et al.* 1996). Alternatively, hydrophobicity, or non-specific aggregation may have been a problem. The results from the cleavage assay argue that WRWYCR is prone to precipitation at high

concentrations. It is possible that the material from the larger double-labeled preparations precipitated post C18 purification, and was never recoverable. If this is the case, then purification in a mild detergent, or alternatively, expression of an active, but less hydrophobic peptide sequence may yield better results.

Chapter 5. Conclusions and Future Directions

Holliday junctions are fascinating structures. The study of these elegant genetic exchange intermediates is a worthwhile pursuit regardless of whether they are ever realized as a theraputic target. Indeed, the peptide inhibitors of site-specific recombination (SSR) were initially pursued to develop molecular tools, not potential theraputics and in that regard, the peptides have contributed greatly to the understanding of HJ processing in by tyrosine recombinases such as Int (Cassell *et al.* 2000; Klemm *et al.* 2000; Cassell *et al.* 2003; Boldt *et al.* 2004; Boldt *et al.* 2007; Hazelbaker *et al.,* 2005), XerC/D (Grainge *et al.,* 2007) NBU1 (Rajeev *et al.,* 2007) and by virally encoded enzymes such as vacinnia virus topoisomerase (Fujimoto *et al.*, 2006) and A22R (Cassell, G., Segall A., unpublished data). The small molecules described herein also show considerable promise as molecular tools and have led to novel insights into the correlation between membrane perturbations and DNA damage (Rostron J., Yitzaki S., Authement N., Rideout M., and Segall A., ms in preparation). Together these compounds create a "molecular toolbox" useful for answering questions about DNA recombination, repair and other aspects of cellular metabolism. Therefore, the evolution of this work described below has been directed towards both tractable theraputics, and better tools.

Addressing the toxicity of the pyrrolidine bis-cyclic guanidines is an important future direction for this class of compounds. While the compounds inhibit HJ resolution *in vitro*, the low MIC values against all bacterial species are linked to non-specific membrane effects as illustrated by studies of potassium leakage, membrane stress reporters, and fluorescence microscopy (Yitzaki S., Rostron J.,

Segall A., unpublished data). Membrane perturbation may be linked to hydroxyl radical-induced DNA damage (Kohanski *et al.* 2007; Kohanski *et al.* 2010; Spindler *et al.* 2011) and therefore using these inhibitors to study DNA repair is complicated by the fact that they may cause DNA damage themselves. Furthermore, if this toxicity is severe, the small molecules may have minimal effects on their primary target (the HJ) while overwhealming the cells with unintended side-effects. Additionally, severe side-effects may decrease the likelihood of establishing toxic specificity toward DNA repair intermediates, such as those frequently found in rapidly dividing bacterial or cancerous cells that are expected to rely heavily on DNA repair for survival. Thus it is important to first decipher the extent of disruption of both bacterial and eukaryotic membranes and second to minimize this characteristic. One important aspect of this is to first determine the cellular concentrations of the small molecules following treatment which is possible via HPLC analysis on cell lysates as was done previously for the peptides (Orchard S., Medina-Cleghorn D., and Segall A., unpublished data) and eukaryotic cells (Patra S., Su L., and Segall A. unpublished data). Additionally, determining cellular localization would provide useful insight and a means for this is discussed below.

As discussed in Chapter 2, several modifications could potentially make the pyrrolidine bis-cyclic guanidines less toxic. Decreasing the hydrophobicity is a promising means of minimizing the toxicity and is straightforward through re-synthesis with less hydrophobic amino acids. For instance, R- and S-hydroxymethyl functionalities both performed well in the positional scanning at positions R^1-R^3 (Figure A - 4 and Figure A - 6) and could easily be incorporated in future compounds. Slightly larger analogs also hold promise for increasing the

effectiveness of these inhibitors as tools for studying DNA repair and also decreasing their toxicity. For instance, the 2-AP data we have modeled for the peptides suggest that a homodimer of WRWYCR (Kepple *et al.* 2008), or a monomer of WRWYRGGRYWRW (York G., Vahi-Ferguson G., Rideout M., Salamon P. Segall A., unpublished data) bind HJs at equilibrium, compared to two molecules of 1609-10 (Chapter 2). If this is the case, then perhaps a larger pyrrolidine (tri- or tetra-) cyclic guanidine may bind with a simpler stoichiometry and better affinity. This modification is also straightforward by coupling additionaly amino acid during synthesis, and would yield additional functionalities that could be modified with more polar groups (see synthesis described in Chapter 2). Furthermore, the present functionalities would not need to be sacrificed for inclusion of more polar ones. Additionaly, a subset of compounds could contain a 9-anthrylmethyl functionality (derived from anthracene). While this would yield a slight increase in hydrophobicity (in comparison to the 2-naphthylmethyl functionalities present), anthracene is fluorescent, making such compounds useful for *in vivo* tracking and thus cellular localization studies. Furthermore, the emission range is distinct from that of DNA meaning that it could be possible to monitor binding without the use of a 2-AP reporter. These modifications are straightforward using the established synthesis pathway. Alternatively, the incorporation of Boc-protected lysine at position R_1 would provide two primary amines useful for creating a branched analog. In this scenario, both the N-terminal amine and the □-amine of lysine would be sites for coupling of subsequent amino acids and this would create the branches.

It is possible that the toxicity of the pyrrolidine-biscyclic guanidines can not be minimized. An alternative approach to less toxic, and potentially more effective, small molecules is to re-screen combinatorial libraries for compounds with characteristics other than inhibition of SSR. We have recently developed membrane stress and DNA damage reporters that are effective in 96-well format and could be used to screen for positional scanning mixtures that illicit low membrane stress, but cause DNA damage. Promising mixtures of compounds could then be tested for HJ binding using the 2-AP fluorescence assay adapted to a 96-well format. Screening for antibacterial activity by determining MIC values in a 96-well plate format would be important to ensure that bacterial growth inhibition is retained. This approach would allow investigation of libraries that were previously overlooked for instance a pyrrolidine- bis-cyclic thiourea library that would offer a dimerized version of the original cyclic thiourea small molecule, 1530-1 (Ranjit *et al.* 2010). Finally, an important caveat is to test libraries that are not peptide, or peptide-derived. One of the most significant limitations of the combinatorial libraries is that the compounds identified are all inherently analogs of each other. As such, they occupy relatively narrow regions of "chemical space." Libraries that are synthesized using "non-peptide" chemistry offer another level of chemical diversity that would be interesting to explore.

WRWYCR, WRWYRGGRYWRW, and their analogs described in this work and elsewhere, are a special class of CAMPs that are likely to have multiple modes of action. For instance, pulsed-field and 2-D gel electrophoresis studies with DNA repair mutants support DNA repair as an *in vivo* target of wrwycr and wrwyrggrywrw (Gunderson C., Marcusson L., Medina-Cleghorn D., and Segall A., unpublished

data). Additional studies suggest that iron homeostasis may also be affected by peptide treatment (Orchard S., Segall A., unpublished data). In spite of this, microscopy, potassium efflux measurements and membrane stress reporters, indicate that the peptides also disrupt bacterial membranes (Rostron J., Naili I., Segall A., unpublished data). Most CAMPs perturb membranes as one, if not the primary mode of action (Nguyen *et al.* 2011) and the extent of membrane damage caused by wrwycr and its analogs is now being studied in our lab. There are various mechanisms of CAMP-induced membrane disruption all of which are dictated by peptide folding (Nguyen *et al.* 2011). The peptide labeling strategy presented in Chapter 4 can be directly employed to address both peptide folding and cellular localization. For instance, solid-state NMR is routinely used to determine peptide structure in lipid environments (see examples in (Nguyen *et al.* 2011)) and the ^{13}C, ^{15}N isotope enrichment strategy would be useful in these studies. Alternatively, ^{3}H labeling would provide a convenient way of tracking the peptides for determining cellular localization in both bacterial and eukaryotic cells. Notably, one of the strengths of this isotope enrichment strategy is that it yields intrinsically labeled peptides that maintain all of their native characteristics in contrast to extrinsically coupled labels such as rhodamine.

The peptide labeling strategy also makes it possible to deliver toxic peptides *in vivo.* The peptide ubiquitin fusions are stable and an expression strain carrying the ubiquitin hydrolase, on a compatible plasmid and with a different inducible promoter, may allow the fusion to be cleaved in a regulated manner. This would deliver the peptide *in vivo*, while eliminating the effects of membrane penetration or extracellular effects on iron (such as iron binding). This could be extremely valuable

to separate the effects of DNA damage caused by membrane penetration, from DNA damage caused by inhibition of DNA repair. One drawback to this is that expression will yield L-stereoisomers of the peptides which will likely not be as stable as the D-stereoisomers. Alternatively, if the peptides affect iron homeostasis by binding external iron, then it is possible to eliminate this activity by *in vivo* expression. Finally, the system described could be used to look at peptide efflux. We have previously seen that cells treated with wrwycr or its analogs recover over time; thus it is likely that the peptides are effluxed. However, efflux measurements are difficult since the peptide is applied externally; *in vivo* expression could eliminate this complication.

Another important aspect yet to be addressed is the optimal size of the peptide inhibitors necessary for HJ binding, inhibition of SSR or HJ resolution. It is entirely possible that the peptide inhibitors of SSR described in this work and elsewhere are too large for optimal HJ binding. While it is clear that disulfide bridged hexamers and the single chain dodecamers are potent in our assays, the optimal size might be between 7 and 12 amino acids. Alanine substitutions of WRWYRGGRYWRW suggest that the C-terminal tryptophan is not important for HJ binding by EMSA or 2-AP quenching and thus it may actually be sticking out of the center of the junction. A similar type of binding can be seen for supramolecular metallo helicate described in Chapter 1 (Oleksy *et al.* 2006). This question of size may be straightforward to address for the peptides using the power of the combinatorial libraries and a variation of the "scaffold-ranking" strategy described in Chapter 2. In this scenario, the "scaffolds" tested would be peptides of varying backbone length (i.e. 6, 7, 8, 9, 10, 11, and 12 amino acids). Selection of the

appropriately sized "scaffold" would be followed by screening a single positional scanning library to identify potent peptide sequences, as done previously (Cassell *et al.* 2000; Boldt *et al.* 2004). If the scaffold ranking strategy does not work, then a similar strategy as used to determine the optimal length of peptides that bind CD4$^+$ T-cell receptors (Hemmer *et al.* 2000) could be employed. In this strategy, each positional scanning library was screened and here a high-throughput 2AP HJ-binding assay would be imperative due to the numbers of mixtures necessary for testing.

Identification of optimal peptide length may significantly aid in endeavors to obtain an atomic level crystal- or NMR-structure of a peptide bound to a HJ. Presently, structural studies are complicated by the fact that the peptides are structure-specific, rather than sequence-specific, ligands. They bind to protein-free HJs regardless of the sequence or the ability to branch migrate. Indeed, if they are to bind junctions *in vivo* in the context of DNA repair, then they likely to bind in a variety of orientations. It is analogous to putting a penny in a gumball machine. Whether the penny is heads-up or tails-up is irrelevant so long as it's the size and shape of a penny. In this case, while flexibility is an attribute for inhbitor efficacy, it may be problematic when trying to obtain a single uniform ligand conformation. Having a ligand that can fit in the junction in a single orientation is therefore an important pursuit, and peptides of an optimal size for HJ binding may yield better substrates for structural studies.

Finally, crystallization studies (ongoing) have been yielding positive results and will continue to be pursued by others. WRWYCR in complex with a modified

HJ1 (Kallenbach, 1983) containing single base overhangs routinely produces crystals that diffract to better than 6 Å (York G., Rideout M., Huxford T., and Segall A., unpublished data). These crystals also grow in the presence of brominated WRWYCR, which has similar *in vitro* activity to the native sequence, and this may be useful for providing phase variations necessary to solve the structure. Diffraction quality is likely to be influenced by the species present and therefore determining the optimal length of peptides for HJ binding could proved useful for crystallography. Additionally said peptide crystallizations should be attempted with a recombinase such as Cre. The Van Duyne lab has had success with Cre in crystallizations, including the only known crystal with a peptide inhibitor; however, that inhibitor WKHYNY was disordered in the crystal structure (Ghosh *et al.* 2005). The disorder seen is due to 2 or more peptides in the center of the HJ and it may be that they are bound in different orientations. As mentioned in Chapter 4, Cre-crystallizations with WRWYRGGRYWRW have been unsuccessful and this may be due to the fact that this ligand is too large. Therefore, peptides of the appropriate length could be useful in co-crystallization studies with Cre. Here too, the 2-AP quenching data used for the screening would be incredibly useful if it is concomitantly modeled to determine if 1 or 2 ligands are likely to be bound to the HJ.

Chapter 6. Description of experimental procedures

Section 6.1. Materials and methods for Chapter 2

Libraries and compound synthesis The mixture-based libraries that were screened were synthesized at Torrey Pines Institute for Molecular Studies (TPIMS). Based on the results of the screens, individual compound synthesis was also performed at TPIMS as described in Section 2.2.4. All reagents for the synthesis were purchased from commercial suppliers, and were used without further purification. All synthesis controls that were analyzed by MS were dissolved at a concentration of 1.0 mg/mL in 50% acetonitrile in water (ACN/water) and a 20 µL aliquot was injected onto a C-18 column on a Finnegan LC-MS system (Finnegan HPLC equipped with a Finnegan Surveyor photodiode array detector (PDA) and a Finnegan LCQ duo Mass Spectrophotometer). All solvents for liquid chromatography contained 0.05% TFA as a buffer. Compounds were eluted from the column using a gradient of 5% (ACN/water) to 95% (ACN/water) over 6 minutes with a flow rate of 250 µL/min. The presence of the desired compounds was confirmed by their mass and purity of the crude material was determined to be 70-80% as judged by UV absorption at 254 nm.

Small Molecule Purification. Pyrrolidine bis-cyclic guanidine compounds (1609: 1, 3, 10, and 12) were purified as follows. Each crude compound was initially solubilized in 2 mL of 50% (ACN/water) and then diluted to 10% (ACN/water), causing a precipitate to form. Concentrated HCl (2.5% (v/v)) was added and the compounds were sonicated for 5 minutes to help solubilize them. A 20 µL aliquot of each compound solution was injected onto the Finnegan LC-MS. The product with

the desired molecular weight was identified and, based on its retention time, a unique gradient was created for the purification of each molecule. The crude compounds were purified on an Agilent 1100 HPLC with a semi-prep C18 column using the established gradient and an initial mobile phase of 10% (ACN/water) with a flow rate of 10 mL/min. In general, peak fractions eluted between 45-75% (ACN/water). Ten ml fractions were collected and each was screened by LC-MS to confirm the purity and correct molecular weight. Fractions were pooled, lyophilized, resuspended in 50% (DMSO/water) and stored at 4°C. An aliquot of the purified material for each compound was analyzed on a Beckman HPLC (Model 128 pump with a model 168 photo diode array detector) and a Phenomenex Jupiter 4μ Proteo 90Å (250 x 4.6 mm) C8 analytical column. The purity of each compound was determined to be 90-95% (compounds 1609–1, 3, and 12) and 82% for 1609-10. Final yields for each purified compound were between 5 and 10 mg.

Biological Assays. All acrylamide gels used in this study were made from 29:1 polyacryamide:bis-acrylamide solutions. Oligonucleotides were purchased from Integrated DNA Technologies and, in the case of oligos used directly as reaction substrates, were purified on 5% native polyacrylamide gels. DNA was visualized by "UV shadowing" using a hand held Mineral lamp, model UVGL-58 (366 nm), and the correct molecular weight product was excised from the gel and eluted using a "crush/soak" method (Sambrook *et al.* 2001). DNA oligomers were precipitated and resuspended at the indicated concentrations for use in PCR, or were directly annealed together to make HJ substrates. DNA substrates were radiolabeled using [γ-^{32}P]-ATP (Perkin Elmer, (BLU-502Z)) and T4 polynucleotide kinase (New England

Biolabs (NEB), as described previously (Boldt *et al.* 2004). Gels were dried on a gel dryer at 80°C under vacuum for 2 hours. Dried gels were exposed to a Molecular Dynamics (MD) PhosphorImager screen, and quantitated with ImageQuant software from MD.

Excision Recombination Assays. The excision assays were performed with the same DNA substrates and exactly as described in (Boldt *et al.* 2004).

Bent-L Recombination Assays. The bent-L assays were performed with the same DNA substrates and exactly as described in (Boldt *et al.* 2004).

RecG Helicase Assays. RecG unwinding assays were performed as described previously (Kepple *et al.* 2005), using the same oligonucleotides as substrates. RecG was the generous gift of Dr. Peter McGlynn (University of Aberdeen).

Restriction enzyme inhibition. pUC19 DNA was purified from RecA⁻ cells. The amount of HindIII restriction enzyme (New England Biolabs) was first titrated in reactions containing 43.2 ng plasmid DNA to establish conditions where 50-70% of the total input DNA was cut after 25 minutes at 37°C with 0.08 units of HindIII per reaction. To examine inhibition, purified small molecules were added to reactions at the indicated concentrations and incubated 10 minutes at 37°C. Reactions were then started with the addition of restriction enzyme and aliquots were taken at either 2 minutes, 5 minutes, 15 minutes, or 25 minutes, and stopped with 2% SDS, 10% glycerol, and 0.1% bromophenol blue. Reactions were electrophoresed on 0.7% agarose gels with a final concentration of 2.5 μg/mL ethidium bromide, at 5V/cm and 0.5X TBE. The DNA was visualized on a Geneflash gel documentation system

(Imgen Technologies) with UV exposure at 258 nm. The image was quantitated for % DNA cleavage using ImageQuant (GE Lifesciences) software.

Electrophoretic Mobility Shift Assay (EMSA) The following oligos were used to assemble a junction with symmetrical arms and a frozen center that cannot branch migrate (oligos shown 5' to 3'):

1. TCCTACCACCAGATACACGCCACAGTTTTTTTTTTGATTA

2. TAATCAAAAAAAAAACTGTGCAGATGCGGAGTGAAGTTCC

3. GGAACTTCACTCCGCATCTGATCTTTGCCGTCTTGTCAAA

4. TTTGACAAGACGGCAAAGAT GCGTGTATCTGGTGGTAGGGA

For these experiments, junctions were purified on an SDS-Tris-Tricine gel. The HJ band was excised, and eluted by the "crush/soak" method, then precipitated and finally resuspended in 1 mM Tris (pH 8.0), 0.1 mM EDTA. Binding reactions were performed with 2 nM HJ in 25 mM Tris (pH 8.0), 1 mM EDTA, 100 mM NaCl, 5% glycerol, with 100 ng of sonicated salmon sperm DNA in a 10 ml volume. 1609-10 was allowed to incubate for 10 minutes on ice. Reactions were electrophoresed through a native 5% polyacrylamide gel at 4°C with 0.5X TBE as running buffer. Gels were dried and analyzed as described above.

2-aminopurine (2-AP) fluorescence binding assays. 2-AP assays were performed as described previously (Kepple *et al.* 2008) and using the same oligonucleotides as substrates. Briefly, 100 nM HJ containing one 2-AP substitution of adenine, as indicated, was titrated with crude compounds at molar ratios of 0:1,

0.5:1, 1:1, 2:1 or 4:1 small molecule:HJ. Fluorescence measurements were performed on a Photon Technology International Model QM-4/2005 scanning spectrofluorometer (Birmingham, NJ, USA). The sample was excited at 315 nm and fluorescence emission values obtained between 365 nm and 375 nm were averaged. Bandpass filters were set at 4 nm for excitation and 8 nm for emission. The averaged values were subtracted from a similar titration of a junction in which the native adenine was present in the junction, instead of 2-AP, to give corrected fluorescence (Fcorr) values, which represent the fluorescence due to the presence of the 2-AP substitution. The Fcorr values were then normalized to untreated reactions (shown in Figure A - 1B). Crude compounds were initially screened using the HJ with the 2-AP site on strand four at position two (4AP2, Figure A - 1). Selected small molecules were screened further using 3 other HJs containing AP substitutions at different sites (1AP1, 3AP1, and 4AP1).

2-AP fluorescence binding of purified 1609-10 for determination of apparent dissociation constant (K_d). Based on the initial 2AP screening and in part upon *in vivo* results, purified 1609–10 was selected for extensive titration in the 2-AP assay in order to model the binding interactions and estimate an apparent binding constant (K_d). HJ4AP2 was used as the reporter and titrated with 1609-10 at 15 or 20 different concentrations ranging from 0 to 900 nM. Fcorr values were determined (as described above), and then expressed as a fraction of the HJ in a complex (Fraction of Complex, or F_c) versus concentration of 1609-10 using the following equation:

$$F_{C_{observed}} = \frac{F_O - F_B}{F_O - F_S}$$

where F_0 is the initial fluorescence of the 2AP HJ, F_B is the fluorescence at a given concentration of 1609-10, and F_S is the fluorescence at saturating concentrations of 1609-10. For each titration the saturation point was set just below the point of maximum fluorescence quenching and used to estimate an apparent K_d.

Fitting of the fluorescence data to describe the binding interactions between 1609-10 and a HJ. We modeled predicted binding curves to the experimentally determined values, shown in Figure 2-8, by testing six possible scenarios of 1609-10 binding to a HJ. These scenarios as well as the equations used to describe the best model are presented in detail in Section 2.3.6.

Stability experiments. Radiolabeled HJs were trapped in excision recombination reactions with a final concentration of 0.5 mM peptide WRWYCR. Reactions were electrophoresed on 5% SDS-Tricine polyacrylamide gels and the HJ band was cut from the gel and eluted overnight using the "crush-soak" method (Sambrook et al. 2001) in 3 volumes of TE (pH 8.0). Junction DNA was precipitated with 10% sodium acetate and 3 volumes cold ethanol, resuspended in TE and quantitated by UV. Recombination reactions were assembled as described above, using the purified junctions (20 pM final) and warmed to 30℃ prior to t he initiation by the addition of a "pre-mix" of the recombination proteins. Reactions were allowed to proceed for 30 min, and were then diluted 20 fold with 1X buffers, 2 mg nonspecific DNA, and a 28-fold molar excess of unlabeled HJ over each inhibitor. Aliquots (200 ml) were taken from diluted reactions at the indicated time points and stopped with 100 ml of 2% SDS. Standard reactions using the same molar amounts of DNA and proteins were assembled in either 10 ml or 200 ml volumes. These were used as controls to judge

inhibition based on reaction volume and were quenched just prior to the 20-fold dilution with either 5 ml or 100 ml of 2% SDS, respectively. Products were separated on SDS-Tricine gels and % HJ resolution/min was calculated.

RuvABC HJ Cleavage Assays. Assays were performed as described previously (Kepple *et al.* 2005) using the same oligonucleotides as substrates. We are grateful to Dr. Robert Lloyd (University of Nottingham) for his generous gifts of RuvA, RuvB, and RuvC proteins.

Minimal Inhibitory Concentration (MIC) assays. Several bacterial strains were used to examine the inhibitory effects of the isolated small molecules. A complete strain list with genotypes can be found in Table 6-1. Overnight cultures were subcultured 1:100 in MHB in culture tubes and grown to an OD_{600} of 0.08-0.1. Concentrations of small molecule tested were 1, 2, 4, 8, 16, 32, 64, 128, 256, and 512 µg/mL. A 96-well plate was prepared with 2X desired small molecule in 100 µL of MHB. Subcultured cells (100 µLper well) were mixed into each well and an initial OD_{600} reading of the plate was taken. Plates were incubated for 16 - 20 hours without shaking at 37° C, and the final OD_{600} reading was determined. The difference between the final and the initial reading was calculated to yield the increase in growth. The MIC is defined as the lowest concentration of compound that inhibits growth (Ferraro 2000).

MTT assays The African green monkey kidney epithelial cell line BSC40 was seeded at 40,000 cells/well in 96-well plates, then incubated overnight at 37˚C in 5% CO_2. The medium was removed and replaced with DMEM containing the indicated treatments, and growth proceeded for 24 hours. Following treatment, 20 ml of 4 -

mg/mL 3-(4, 5-dimethyl-2-thiazolyl)-2, 5-diphenyl-2H-tetrazolium bromide (MTT) solution in 1X PBS was added to each well and incubated for 3 hours. Lysis buffer (100 ml of 20% SDS in water:DMF (1:1), 2% glacial acetic acid, 2% 1M hydrochloric acid) was added and the plates were incubated overnight at 37˚C to aid the dye dispersion. Absorbance of the wells was read at OD570 nm in a SpectraMax384 Molecular Devices microtiter plate reader. Control reactions to test the effect of DMSO (solvent for peptides and small molecules) were performed in identical fashion.

Table 6-1. Bacterial Strain List for Chapter 2

Designation[a]	Species and Strain	Genotype	Source
G90	*E. coli* W3110	N99 Δ(*lacZYA*) *galK rpsL*	R. Menzel
G255	*S. enterica* serovar Typhimurium	LT2	Laboratory collection
G455	*S. enterica* sv. Typhimurium	LT2 *din1001*::MudJ(*lacZ*, Km^R) *rfa* Δ[*gal bio uvrB*] *hisG46*	L. Bossi
G510	*B. subtillis*	Spo$^+$	Alan Grossman
G565	*S. aureus*	ATCC 33591 methicillin-resistant (MRSA)	ATCC via S. Blondelle (TPIMS)

[a]The Segall lab strain designation is given.

Section 6.2. Materials and Methods for Chapter 3

General. All peptides were synthesized either by Sigma Genoysis or Biosynthesis Inc., with C-terminal amidation. These peptides were purified to > 95%, and the correct molecular weights were verified by mass spectroscopy (MS) by the manufacturers. Lyophilized peptides were resuspended as 10 mM stock solutions in 100% anhydrous DMSO and all peptide dilutions for assays were made in nano-pure water. For each experiment, DMSO controls were performed and they correspond to the residual solvent concentration in the highest peptide treatment. All acrylamide gels were made with 29:1 polyacryamide:bis-acrylamide solutions. Oligonucleotides were obtained from Integrated DNA Technologies. For the generation of recombination substrates, oligonucleotides were annealed and directly used as PCR templates as described (Boldt *et al.* 2004). For the generation of HJ substrates oligonucleotides were purified on 5% native polyacrylamide gels, and the DNA was visualized by "UV shadowing" using a hand held mineral lamp, model UVGL-58 (366 nm). The correct molecular weight product was excised from the gel and eluted overnight in TE (pH 8.0) using a "crush/soak" method (Sambrook *et al.* 2001). Eluted DNA was precipitated with three volumes of ethanol and 10% sodium acetate. The DNA was resuspended in TE and, if needed, individual strands were radiolabeled using [γ- 32P]-ATP (Perkin Elmer, (BLU-502Z)) and T4 polynucleotide kinase (PNK, New England Biolabs) according to (Sambrook *et al.* 2001). DNA strands were then directly annealed together to make HJ substrates. Recombination and band shift gels were dried at 80°C under vacuum for 2 hours and were then exposed to a PhosphorImager (PI) screen (GE Lifesciences), and quantitated with

ImageQuant software from GE. The 12% HJ unwinding gels were not dried, but were exposed to PI screens and scanned following overnight exposure.

Excision Recombination assays. Substrates, proteins and assay conditions are described in (Boldt *et al.* 2004).

HJ band shifts. Band shifts (Figure 3-2A and Figure A - 14) were performed in TE (10 mM Tris-HCl (pH 8.0), 1 mM EDTA (pH 7.8)) + 5% glycerol. Radiolabeled HJ DNA was the same as used for the RecG unwinding assay (below). The HJ DNA substrate was included in reactions at 2 nM final concentration. Peptide dilutions were added to reactions and binding was allowed to incubate for 10 minutes on ice. The samples were loaded without loading-dye on 5% native Tris-Borate-EDTA (TBE, pH 7.8) gels. Electrophoresis was done at 240 V for 3 hours at 4°C

Short junction band shifts (Figure 3-2B and Figure A - 15). The oligonucleotides used were the same as described in (Kallenbach *et al.* 1983). Oligo 1 was 5' radioactively end-labeled with T4 PNK as described above. A stock solution of the short HJ was made by combining equimolar amounts of unlabeled oligos 1-4 (concentrations estimated by UV absorbance at 260 nm) with the radiolabeled tracer in 0.5X TAEMg (20 mM Tris-HCl (pH 8.0) 10 mM boric acid, 1 mM EDTA, and 6.25 mM magnesium acetate), and heating to 95°C followed b y slowly cooling to room temperature. The final concentration of the stock was 20 µM unlabeled junction with 20 nM tracer. Once cooled this mix was used without further purification. Peptide was added at the indicated concentrations to 2 µM annealed junction in 0.5X TAEMg and 10% glycerol and the reaction was allowed to incubate at room temperature for 10 minutes. Identical reactions were setup with 20mM DTT or water

and incubated for another 10 minutes. All reactions were then loaded on a 12% polyacrylamide gel containing either 0.5X TBE. Electrophoresis was performed at 240 V for 7 hours at 4°C. Gels were visualized by exposure to a phosphoimager cassette without drying and analyzed using Image Quant software.

RecG unwinding assays. Purified RecG protein was a generous gift from Dr. Peter McGlynn (University of Aberdeen, UK). Unwinding assays were performed as described previously (Kepple *et al.* 2005), using the same oligonucleotides as substrates.

RuvABC HJ cleavage assay. Purified RuvA, RuvB and RuvC proteins were a generous gift from Robert Lloyd (University of Nottingham, UK). HJ cleavage assays were performed as described previously (Kepple *et al.* 2005), using the same oligonucleotides as substrates.

Minimal inhibitory concentrations (MICs). The genotypes of the bacterial strains used to examine the inhibitory effects of the peptides can be found in Table 6-2. Overnight cultures were diluted 1:100 in Mueller Hinton Broth (MHB) in culture tubes and grown to an OD_{600} of 0.08 – 0.1. Concentrations of peptide tested were 1, 2, 4, 8, 16, 32, 64, and 128 µg/mL. A 96-well microtiter plate was prepared with 2X peptide in 100 µL of MHB. Subcultured cells (100 µL per well) were mixed into each well and an initial OD_{600} reading of the plate was taken. Plates were then incubated for 16 to 20 hours without shaking at 37° C. The final OD_{600} reading was determined and the difference between the final and the initial reading was calculated to yield the increase in growth. The MIC values were defined as the lowest concentration of

compound that inhibits growth and are estimated from 3 independent replicates in each experiment (Ferraro *et al.* 2002).

Flow cytometry for bacterial cells. All flow cytometry experiments were performed using a BD FACSAria desktop cell sorter with a 70 μm nozzle (Becton-Dickinson) at the SDSU Flow Cytometry Core Facility. For each sample, 50000 events were recorded. Data acquisition and analysis was performed using FACSDiva software (Becton-Dickinson). In most cases, bacterial cells were identified by counterstaining for DNA content.

Terminal dUTP transferase nick-end labeling (TUNEL) assay. Overnight cultures of bacteria were subcultured 1:100 in MHB and grown until they reached an OD_{600} of 0.08-0.1, and then treated with 2X concentrations of peptide wrwyrggrywrw, or DMSO, in a microtiter plate for 1.5 hours in a 37°C shaker (MTS 2, IKA-Schuttler). The cultures were pelleted, fixed with 4% paraformaldehyde, permeabilized using a solution of 0.1% Triton X-100, 0.1% sodium citrate, and assayed using the In Situ Cell Death Detection Kit Fluorescein (Roche) according to the manufacturer's protocol, except that we resuspended our samples in a final volume of 25 μl of the detection solution. Cells were counterstained with 0.5 μM TOTO-3 (Invitrogen) for 10 minutes to monitor the presence of the chromosome. After treatment, cells were pelleted and resuspended in 1X PBS and quantified by flow cytometry using the blue laser (488 nm; FITC channel) for fluorescein, and the red laser (633 nm; APC channel) for TOTO-3. The percentage of TUNEL-positive cells was calculated as a fraction of the TOTO-3-positive cells.

Hemolytic activity assay. Hemolysis was performed using sheep red blood cells (MP Biochemicals). Peptides wrwycr or wrwyrggrywrw, or the appropriate controls, were resuspended at 2X the indicated concentration in 1X PBS. A 1% solution of red blood cells in an equal volume of 1X PBS were mixed with the peptides in a microtiter plate to bring the final concentrations to 1X and 0.5% solution of red blood cells. The plate was incubated at 37°C in 5% CO_2 for 1 hour, then centrifuged for 5 min at 1500 rpm. 100 µl of supernatant from each sample was transferred into a new clear plate using a multichannel pipette. The optical density was read at 414 nm using a SpectraMax plate reader (Molecular Devices).

Collection of peritoneal macrophages. To harvest peritoneal murine macrophages (PMs), 8- to 12-week-old female BALB/c mice were injected in the peritoneal cavity with 1 ml of thioglycolate (final concentration of 4% in boiling water) to induce macrophage proliferation and were euthanized 4 days later. PMs were harvested by washing the peritoneal space with 10 ml of DMEM (without FBS) and collecting the effluent. The cells were centrifuged for 5 min at 4°C (Sorvall RT6000) at 700 rpm and were then resuspended in DMEM-10% FBS with penicillin and streptomycin (Invitrogen). The cells were counted with a hemocytometer and plated at the appropriate densities.

Live-Dead Assay on PMs PMs were seeded in 96 well culture plates at 40,000 cells per well and the plates were incubated overnight at 37°C in DMEM 5% CO_2 to allow adhesion. The medium was replaced by fresh DMEM with or without peptide wrwyrggrywrw, and the plates were incubated for an additional 24 hours. The cells were washed twice with 1X PBS and then released from the plate by trypsinization

(0.05% trypsin and 0.2% EDTA in 1X PBS). Cells were then treated with the reagents in the Live/Dead viability/cytotoxicity kit for mammalian cells (Invitrogen) according to the manufacturer's instructions, and analyzed using a BD FACSAria desktop cell sorter with a 70 µm nozzle (Becton-Dickinson). We used the blue laser (488 nm) for calcein (FITC channel) and for the ethidium homodimer (PE channel), and performed manual compensation to avoid overlap between the two colors used. We used cells permeabilzed with ethanol at 70% as our positive single color control for ethidium homodimer (dead cells), and untreated cells in DMEM as our positive single color control for calcein (live cells). 30,000 events were recorded for each sample and analyzed using the FACSDiva software (Becton-Dickinson).

MTT reduction assay on PMs PMs were seeded in 96 well plates at 40,000 cells per well, and the plates were incubated at 37°C in DMEM and 5% CO_2 overnight to allow adhesion. For treatments the medium was removed and replaced with fresh DMEM containing DMSO or wrwyrggrywrw at the indicated concentrations for 24 hours. Following treatment, 20 µl of a 4-mg/mL 3-(4,5-dimethyl-2-thiazolyl)-2,5-diphenyl-2H-tetrazolium bromide (MTT) solution in 1X PBS was added to each well and the cells were incubated 37°C in 5% CO_2 for up to 3 hours to allow the reduction of the MTT. 100 µl of lysis buffer (20% SDS in 1:1 water-dimethyl formamide, 2% glacial acetic acid, 2% 1M hydrochloric acid) was added to each well, and the plates were incubated at 37°C overnight help disperse the dye. The optical density of the reaction mixtures was read at 575 nm the next day with a SpectraMax Plus plate reader (Molecular Devices).

Live-dead assay on human colorectal cancer cells (HCT 116). HCT116 (p53 +/+) cells were seeded at 400,000 cells per well in 6-well tissue culture plates and incubated overnight at 37˚C with 5% CO_2 in complete growth media (DMEM with 10% FBS and 100 μg/mL of Penicillin/Streptomycin). Treatments were conducted in complete growth media as described above and analysis was as described above (section 2.11).

MTT reduction assay human colorectal cancer cells (HCT 116) HCT cells (p53 +/+) were seeded at 10,000 cells/well in 96-well plates, then incubated overnight at 37˚C with 5% CO_2 in complete growth media (DMEM with 10% FBS and 100 μg/mL of Penicillin/Streptomycin). Treatments were conducted in complete growth media as described above and analysis was as described above (section 2.12)

Table 6-2. Bacterial Strain List for Chapter 3

Designation[a]	Species and Strain	Genotype	Source
G255	*S. enterica* serovar Typhimurium	LT2	Laboratory collection
G455	*S. enterica* sv. Typhimurium, AMES	LT2 *din1001*::MudJ(*lacZ*, Km^R) *rfa* Δ[*gal bio uvrB*] *hisG46*	L. Bossi
G582	*E. coli*, MG1655	*rph*-1	S. Lovett
G1018	*P. aeruginosa*	Clinical lung isolate (small colony variant)	F. Rohwer
G510	*B. subtillis*	Spo$^+$	D. Conrad
G565	*S. aureus* MRSA	ATCC 33591 methicillin-resistant	S. Blondelle (TPIMS)
G748	*S. aureus* Newman	Clinical isolate	V. Nizet
G762	*S.pyogenes*, M49	Clinical isolate	V. Nizet

[a]The Segall lab strain designation is given.

Section 6.3. Materials and Methods for Chapter 4

Cloning of peptides WRWYCR and WKHYNY, C-terminal to 6x His-tagged Ubiquitin. The ubiquitin fusion vector was a generous gift from Dr. John Love at SDSU. Primers for the WRWYCR insert (MRP1F and MRP1R, Section 6.3) and the WKHYNY insert (MRP4F and MRP4R, Section 6.3) were synthesized on an ABI 392 DNA synthesizer using standard phosphoramidite chemistry and leaving the Dimethoxytrityl (DMT) group on the 5' end of the oligos for purification. DMT "on" products were purified on a reverse phase, C18 column using 100mM triethylammonium acetate as a buffer and a gradient of 5%-95% acetonitrile for elution. Oligos were ethanol precipitated and the pellet was resuspended in water and treated with 80% glacial acetic acid for 10 minutes to remove the DMT group. The oligos were ethanol precipitated again, and the pellet resuspended in TE buffer. Oligos were quantitated by UV spectrophotometry, annealed in 1X PNK buffer (New England Biolabs, NEB) by mixing at a 1:1 ratio, heating to 95°C for 15 minutes, and then cooling slowly to room temperature. The annealed insert was then used without further purification or phosphorlyation. The fusion vector (0.5 µg) containing an unrelated protein (pUBQ::Engrailed protein) was restricted with 10 Units of KspI (Roche) and 10U of BamHI (NEB) in BamHI buffer (NEB) for 2 hours at 37°C. The cut vector was purified on a 1% agarose gel run at 100V for 4.5 hours in 0.5X TBE (pH 8.0). The gel was stained with 50 µg of ethidium bromide and the bands were visualized using a hand held UV lamp (302nm), excised, and purified from the gel slice using a DNA ultraclean 15 kit (Mo-Bio) following the instructions therein. The cut vector quantitated by UV and was used without further treatment. The annealed insert (100 – 200 ng) and the cut vector (8 – 20 ng) were ligated together in 1X T4

DNA ligase buffer (NEB) with 40 Units of T4 DNA ligase (NEB) at 16 degrees overnight. The reaction was drop-dialyzed against water on a 10000 M.W.C.O. filter, and electroporated into *E. coli* S17 cells for stable maintenance of the plasmid (Strain 1259, Section 6.3), and into an *E. coli* BL21 (DE3) expression strain (Strain G 274, Section 6.3). Following electroporation, cells were allowed 1 hour of recovery in LB at 37° C with shaking, before plating on LB pl ates containing 100 µg/mL ampicillin. Transformants were screened in the PCR assay described below, and then selected clones were sequence verified at the DNA Core facility.

Cloning of peptide WRWYRGGRYWRW, C-terminal to 6x His-tagged Ubiquitin. The plasmid with the WRWYCR insert (above) was used as a template. Primer 1 and 2, (Section 6.3, (Integrated DNA Technologies, IDT)) were used without further purification. PCR amplification used to create the first product was as follows:

1. 95 for 3 minutes
2. 93 for 30 seconds
3. 47 degrees for 30 seconds
4. 72 for 30 seconds
5. Step 2 (repeat 19X)
6. 72 for 15 minutes

Primer 3 (IDT) was combined with the PCR product at a 2:1 molar ratio. This mixture denatured at 95 degrees for 5 minutes, and then cooled slowly to room temperature. This annealed product was used as a template for fill-in PCR with 5U of Klenow (Large Fragment, NEB) in NEB buffer # 3, with 10mM dNTP's, 5% DMSO, 1mM $MgSO_4$, at room temp for 15 minutes. The reaction was monitored on a 2% agarose gel, and was subsequently purified with a DNA Clean-up Kit (Mo-Bio).

The purified fill-in product double digested 20 U of NdeI (NEB) and BamHI (NEB) in Bam Buffer (NEB) and was ligated into the cut vector as described above. *E. coli* S17 cells (Strain 1457, Section 6.3) and BL-21 (DE3, Strain 1458, Section 6.3) cells were transformed, screened, and sequenced as described above.

Colony PCR to screen peptide inserts C-terminal to 6x His-tag Ubiquitin protein. Oligos 8-11 (Section 6.3) were ordered from IDT and used without further purification. Colony PCR was performed in 25 µL reaction volumes with 1X Biolase reaction buffer (Bioline), 4mM Mg^{+2}, 5% DMSO, 200 µM dNTP's, 1 µM primers, and 2 Units of Biolase Taq Polymerase (Bioline). Colonies were stabbed gently with a toothpick, and this was used to inoculate PCR reactions. Thermal cycler program was as follows:

Cycling: Program RIDE2

1. 95 for 5
2. 95 for 30 sec
3. 62 for 30 sec
4. 72 for 1 min
5. Step 2 (repeat 29X)

The products were run on a 0.8% agarose gel for 50 minutes at 70 V, and then stained with 50 µg of ethidium bromide.

Analysis of growth rates and protein expression. 20 mL cultures, subcultured (1:100) from overnights, were grown in LB amp^{100}. OD_{600} readings were taken in microtiter plates in a Spectramax plate reader (Molecular Devices) on 200 µL culture aliquots at the indicated time points. Cultures were treated with IPTG

(0.5mM final) or media (control) at an OD_{600} of between 0.4-0.6. Cultures were allowed to continue to grow for several hours, and then cells were collected. Cell pellets were resuspended in 50 mM Tris (pH 8.0), 100mM NaCl, sonicated (Cell Disrupter, Fisher) three times on 50% duty cycle at room temperature and cell debris were separated by centrifugation. Protein concentrations of the supernatants were equalized using the same re-suspension buffer based on OD_{280} readings. Equal amounts of each sample were loaded on a 4-20% Tris-Glycine SDS gel (Invitrogen) and run at 170V for 50 minutes.

Ubiquitin-peptide fusion expression from minimal media with isotope enriched supplements. Overnight cultures were started from glycerol freezer stocks and grown in LB + amp[100] for no more than 10 hours. Overnights were used directly, without media exchange, to inoculate 1L cultures of 1.5X M9 minimal media (1.5X = 71 mM Na_2HPO_4, 33 mM K_2HPO_4, 51 mM NaCl, supplemented with 10 mL of 100 X Eagle Medium Vitamin solution (Gibco), 3 mM $MgSO_4$, and 0.15mM $CaCl_2$), containing 2g of uniformly labeled ^{13}C glucose (Cambridge isotopes) and 1g of ^{15}N ammonium sulfate (Cambridge isotopes) and ampicillin (50 µg/mL). Expression of the fusion protein was induced at OD_{600} of 0.4-0.6 with 0.5 mM IPTG and then the cells were allowed to grow for another 6 hours. Final OD_{600} values were between 1-1.2. Cells were harvested by centrifugation and frozen immediately at -80.

Cell lysis and affinity column purification. Cells were thawed at room temp in a small volume of 50 mM Tris-HCl (pH 8.0), 100 mM NaCl (Buffer A). Cells were lysed by sonication on ice using a Cell Disrupter (Fisher) on 50% duty cycle continuously

for 3 minutes. Lysate was clarified by centrifugation and the supernatant was filtered through a 0.45 um syringe filter. For each peptide fusion a dedicated 10mL cobalt chelation column (Talon resin, BD) was packed. Purifications were done at room temperature and fusion was eluted from the column in Buffer A + 500mM imidazole (Buffer B) using a segmented gradient from 0% to 50% Buffer B in 1 column volume (CV, variable depending upon the size of the column). The gradient was then held at 50% Buffer B until the absorbance readings at OD 280 were no longer increasing. The column is then washed with 100% Buffer B for 5 minutes. The fusion protein usually eluted at approximately 25% of Buffer B. Fractions containing fusion were verified on 4-20% Tris-Glycine SDS gels, pooled based on the results and were immediately treated with the ubiquitin hydrolase without dialysis.

UCH-L3 hydrolase cleavage. The UCH-L3 expression vector was a generous gift from John Love. UCH-L3 was expressed and purified as described above, except that it was grown in LB + amp[100] and purified over a dedicated cobalt column using the same gradient as described above. Fractions containing the UCH-L3 were pooled and the concentration of the undialyzed hydrolase was calculated using a Bradford assay. A 1:100 molar ratio (UCH-L3: peptide fusion) in the undialyzed purification buffers were mixed overnight at 37 degrees in a shaking incubator. Cleavage was monitored on a 4-20% Tris-Glycine SDS gel (as described above) monitoring the change in mobility of the ubiquitin carrier. In the case of WRWYCR, cleavage of the peptide fusion led to a fluffy white precipitate that was collected by centrifugation at 15,000 rpm, for 1 hour. The insoluble material was separated from the soluble fraction and then redissolved in 6M guanidinium HCl (GHCl). This

material was dialyzed against buffer A to 2M GHCl and both fractions were purified as described below.

Peptide purification. Material from the cleavage reaction was loaded on a low-pressure disposable SillaSep Flash Chromatography C18 column (Silicycle) run on an AKTA Protein Explorer (GE Lifesciences). The mobile phase running buffer was 0.1% TFA in water and elution buffer was 0.1% TFA in Acetonitrile with a flow rate of 4mL / min. Separation of peptide from contaminating material was achieved by using a linear segmented gradient as follows:

1. 0% B until flow-thru was complete (OD 280 was no longer increasing)

2. 20% B in 5 minutes; then hold at 20% B for 15 minutes

3. 30% B in 5 minutes; then hold at 30% B for 15 minutes

4. 50% B in 5 minutes; then hold at 50% B for 5 minutes

5. 100% B in 5 minutes; then hold at 100% B for 5 minutes

5 mL fractions were collected and tested in recombination reactions without further workup.

Excision recombination reactions. Reactions were performed as described in (Boldt *et al.* 2004), with 2 μL of each fraction from the C18 purification added to each reaction to test inhibition. Controls consisted of 2 μL of the mobile phase at approximately the same acetonitrile concentration.

Liquid chromatography-coupled mass spectrometry (LC-MS). Analysis of the fractions by LCMS was conducted exactly as described for the 1609 series of small molecules in the Appendix.

Nuclear Magnetic Resonance. The purified, lyophilized labeled peptides were resuspended in DMSO-d_6 (Sigma) to 600-700 μL. Concentrations for ^{15}N-WRWYCR was approximately 650 mM and ^{13}C-^{15}N WKHYNY was approximately 1.1 mM as judged by UV absorption at 280 nm. Data were recorded on a Varian 600 MHz spectrophotometer equipped with a Varian Auto X ^{1}H[^{13}C/^{15}N] 5mm PFG triple resonance probe. The 2D spectra for WRWYCR were collected at 25° C with 128 t1 increments in the nitrogen dimension with a sweep width of 32 ppm. In the proton dimension, a pulse width of 6.5 and power setting of 60 were used to collect 642 complex points with 8 scans per point over a 12.6 ppm sweep width. A one second relaxation delay was used. Experiments for WKHYNY were collected at 20° C. The 2D HSQC was collected as for WRWYCR, except that a sweep width of 20ppm was used in the nitrogen dimension, and a pulse width of 8.75 and a power setting of 54 were used to collect 1024 points in the proton dimension with 16 scans per point. For the gradient HNCACB experiment on WKHYNY 80 points were collected in the carbon dimension and 918 points in the proton dimension with 8 scans per point and a 1.2 second relaxation time. Spectral widths were 18.4 ppm, 79.6 ppm, and 32.9 ppm for proton, carbon, and nitrogen, respectively. Data analysis for all spectra were performed using NMRDraw and NMRPipe software (Delaglio *et al.* 1995)

Peptide/HJ stability assay. This assay was performed as described in Section 6.2. For HJ analysis and purification by HPLC, junctions were annealed in 0.5X TAEMg

following the standard procedure. Junction DNA was purified over a 5mL anion exchange column (Hi-trap Q FF, G.E. Life Sciences) on a AKTA Protein Explorer (G.E. Life Sciences) using 20 mM Na_3PO_4 (pH 7.0) as a running buffer, and 20 mM Na_3PO_4 (pH 7.0) plus 2 M NaCl as the elution buffer delivered in a linear gradient from 0 to 1M over 30 minutes. DNA was monitored by UV absorption at 260 nm, and fractions were collected for analysis by HPLC. An aliquot from each fraction was passed through individual desalting columns (P6 resin and spin columns from Bio-Rad) and then injected on an analytical anion exchange column (DNApac, Dionex) run on a System Gold HPLC (Beckman, model 168). Retention times and peak characteristics for each fraction were compared with individual strands, or combinations of strands, annealed in 0.5X TAEMg as described above. Samples from the desalting columns were also radioactively end-labeled with T4 PNK as described previously. Prior to electrophoresis, 0.5X TAEMg was added, and the samples were run (without re-annealing) on a 0.5X TAEMg gel as described previously.

Table 6-3. Bacterial Strain List for Chapter 4

Designation[a]	Species and Strain	Genotype	Source
EDT1184	*E.coli* BL21	DE3, pUBQ::WRWYCR	This study
EDT1191	*E.coli* BL21	DE3, pUBQ (empty vector)	This study
EDT1192	*E.coli* BL21	DE3, pUCH-L3	This study
EDT1193	*E.coli* BL21	DE3, pUBQ::WKHYNY	This study
EDT1259	*E.coli*	S-17-1 λpir, pUBQ::WRWYCR	This study
EDT1260	*E.coli*	S-17-1 λpir, pUBQ	This study
EDT1261	*E.coli*	S-17-1 λpir, pUBQ::WKHYNY	This study
EDT1262	*E.coli*	S-17-1 λpir, pUCH-L3	This study
EDT1457	*E.coli*	S-17-1 λpir, pUBQ::WRWYRGGRYWRW	This study
EDT1458	*E.coli*	DE3, pUBQ::WRWYRGGRYWRW	This study

[a]The Segall lab strain designation is given.

Oligonucleotides used in Chapter 4.

5' – GGT GGT TGG CGT TGG TAT TGC CGT TAA TAG G – 3' (MRP1F)

5' – GATCCCTATTAACGGCAATACCAACGCCAACCACCGC – 3' (MRP1R)

5' – GGT GGT TGG AAA CAT TAT AAC TAT TAA TAG G – 3' (MRP4F)

5' – GATCCCTATTAATAGTTATAATGTTTCCAACCACCGC – 3' (MRP4R)

5' – TTG TTT AAC TTT AAG AAG GAG ATA TAC – 3' (Primer 1)

5' – ATA CCA ACG CCA ACC – 3' (Primer 2)

5' – GGC TTT GTT AGC AGC CGG ATC CCT ATT ACC AAC GCC AAT AAC GGC
CAC CTC GAT ACC AAC GCC AAC CAC C – 3' (Primer 3)

5' – CAC CAC CAT CAC CAT CAC GGT GGT TCC – 3' (MR_pUBQ_insert_screen)

5' – CTA TTA ACG GCA ATA CCA ACG CCA – 3' (MR_pUBQ_screen_peptide_8)

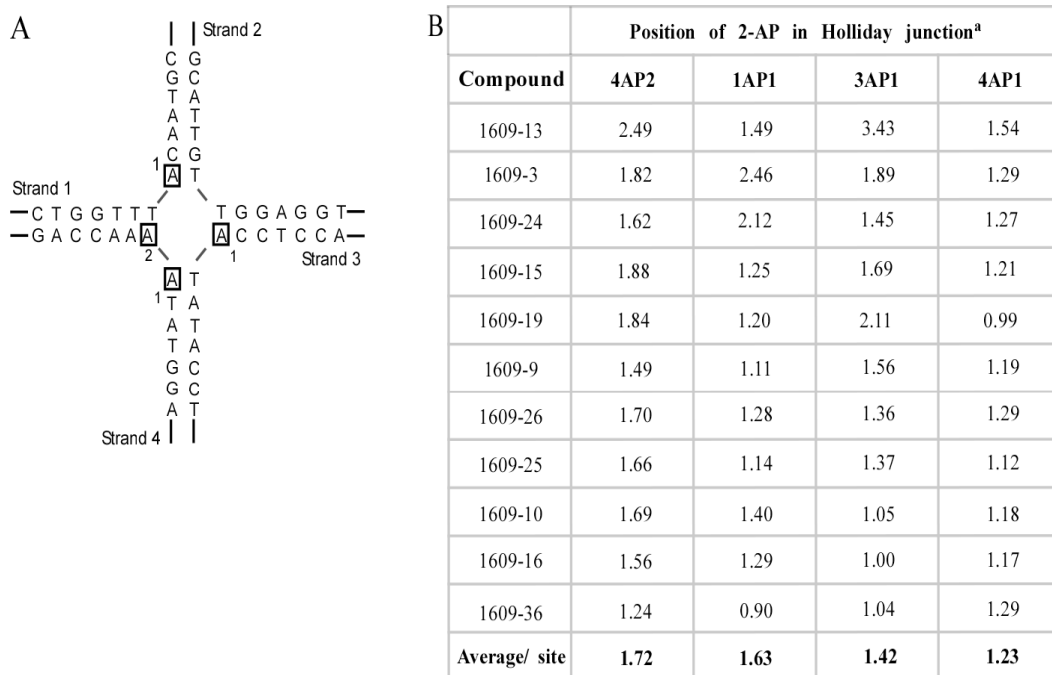5' – CTACCACCAACGCCAACAACGGCCACCTCGATACCAACGCCA – 3' (MRP2
screen)

5' – CGC AAT CCT GAG CAC G – 3' (Chazin 1)

5' – CGT GCT CAC CGA ATG C – 3' (Chazin 2)

5' – GCA TTC GGA CTA TGG C – 3' (Chazin 3)

5' – GCC ATA GTG GAT TGC G – 3' (Chazin 4)

Appendix. Supplemental information for all chapters.

A

```
              |  | Strand 2
              C  G
              G  C
              T  A
              A  T
              A  T
            1 C  G
             [A] T
Strand 1
—C T G G T T T        T G G A G G T—
—G A C C A A[A]      [A] C C T C C A—
            2          1        Strand 3
             [A] T
            1 T  A
              A  T
              T  A
              G  C
              G  C
              A  T
   Strand 4  |  |
```

B

	Position of 2-AP in Holliday junction[a]			
Compound	4AP2	1AP1	3AP1	4AP1
1609-13	2.49	1.49	3.43	1.54
1609-3	1.82	2.46	1.89	1.29
1609-24	1.62	2.12	1.45	1.27
1609-15	1.88	1.25	1.69	1.21
1609-19	1.84	1.20	2.11	0.99
1609-9	1.49	1.11	1.56	1.19
1609-26	1.70	1.28	1.36	1.29
1609-25	1.66	1.14	1.37	1.12
1609-10	1.69	1.40	1.05	1.18
1609-16	1.56	1.29	1.00	1.17
1609-36	1.24	0.90	1.04	1.29
Average/ site	1.72	1.63	1.42	1.23

[a]Positions are noted 1st with the strand (oligo) number, then with the position of the substitution relative to the 5' end of the oligo.

Figure A - 1. 2-aminopurine fluorescence assay for HJ binding

All 36 crude compounds were tested for the ability to quench the fluorescence of a 2-aminopurine substitution placed in the center of a synthetic HJ, at position 2 in strand 4 (4AP2, boxed in panel A). Fluorescence quenching was determined as specified in Materials and Methods and is expressed as a positive ratio: the higher the number, the greater quenching of fluorescence (B). Based on the initial results, 11 small molecules were selected for further examination at the other indicated positions (1AP1, 3AP1, and 4AP1). The decrease in quenching seen at the 4:1 ratio is attributable to the intrinsic fluorescence of the small molecules themselves, and this decrease is also seen with the purified compounds. The fluorescence signal varied based on its location in the junction as demonstrated by the variation in the average/site. The compounds were ranked based on their performance at all four sites.
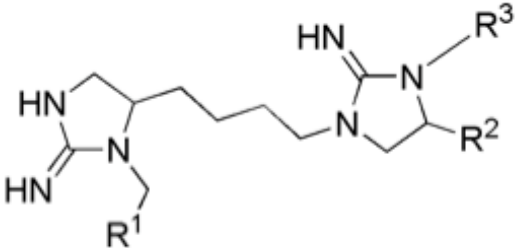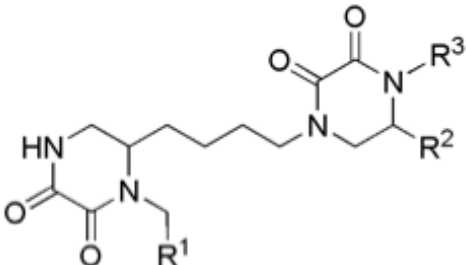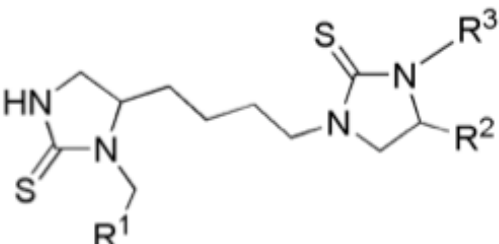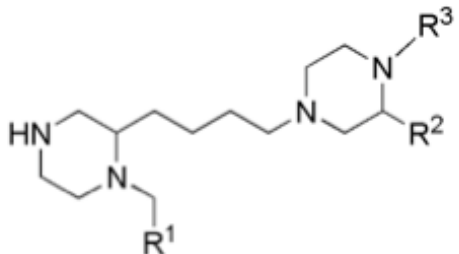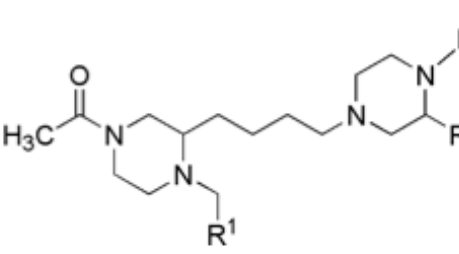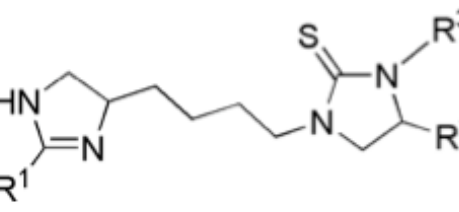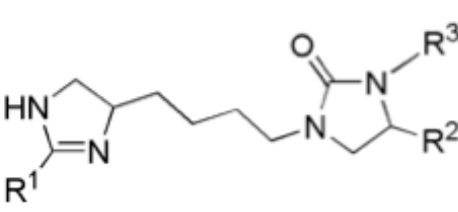
Library	Chemical Name	Structure	Mixtures	Number of Compounds
TPI 1169	Bis-cyclic guanidine		110	45,864
TPI 1170	Bis-diketopiperazine		110	45,864
TPI 1171	Bis-cyclic thiourea		110	45,864

Figure A - 2. Small molecule combinatorial libraries tested.

Shown are the scaffolds upon which the libraries are built. The libraries were selected for their relative two-fold symmetry around the "center" of the scaffold. The number of mixtures in the library is defined as the sum of the functionalities possible for each R group (shown on each scaffold as R^1 - R^3 or R^1 – R^4). Thus, the diversity is defined as the number of functionalities multiplied together. For example, TPI1346 contains 120 mixtures (26 R^1 + 26 R^2 + 26 R^3 + 42 R^4) and a total of 738,192 individual compounds (26 R^1 * 26 R^2 * 26 R^3 * 42 R^4).
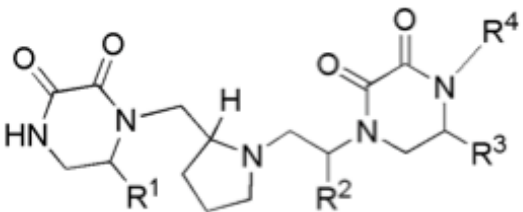
Library	Chemical Name	Structure	Mixtures	Number of Compounds
TPI 1172	Bis-piperazine		110	45,864
TPI 1174	N-acylated bis-piperazine		110	45,864
TPI 1276	Dihydro imidazolyl-butyl-cyclic thiourea		116	56,610
TPI 1319	Dihydro imidazolyl-butyl-cyclic urea		116	56,610

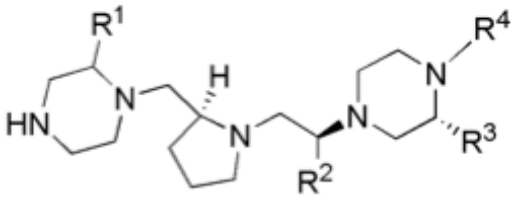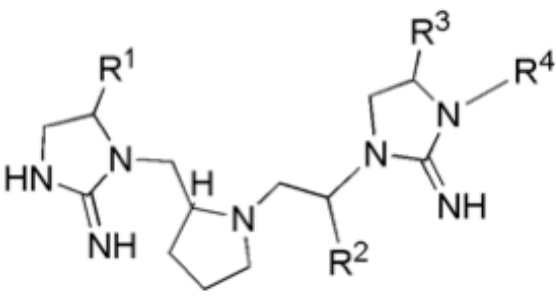**Figure A - 2. Small molecule combinatorial libraries tested (Continued)**
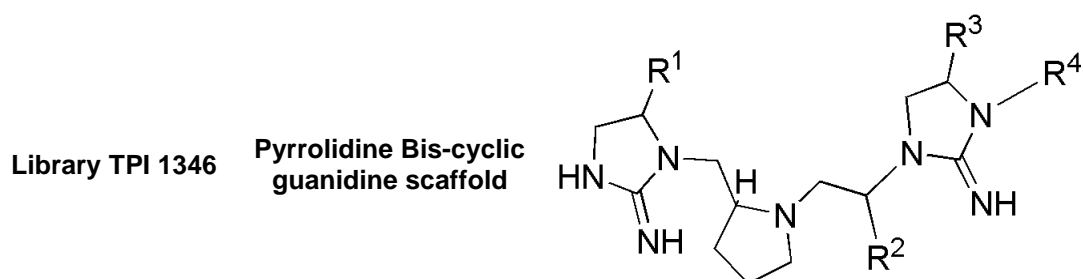
Library	Chemical Name	Structure	Mixtures	Number of Compounds
TPI 1344	Pyrrolidine bis-diketo piperazine		120	738,192
TPI 1345	Pyrrolidine Bis-piperazine		120	738,192
TPI 1346	Pyrrolidine bis-cyclic guanidine		120	738,192

Figure A - 2. Small molecule combinatorial libraries tested (continued).

| Library TPI 1346 | Pyrrolidine Bis-cyclic guanidine scaffold | |

Summary of mixture library TPI1346:

R^1 = 26 amino acids / each mixture = 28,392 compounds

R^2 = 26 amino acids / each mixture = 28,392 compounds

R^3 = 26 amino acids / each mixture = 28,392 compounds

R^4 = 42 carboxylic acids / each mixture = 17,576 compounds

Total diversity = 738,192 compounds

Parent amino acid	Mixture #[a]				Name of Incorporated Functionality
	R^1	R^2	R^3	R^4	
Boc-L-Ala	1	27	53	X	S-methyl
Boc-L-Phe	2	28	54	X	S-benzyl
Boc-Gly	3	29	55	X	hydrogen
Boc-L-Ile	4	30	56	X	S-2-butyl
Boc-L-Leu	5	31	57	X	S-isobutyl
Boc-L-Ser(Bzl)	6	32	58	X	R-hydroxymethyl
Boc-L-Thr(Bzl)	7	33	59	X	(R,R)-1-hydroxyethyl
Boc-L-Val	8	34	60	X	S-isopropyl
Boc-L-Tyr(BrZ)	9	35	61	X	S-4-hydroxybenzyl
Boc-D-Ala	10	36	62	X	R-methyl
Boc-D-Phe	11	37	63	X	R-benzyl
Boc-D-Ile	12	38	64	X	R-2-butyl
Boc-D-Leu	13	39	65	X	R-isobutyl
Boc-D-Ser(Bzl)	14	40	66	X	S-hydroxymethyl
Boc-D-Thr(Bzl)	15	41	67	X	(S,S)-1-hydroxyethyl
Boc-D-Val	16	42	68	X	R-isopropyl
Boc-D-Tyr(BrZ)	17	43	69	X	R-4-hydroxybenzyl
Boc-L-Phenylglycine	18	44	70	X	S-phenyl
Boc-L-Norvaline	19	45	71	X	S-propyl
Boc-D-Norvaline	20	46	72	X	R-propyl
Boc-L-Norleucine	21	47	73	X	S-butyl
Boc-D-Norleucine	22	48	74	X	R-butyl

Figure A - 3. R group functionalities and corresponding building blocks.

Parent amino acid	Mixture # [a]				Name of Incorporated Functionality
	R[1]	R[2]	R[3]	R[4]	
Boc-L-Naphthylalanine	23	49	75	X	S-2-naphthylmethyl
Boc-D-Naphthylalanine	24	50	76	X	R-2-naphthylmethyl
Boc-L-Cyclohexylalanine	25	51	77	X	S-cyclohexyl
Boc-D-Cyclohexylalanine	26	52	78	X	R-cyclohexyl

Parent carboxylic acid	Mixture # [a]				Name of Incorporated Functionality
	R[1]	R[2]	R[3]	R[4]	
1-Phenyl-1-Cyclopropanecarboxylic Acid	X	X	X	79	(1-phenyl-cyclopropyl)-methyl
2-Phenylbutyric Acid	X	X	X	80	2-phenylbutyl
3-Phenylbutyric Acid	X	X	X	81	3-phenylbutyl
m-Tolylacetic Acid	X	X	X	82	*m*-tolylethyl
3-Fluorophenylacetic Acid	X	X	X	83	2-(3-fluoro-phenyl)-ethyl
3-Bromophenylacetic Acid	X	X	X	84	2-(3-bromo-phenyl)-ethyl
(Alpha-Alpha-Alpha-Trifluoro-m-Tolyl) acetic acid	X	X	X	85	2-(3-trifluoromethyl-phenyl)-ethyl
p-Tolylacetic Acid	X	X	X	86	*p*-tolylethyl
4-Fluorophenylacetic Acid	X	X	X	87	2-(4-fluoro-phenyl)-ethyl
3-Methoxyphenylacetic Acid	X	X	X	88	2-(3-methoxy-phenyl)-ethyl
4-Bromophenylacetic Acid	X	X	X	89	2-(4-bromo-phenyl)-ethyl
4-Methoxyphenylacetic Acid	X	X	X	90	2-(4-methoxy-phenyl)-ethyl
4-Ethoxyphenylacetic Acid	X	X	X	91	2-(4-ethoxy-phenyl)-ethyl
4-Isobutyl-alpha-Methylphenylacetic Acid	X	X	X	92	2-(4-Isobutyl-phenyl)-propyl
3,4-Dichlorophenylacetic Acid	X	X	X	93	3,4-dichlorophenethyl
3,5-Bis(Trifluoromethyl)-Phenylacetic Acid	X	X	X	94	2-(3,5-bis-trifluoromethyl-phenyl)-ethyl
3-(3,4-Dimethoxyphenyl)-Propionic Acid	X	X	X	95	3-(3,4-dimethoxy-phenyl)-propyl
Phenylacetic Acid	X	X	X	96	phenethyl
3,4,5-Trimethoxybenzoic Acid	X	X	X	97	3,4,5-trimethoxy-benzyl
Butyric Acid	X	X	X	98	butyl
Heptanoic Acid	X	X	X	99	heptyl
Isobutyric Acid	X	X	X	100	isobutyl
2-Methylbutyric Acid	X	X	X	101	2-methylbutyl
Isovaleric Acid	X	X	X	102	3-methylbutyl

Figure A - 3. R group functionalities and corresponding building blocks (Continued).

Parent Carboxylic Acid	Mixture # [a]				Name of Incorporated Functionality
	R^1	R^2	R^3	R^4	
3-Methylvaleric Acid	X	X	X	103	3-methylpentyl
4-Methylvaleric Acid	X	X	X	104	4-methylpentyl
p-Toluic Acid	X	X	X	105	4-methyl-benzyl
Cyclopentanecarboxylic Acid	X	X	X	106	cyclopently-methyl
Cyclohexanecarboxylic Acid	X	X	X	107	cyclohexyl-methyl
Cyclohexylacetic Acid	X	X	X	108	cyclohexyl-ethyl
Cyclohexanebutyric Acid	X	X	X	109	cyclohexyl-butyl
Cycloheptanecarboxylic Acid	X	X	X	110	cycloheptyl-methyl
2-Methylcyclopropanecarboxylic Acid	X	X	X	111	(2-methyl-cyclopropyl)-methyl
Cyclobutanecarboxylic Acid	X	X	X	112	cyclobutyl-methyl
3-Cyclopentylpropionic Acid	X	X	X	113	3-cyclopentyl-propyl
Cyclohexanepropionic Acid	X	X	X	114	cyclohexyl-propyl
4-Methyl-1-Cyclohexanecarboxylic Acid	X	X	X	115	4-methyl-1-cyclohexyl-methyl
4-tert-Butyl-Cyclohexanecarboxylic Acid	X	X	X	116	4-*tert*-butyl-cyclohexyl-methyl
4-Biphenylacetic Acid	X	X	X	117	2-Biphenyl-4-yl-ethyl
1-Adamantanecarboxylic Acid	X	X	X	118	adamantan-1-yl-methyl
1-Adamantaneacetic Acid	X	X	X	119	2-adamantan-1-yl-ethyl
2-Norbornaneacetic Acid	X	X	X	120	2-Bicyclo[2.2.1]hept-2-yl-ethyl

Figure A - 3. R group functionalities and corresponding building blocks (Continued).

[a]Mixture # references the incorporated functionality (listed) to the indicated R group on the pyrrolidine bis-cyclic guanidine scaffold. An "X" denotes the presence of an nearly equamolar-mixture of all possible functionalities (for any given R group). Since the same functionalities were used for positions R^1 – R^3 these functionalities have been grouped and the "X's" have been excluded. For instance, mixture 1 contains the defined functionality, S-methyl at position R^1 and mixtures at positions R^2 – R^4.
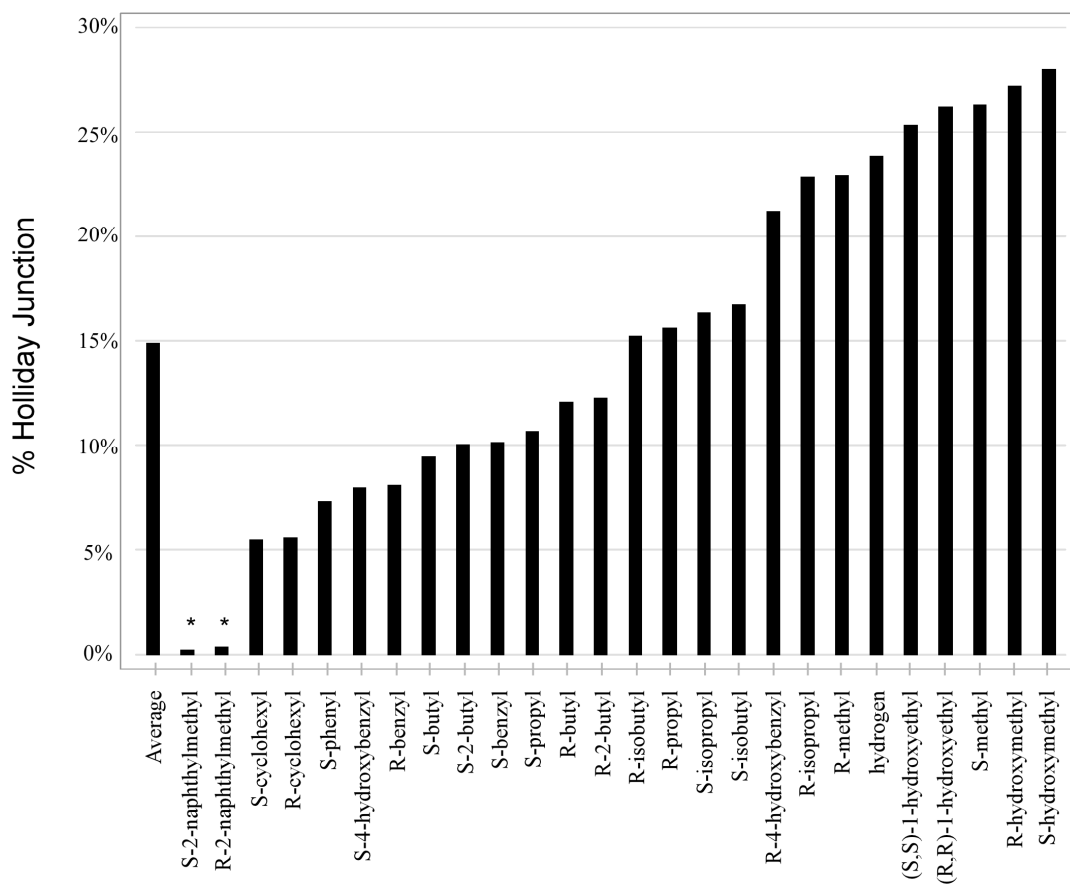
Figure A - 4. Deconvolution of R^1 mixtures in library TPI1346.

Two concentrations (final in the reactions) were tested to differentiate among R groups: 1 mg/mL (shown above) and 0.5 mg/mL (not shown). The activity of S-2-naphthylmethyl and R-2-naphthylmethyl, marked with an asterisk, are consistent with a situation in which too high a concentration of compound inhibits the 1st cleavage step, thereby also reducing the% HJ formed (see Figure 2-1A). Both of these functionalities performed better than all others at 0.5 mg/mL and were selected for synthesis. The screening results shown in Figure A - 4 were performed by Jeff Boldt.
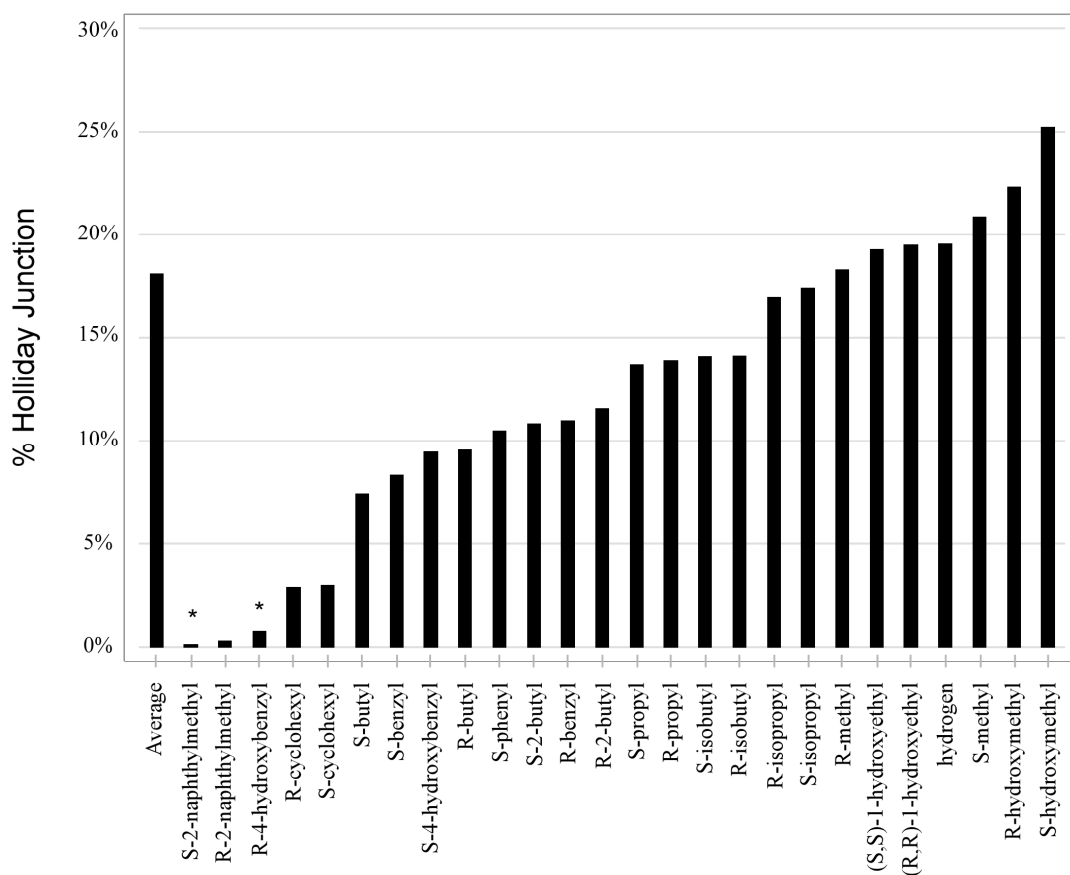
Figure A - 5. Deconvolution of R^2 mixtures in library TPI1346.

Two concentrations (final in the reactions) were tested to differentiate among R groups: 1 mg/mL (shown above) and 0.5 mg/mL (not shown). The activity of S-2-naphthylmethyl and R-4-hydroxybenzyl, marked with an asterisk, are consistent with a situation in which too high a concentration of compound inhibits the 1st cleavage step, thereby also reducing the% HJ formed (see Figure 2-1A). Both of these functionalities performed better than all others at 0.5 mg/mL and were selected for synthesis. The screening results shown in Figure A - 5 were performed by Jeff Boldt.
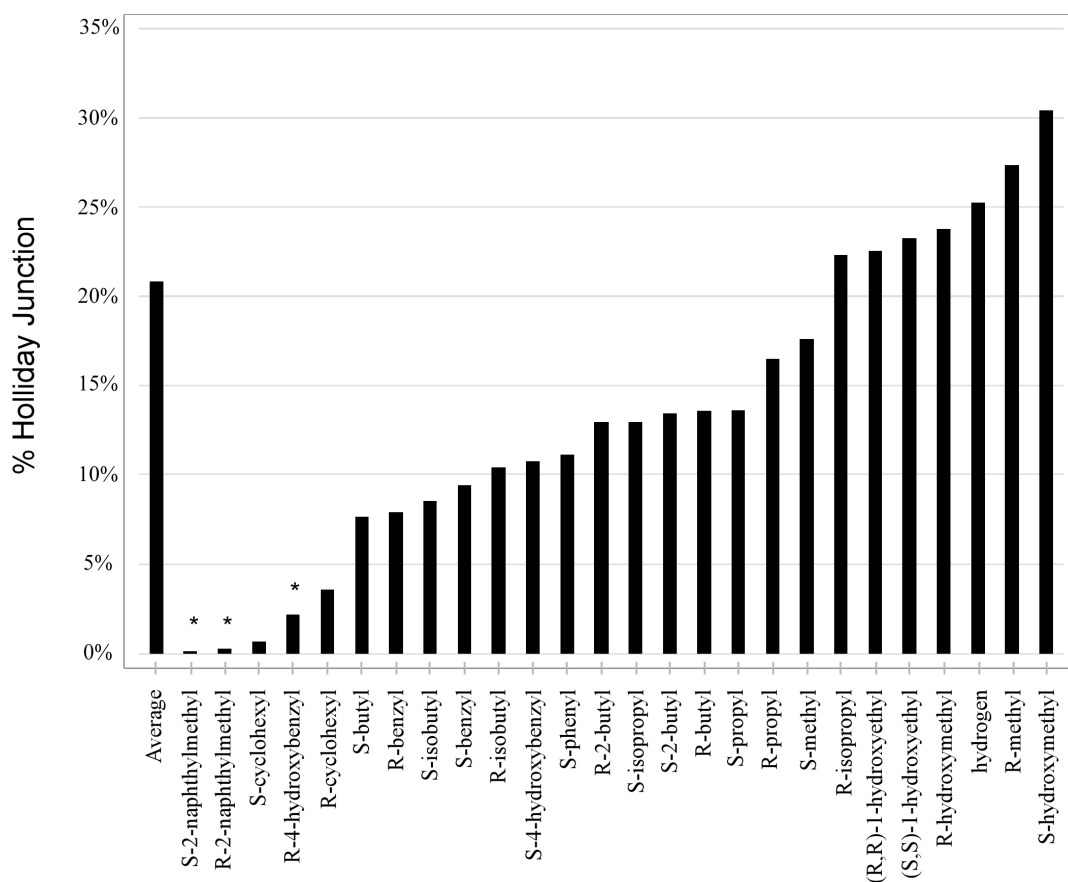
Figure A - 6. Deconvolution of R^3 mixtures in library TPI1346.

Two concentrations (final in the reactions) were tested to differentiate among R groups: 1 mg/mL (shown above) and 0.5 mg/mL (not shown). The activity of S-2-naphthylmethyl, R-2-naphthylmethyl, and R-4-hydroxybenzyl, marked with an asterisk, are consistent with a situation in which too high a concentration of compound inhibits the 1st cleavage step, thereby also reducing the% HJ formed (see Figure 2-1A). All three of these functionalities performed better than the others when included in reactions at 0.5 mg/mL and were selected for synthesis. The screening results shown in Figure A - 6 were performed by Jeff Boldt.
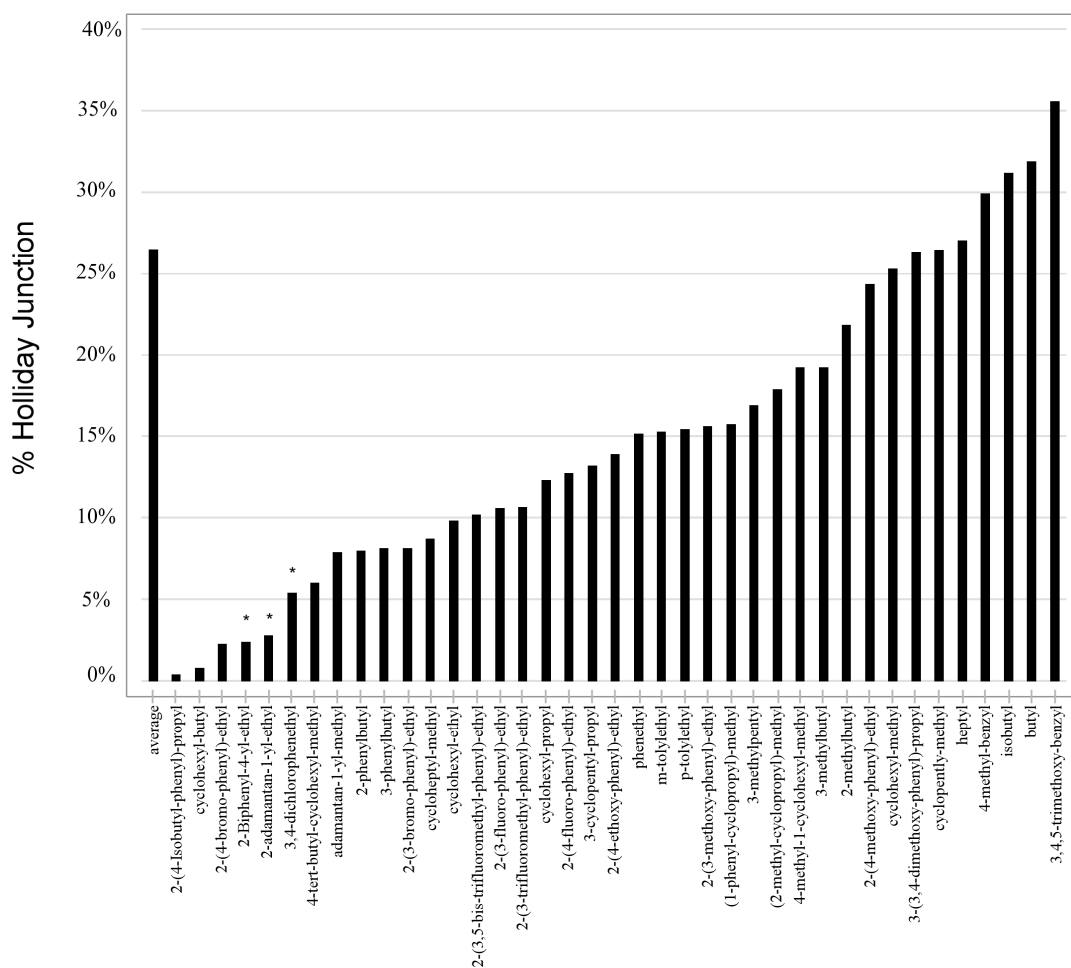
Figure A - 7. Deconvolution of R^4 mixtures in library TPI1346.

Two concentrations (final in the reactions) were tested to differentiate among R groups: 1 mg/mL (shown above) and 0.5 mg/mL (not shown). The activity of 2-biphenyl-4-yl-ethyl, and 3,4-dichlorophenylethyl are consistent with a situation in which too high a concentration of compound inhibits the 1st cleavage step, thereby also reducing the% HJ formed (see Figure 2-1A). These two functionalities performed better than the others when included in reactions at 0.5 mg/mL and were selected for synthesis. 2-adamantan-1-yl-ethyl, was selected for its bulky, non-aromatic structure (see discussion). The screening results shown in Figure A - 7 were performed by Jeff Boldt.
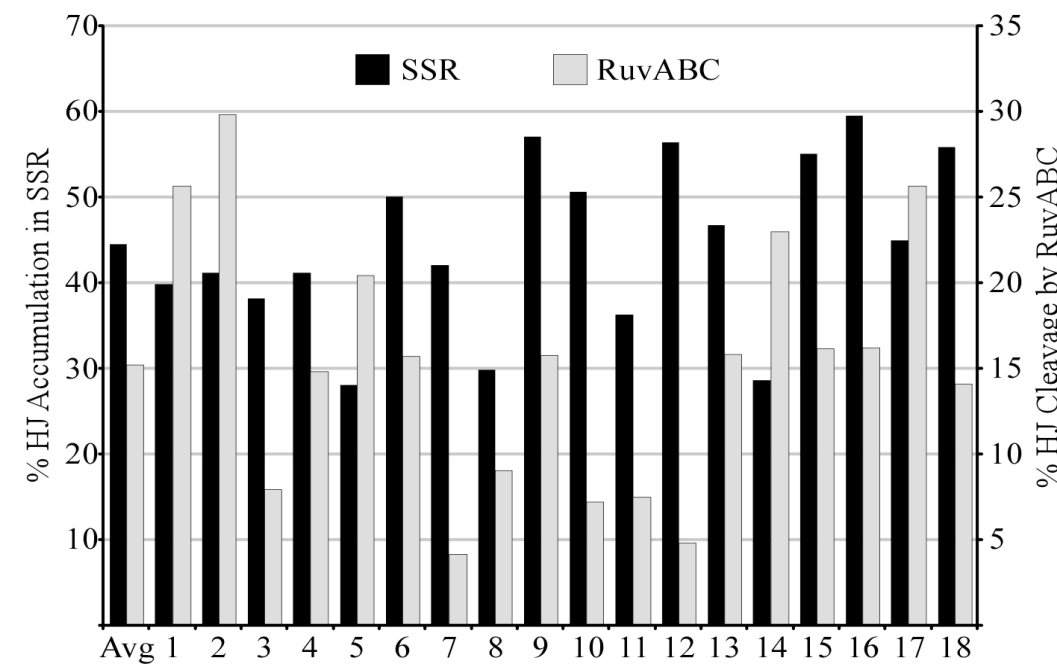
Figure A - 8. Preliminary characterization of crude compounds

Selected compounds (1 – 18, shown on the X axis) were tested in recombination reactions at a final concentration 1 mg/mL and gels were quantitated for the% of HJ accumulated (shown on left Y axis). The crude compounds were also tested for ability to inhibit HJ cleavage by the RuvABC complex of proteins at a final concentration 1 µg/mL. Gels were quantitated for% cleavage normalized to an untreated reaction (right Y axis). The screening of the crude compounds shown was performed by Jeff Boldt.
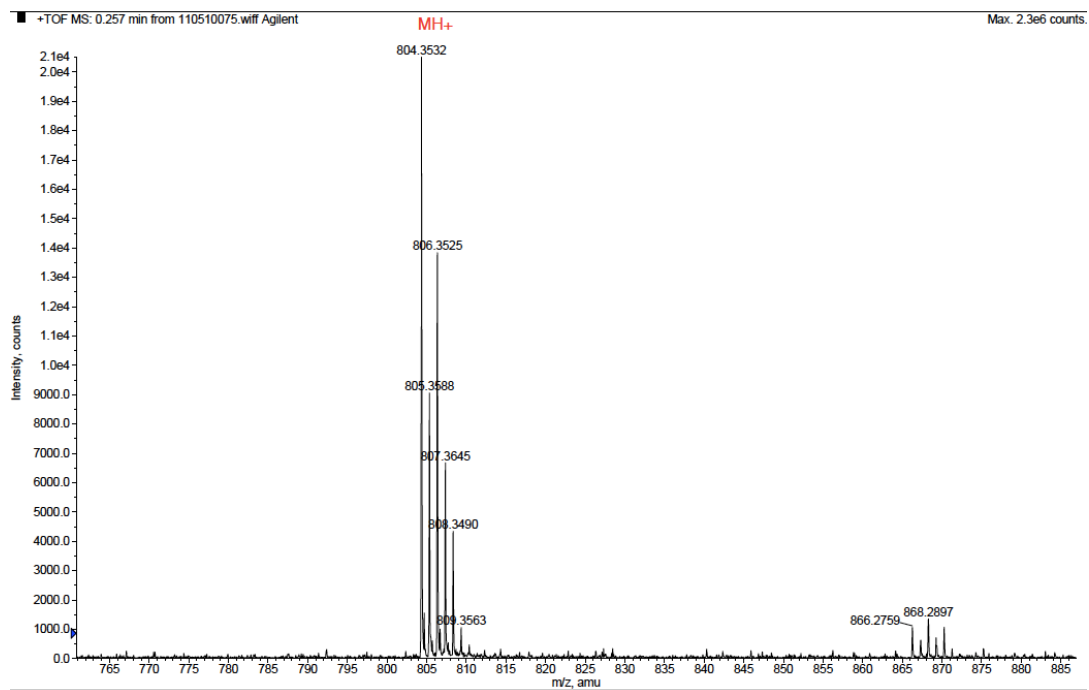
Figure A - 9. High resolution mass spectrum (ESI-TOF) of 1609-1.

1609-1 has an exact mass: 803.3481. The species of approximately + 63 seen in this spectrum are a minor contaminant as judged by LC-MS that represent < 1% of the final product.

Figure A - 10. High resolution mass spectrum (ESI-TOF) of 1609-3.

Compound 1609-3 has an exact mass: 811.4573. The species of approximately + 63 seen in this spectrum are a minor contaminant as judged by LC-MS that represent < 1% of the final product.

Figure A - 11. High resolution mass spectrum (ESI-TOF) of 1609-10.

Compound 1609-10 has an exact mass: 837.3688. The species of approximately + 63 seen in this spectrum are a minor contaminant as judged by LC-MS that represent < 1% of the final product.
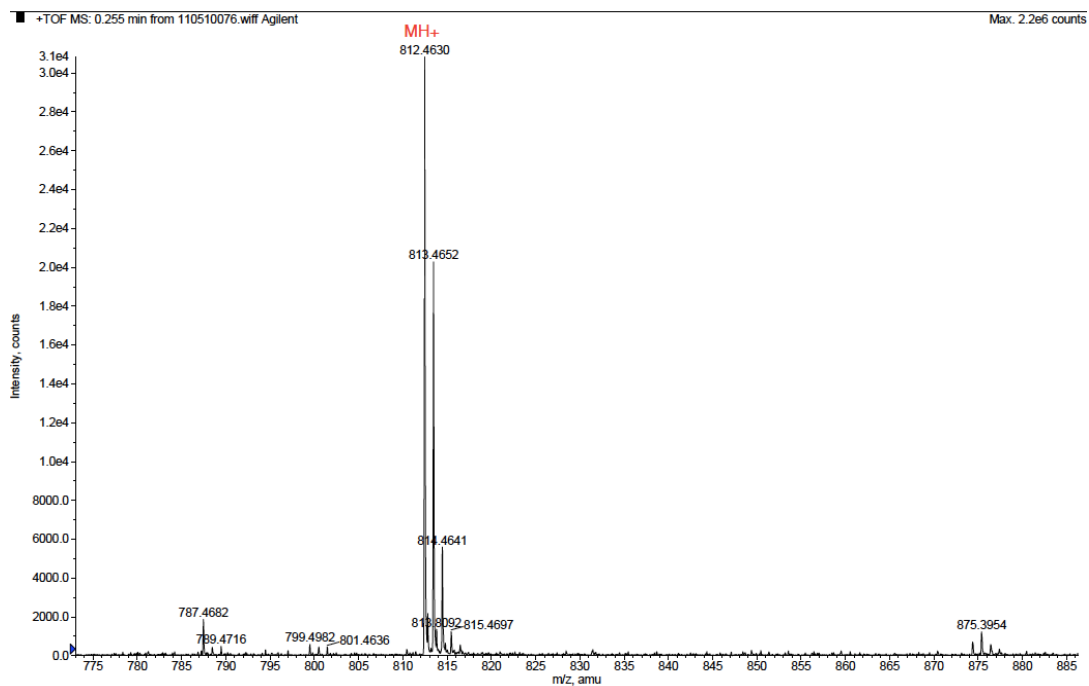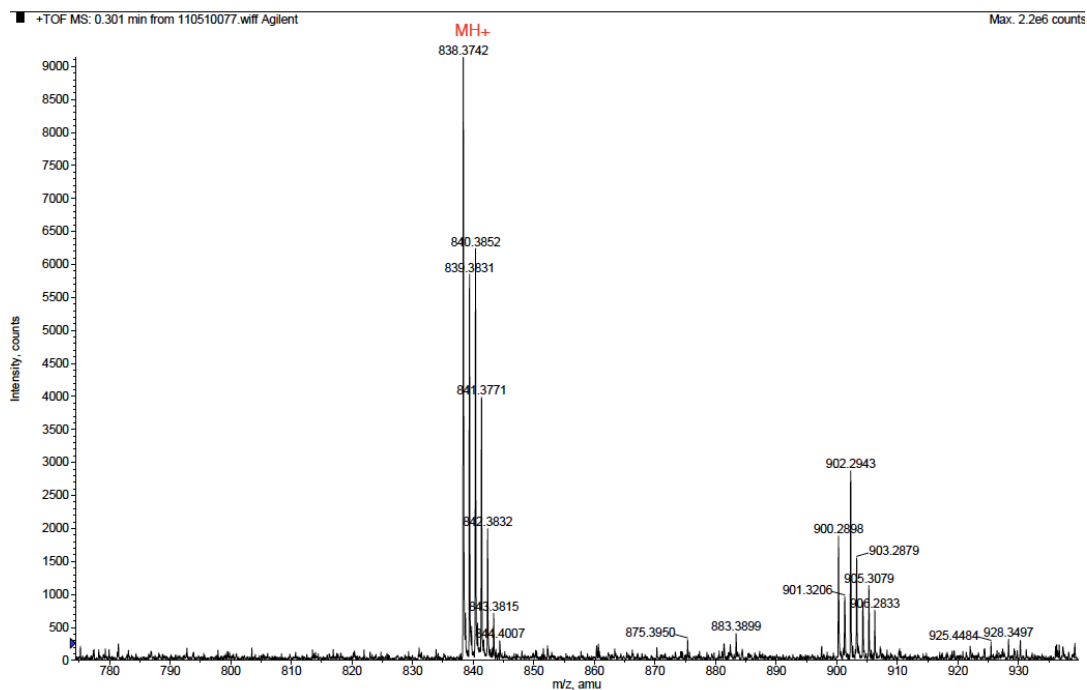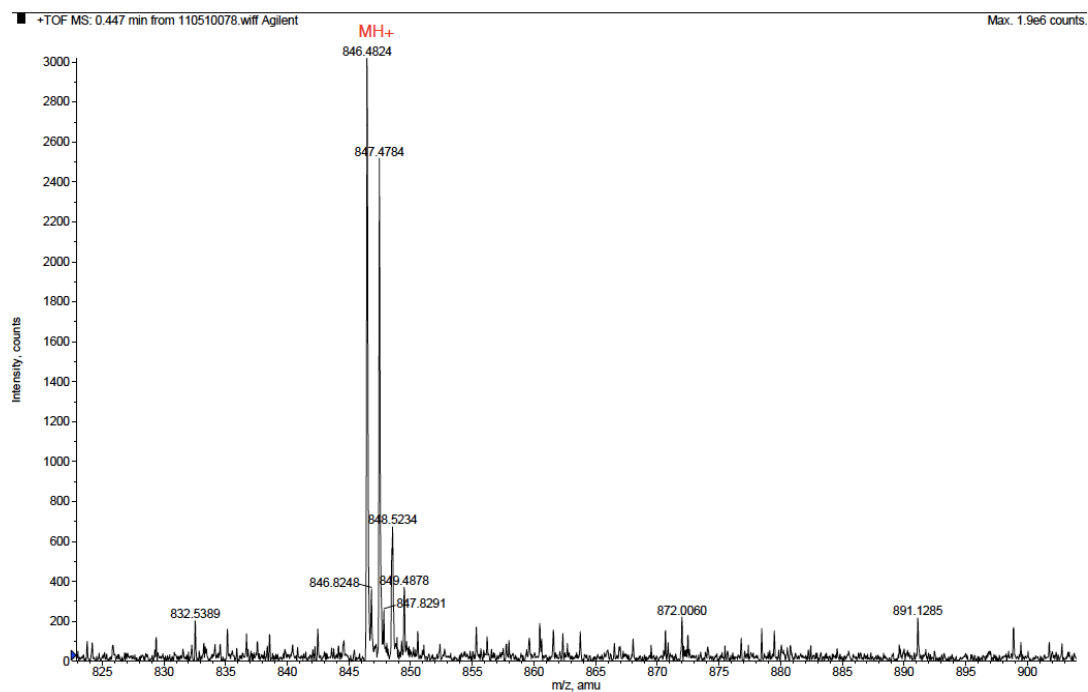
Figure A - 12. High resolution mass spectrum (ESI-TOF) of 1609-12.

Compound 1609-12 has an exact mass: 845.4780.
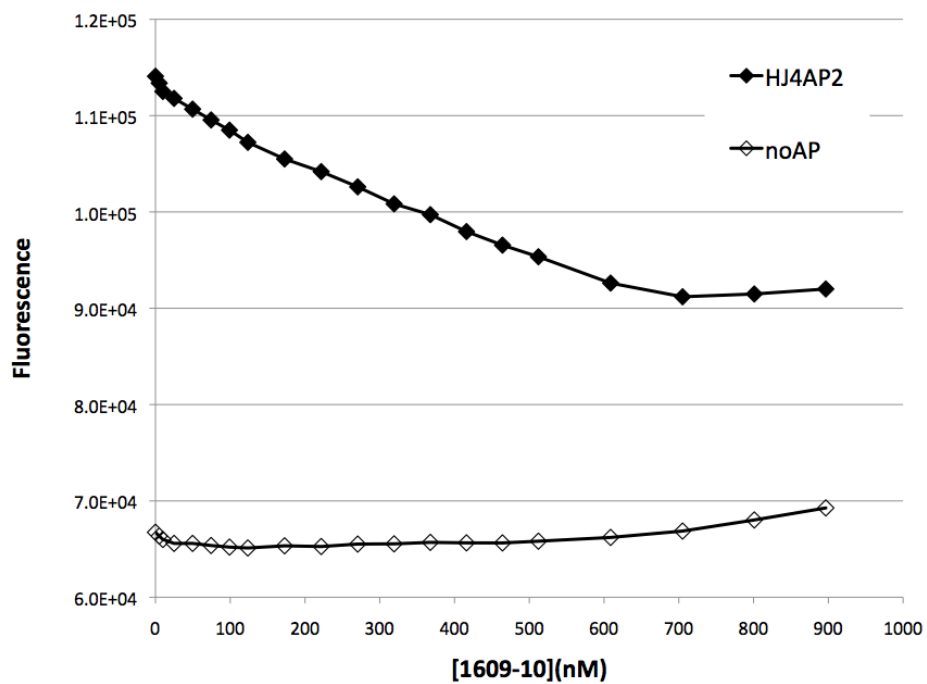
Figure A - 13. Example 2-aminopurine titration set with 1609-10.

Shown are raw fluorescence readings from titrations of HJ4AP2 or noAP junctions with purified 1609-10. Inclusion of 1609-10 leads to a decrease in fluorescence in HJ4AP2 but not the noAP junctions. At high concentrations, 1609-10 has some auto-fluorescence as indicated by the gradual rise in signal. The minimum of quenching seen in the HJ4AP2 curve was used as the saturation point for the modeling described in section 2.2.7.

Analysis of stereochemistry.

To examine the effect of R-group stereochemistry we synthesized molecules with differences in chirality at defined positions. Eighteen comparisons can be made between the R and S isomers of 2 - naphthylmethyl at position R^1 (compounds 1609 – 1 versus 1609 – 19, 2 vs. 20, 3 vs. 21, etc., see Table 1 in main text) and 12 comparisons can be made for the same functional group isomers at positions R^3 (compounds 4 – 6 vs. 7 – 9 and 13 – 15 vs. 16 – 18; or 22 – 24 vs. 25 – 27, and 31 – 33 vs. 34 – 36, Table 1). Comparisons of the data for the 36 crude compounds showed little variationin regards to efficacy in any of our *in vitro* assays, including excision, *ruvABC* cleavage, 2AP fluorescence quenching, or MIC determinations against 4 different bacterial strains [3]). While it is possible that a common contaminant(s) in the crude samples masks the effects of stereochemistry, comparisons of the four purified compounds (1609 – 1, 3, 10 or 12) showed few differences in either excision or MIC values when compared to the values obtained for the crude compounds [3]. This suggests that, first, the crude syntheses have few or no contaminants with activities in our assays, and second, the lack of stereo-specificity for activity *in vitro* HJ processing assays suggests that, given an appropriately flexible scaffold, these compounds may bind to the HJ substrates in several different orientations. This hypothesis is consistent with studies showing similarities *in vitro* between peptides comprised of L versus d amino acids including recombination assays, RecG-mediated HJ unwinding, RuvABC-mediated HJ cleavage, and protein-free HJ binding ([4]; J. Boldt, A. Flores-Fujimoto, M. Rideout, T. Nater, and A. Segall, data not shown). Indeed, if any of our inhibitors are to successfully trap HJ in the context of a growing cell, they should be able to bind in a

variety of conformations to different DNA repair intermediates. *In vivo,* these results support the hypothesis that the molecules may have several modes of action and thus do not require the stereochemistry of a particular functionality, but merely its presence on the scaffold.

Table A - 1. Activities of single-chain linear peptides in site-specific recombination

Parent peptide	Peptide sequence	Excision (IC$_{50}$) (μM)	Excision (IC$_{50}$) (μM)
		(-) DTT	(+) DTT
WRWYCR	WRWYCR[a]	0.021[b]	0.5
	WRWYGGYWRW	0.05	0.15
	WYCRGGRCYW	2	3
	WRWYRGGRYWRW	0.025	0.055
KWWCRW	KWWCRW[a]	1.1[c]	NT
	KWWRGGRWWK	0.25	0.25

[a] WRWYCR and KWWCRW are listed as concentrations of dimer equivalents
[b,c] published (Boldt *et al.* 2004; Gunderson *et al.* 2006)
The data shown are contributions from Jeff Boldt and Marc Rideout
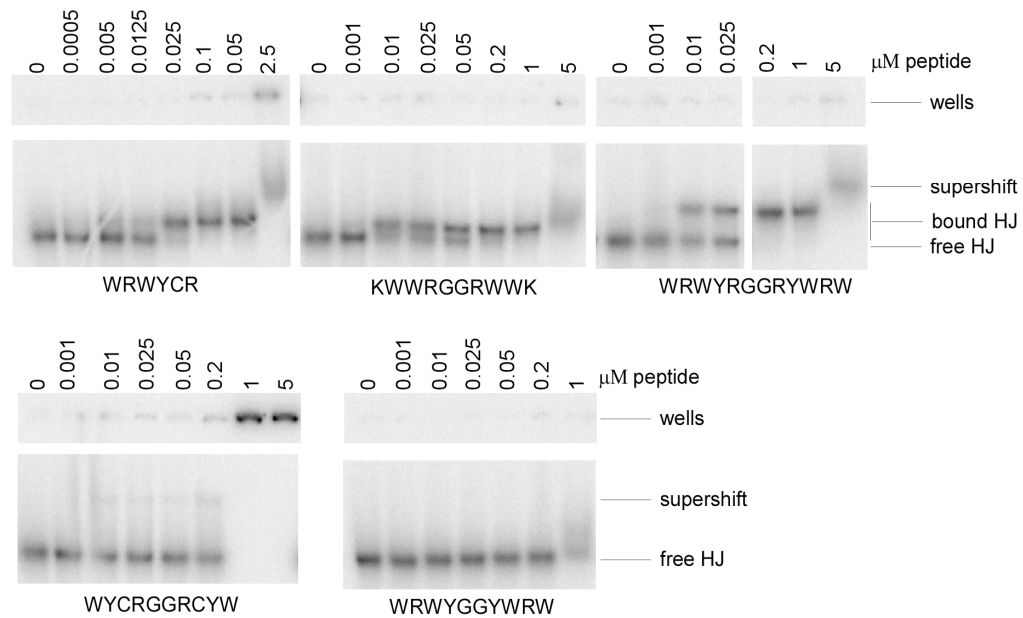
Figure A - 14. Band shifts of WRWYCR, and single-chain linear peptides.

Binding reactions were done in TE + 5% glycerol and were allowed 10 minutes to bind on ice before being electrophoresed on 5% native polyacrylamide gels in 0.5X TBE. Specific shifts can be seen for some of the peptides, and supershifts are likely the result of non-specific interactions. Note that WRWYCR is expressed in terms of dimer equivalents. The band shifts shown were performed by America Flores-Fujimoto.

Figure A - 15. Peptide/HJ stability assay.

WRWYCR (top) or WRWYRGGRYWRW (bottom) are incubated with a short HJ that is not stable for electrophoresis in the absence of Mg^{+2} (no peptide lanes). In the absence of DTT, either peptide can bind the junction together which is seen as a band (HJ) that runs above the 55 nucleotide (nt). In the presence of DTT, only WRWYRGGRYWRW can bind the junction together.

References

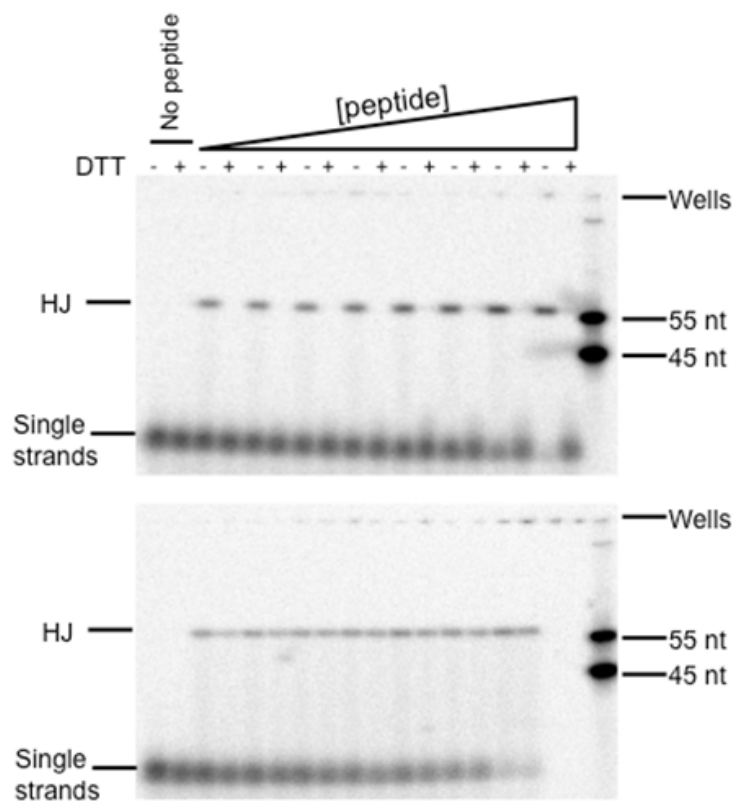Akaike, H (1980). Likelihood and the Bayes procedure. Bayesian Statistics. M. H. DeGroot J. M. Bernardo, D. V. Lindley and A. F. M. Smith (eds). Valencia, Spain, University Press.

Allen, C., A. K. Ashley, R. Hromas and J. A. Nickoloff (2011). "More forks on the road to replication stress recovery." J Mol Cell Biol 3(1): 4-12.

Ames, B. N., F. D. Lee and W. E. Durston (1973). "An improved bacterial test system for the detection and classification of mutagens and carcinogens." Proc Natl Acad Sci U S A 70(3): 782-786.

Ariyoshi, M., T. Nishino, H. Iwasaki, H. Shinagawa and K. Morikawa (2000). "Crystal structure of the holliday junction DNA in complex with a single RuvA tetramer." Proc Natl Acad Sci U S A 97(15): 8257-8262.

Azaro, M. A.; Landy, A. , Ed. (2002). λ Integrase and the λ Int family. Mobile DNA II. Washington D.C., ASM Press.

Bartek, J., C. Lukas and J. Lukas (2004). "Checking on DNA damage in S phase." Nat Rev Mol Cell Biol 5(10): 792-804.

Biroccio, A. and C. Leonetti (2004). "Telomerase as a new target for the treatment of hormone-refractory prostate cancer." Endocr Relat Cancer 11(3): 407-421.

Biswas, T., H. Aihara, M. Radman-Livaja, D. Filman, A. Landy and T. Ellenberger (2005). "A structural basis for allosteric control of DNA recombination by lambda integrase." Nature 435(7045): 1059-1066.

Boldt, J. L. (2006). Second Generation Small Molecule Inhibitors of Lambda Recombination with Enhanced Antimicrobial Activity. Biology. San Diego, San Diego State Universty. Masters.

Boldt, J. L., C. Pinilla and A. M. Segall (2004). "Reversible inhibitors of lambda integrase-mediated recombination efficiently trap Holliday junction intermediates and form the basis of a novel assay for junction resolution." J Biol Chem 279(5): 3472-3483.

Bolla, M. L., E. V. Azevedo, J. M. Smith, R. E. Taylor, D. K. Ranjit, A. M. Segall and S. R. McAlpine (2003). "Novel antibiotics: macrocyclic peptides designed to trap Holliday junctions." Org Lett 5(2): 109-112.

Brogden, A. L., N. H. Hopcroft, M. Searcey and C. J. Cardin (2007). "Ligand bridging of the DNA Holliday junction: molecular recognition of a stacked-X four-way junction by a small molecule." Angew Chem Int Ed Engl 46(21): 3850-3854.

Bryan, T. M., A. Englezou, L. Dalla-Pozza, M. A. Dunham and R. R. Reddel (1997). "Evidence for an alternative mechanism for maintaining telomere length in human tumors and tumor-derived cell lines." Nat Med 3(11): 1271-1274.

Cano, D. A., M. G. Pucciarelli, F. Garcia-del Portillo and J. Casadesus (2002). "Role of the RecBCD recombination pathway in Salmonella virulence." J Bacteriol 184(2): 592-595.

Cassell, G. D. and A. M. Segall (2003). "Mechanism of inhibition of site-specific recombination by the Holliday junction-trapping peptide WKHYNY: insights into phage lambda integrase-mediated strand exchange." J Mol Biol 327(2): 413-429.

Cesare, A. J. and R. R. Reddel (2010). "Alternative lengthening of telomeres: models, mechanisms and implications." Nat Rev Genet 11(5): 319-330.

Champoux, J. J. (2001). "DNA topoisomerases: structure, function, and mechanism." Annu Rev Biochem 70: 369-413.

Cheng, C., P. Kussie, N. Pavletich and S. Shuman (1998). "Conservation of structure and mechanism between eukaryotic topoisomerase I and site-specific recombinases." Cell 92(6): 841-850.

Chopra, I., L. Hesse and A. J. O'Neill (2002). "Exploiting current understanding of antibiotic action for discovery of new drugs." Symp Ser Soc Appl Microbiol(31): 4S-15S.

Connolly, B., C. A. Parsons, F. E. Benson, H. J. Dunderdale, G. J. Sharples, R. G. Lloyd and S. C. West (1991). "Resolution of Holliday junctions *in vitro* requires the Escherichia coli ruvC gene product." Proc Natl Acad Sci U S A 88(14): 6063-6067.

Cox, M. M., M. F. Goodman, K. N. Kreuzer, D. J. Sherratt, S. J. Sandler and K. J. Marians (2000). "The importance of repairing stalled replication forks." Nature 404(6773): 37-41.

Cromie, G. A., J. C. Connelly and D. R. Leach (2001). "Recombination at double-strand breaks and DNA ends: conserved mechanisms from phage to humans." Mol Cell 8(6): 1163-1174.

de Lange, T. (2004). "T-loops and the origin of telomeres." Nat Rev Mol Cell Biol 5(4): 323-329.

Declais, A. C. and D. M. Lilley (2000). "Extensive central disruption of a four-way junction on binding CCE1 resolving enzyme." J Mol Biol 296(2): 421-433.

Declais, A. C. and D. M. Lilley (2008). "New insight into the recognition of branched DNA structure by junction-resolving enzymes." Curr Opin Struct Biol 18(1): 86-95.

Delaglio, F., S. Grzesiek, G. W. Vuister, G. Zhu, J. Pfeifer and A. Bax (1995). "NMRPipe: a multidimensional spectral processing system based on UNIX pipes." J Biomol NMR 6(3): 277-293.

Dwyer, D. J., M. A. Kohanski, B. Hayete and J. J. Collins (2007). "Gyrase inhibitors induce an oxidative damage cellular death pathway in Escherichia coli." Mol Syst Biol 3: 91.

Ferraro, M. J. (2000). National Committee for Clinical Laboratory Standards Methods for Dilution Antimicrobial Susceptibility Tests for Bacteria that Grow Aerobically: Approved Standard. . Wayne, PA: 36.

Ferraro, Mary Jane and National Committee for Clinical Laboratory Standards. (2002). Performance standards for antimicrobial susceptibility testing : twelfth informational supplement. Wayne, PA, National Committee for Clinical Laboratory Standards.

Fujimoto, D. F., C. Pinilla and A. M. Segall (2006). "New peptide inhibitors of type IB topoisomerases: similarities and differences vis-a-vis inhibitors of tyrosine recombinases." J Mol Biol 363(5): 891-907.

Fujimoto, D. F., C. Pinilla and A. M. Segall (2006). "New peptide inhibitors of type IB topoisomerases: similarities and differences vis-a-vis inhibitors of tyrosine recombinases." J Mol Biol 363(5): 891-907.

Georgescu, R. E., N. Y. Yao and M. O'Donnell (2010). "Single-molecule analysis of the Escherichia coli replisome and use of clamps to bypass replication barriers." FEBS Lett 584(12): 2596-2605.

Ghosh, K., C. K. Lau, F. Guo, A. M. Segall and G. D. Van Duyne (2005). "Peptide trapping of the Holliday junction intermediate in Cre-loxP site-specific recombination." J Biol Chem 280(9): 8290-8299.

Goodarzi, A. A., P. Jeggo and M. Lobrich (2010). "The influence of heterochromatin on DNA double strand break repair: Getting the strong, silent type to relax." DNA Repair (Amst) 9(12): 1273-1282.

Grainge, I., M. Bregu, M. Vazquez, V. Sivanathan, S. C. Ip and D. J. Sherratt (2007). "Unlinking chromosome catenanes in vivo by site-specific recombination." EMBO J 26(19): 4228-4238.

Grindley, N. D., K. L. Whiteson and P. A. Rice (2006). "Mechanisms of site-specific recombination." Annu Rev Biochem 75: 567-605.

Gunderson, C. W. and A. M. Segall (2006). "DNA repair, a novel antibacterial target: Holliday junction-trapping peptides induce DNA damage and chromosome segregation defects." Mol Microbiol 59(4): 1129-1148.

Gunderson, C. W., J. L. Boldt, R. N. Authement and A. M. Segall (2009). "Peptide wrwycr inhibits the excision of several prophages and traps holliday junctions inside bacteria." J Bacteriol 191(7): 2169-2176.

Haussler, S. (2004). "Biofilm formation by the small colony variant phenotype of Pseudomonas aeruginosa." Environ Microbiol 6(6): 546-551.

Hazelbaker, D., M. Radman-Livaja and A. Landy (2005). "Receipt of the C-terminal tail from a neighboring lambda Int protomer allosterically stimulates Holliday junction resolution." J Mol Biol 351(5): 948-955.

Heitman, J., T. Ivanenko and A. Kiss (1999). "DNA nicks inflicted by restriction endonucleases are repaired by a RecA- and RecB-dependent pathway in Escherichia coli." Mol Microbiol 33(6): 1141-1151.

Heller, R. C. and K. J. Marians (2006). "Replisome assembly and the direct restart of stalled replication forks." Nat Rev Mol Cell Biol 7(12): 932-943.

Hemmer, B., T. Kondo, B. Gran, C. Pinilla, I. Cortese, J. Pascal, A. Tzou, H. F. McFarland, R. Houghten and R. Martin (2000). "Minimal peptide length requirements for CD4(+) T cell clones--implications for molecular mimicry and T cell survival." Int Immunol 12(3): 375-383.

Hensler, Mary E., Gregory Bernstein, Victor Nizet and Adel Nefzi (2006). "Pyrrolidine bis-cyclic guanidines with antimicrobial activity against drug-resistant Gram-positive pathogens identified from a mixture-based combinatorial library." Bioorganic & Medicinal Chemistry Letters 16(19): 5073-5079.

Holliday, R. (1964). "A mechanism for gene conversion in fungi." Genet Res 5: 282-304.

Houghten, R. A. (1985). "General method for the rapid solid-phase synthesis of large numbers of peptides: specificity of antigen-antibody interaction at the level of individual amino acids." Proc Natl Acad Sci U S A 82(15): 5131-5135.

Houghten, R. A., C. Pinilla, J. R. Appel, S. E. Blondelle, C. T. Dooley, J. Eichler, A. Nefzi and J. M. Ostresh (1999). "Mixture-based synthetic combinatorial libraries." J Med Chem 42(19): 3743-3778.

Houghten, R. A., C. Pinilla, M. A. Giulianotti, J. R. Appel, C. T. Dooley, A. Nefzi, J. M. Ostresh, Y. Yu, G. M. Maggiora, J. L. Medina-Franco, D. Brunner and J. Schneider (2008). "Strategies for the use of mixture-based synthetic combinatorial libraries: scaffold ranking, direct testing *in vivo*, and enhanced deconvolution by computational methods." J Comb Chem 10(1): 3-19.

Ishioka, K., H. Iwasaki and H. Shinagawa (1997). "Roles of the recG gene product of Escherichia coli in recombination repair: effects of the delta recG mutation on cell division and chromosome partition." Genes Genet Syst 72(2): 91-99.

Johnson, R. C. (2002). Bacterial Site-specific DNA inversion systems. Mobile DNA II N. L.; Cragie Craig, R.; Gellert, R.; Lambowitz, A. M. Washington D.C., ASM press: 230-271.

Joo, C., S. A. McKinney, D. M. Lilley and T. Ha (2004). "Exploring rare conformational species and ionic effects in DNA Holliday junctions using single-molecule spectroscopy." J Mol Biol 341(3): 739-751.

Kallenbach, N. R., R. I. Ma, A. J. Wand, G. H. Veeneman, J. H. van Boom and N. C. Seeman (1983). "Fourth rank immobile nucleic acid junctions." J Biomol Struct Dyn 1(1): 159-168.

Kepple, K. V., J. L. Boldt and A. M. Segall (2005). "Holliday junction-binding peptides inhibit distinct junction-processing enzymes." Proc Natl Acad Sci U S A 102(19): 6867-6872.

Kepple, K. V., N. Patel, P. Salamon and A. M. Segall (2008). "Interactions between branched DNAs and peptide inhibitors of DNA repair." Nucleic Acids Res 36(16): 5319-5334.

Klemm, M., C. Cheng, G. Cassell, S. Shuman and A. M. Segall (2000). "Peptide inhibitors of DNA cleavage by tyrosine recombinases and topoisomerases." J Mol Biol 299(5): 1203-1216.

Kohanski, M. A., D. J. Dwyer and J. J. Collins (2010). "How antibiotics kill bacteria: from targets to networks." Nat Rev Microbiol 8(6): 423-435.

Kohanski, M. A., D. J. Dwyer, B. Hayete, C. A. Lawrence and J. J. Collins (2007). "A common mechanism of cellular death induced by bactericidal antibiotics." Cell 130(5): 797-810.

Kohno, T., H. Kusunoki, K. Sato and K. Wakamatsu (1998). "A new general method for the biosynthesis of stable isotope-enriched peptides using a decahistidine-tagged ubiquitin fusion system: an application to the production of mastoparan-X uniformly enriched with 15N and 15N/13C." J Biomol NMR 12(1): 109-121.

Kramer, A., T. Keitel, K. Winkler, W. Stocklein, W. Hohne and J. Schneider-Mergener (1997). "Molecular basis for the binding promiscuity of an anti-p24 (HIV-1) monoclonal antibody." Cell 91(6): 799-809.

Lamarche, B. J., N. I. Orazio and M. D. Weitzman (2010). "The MRN complex in double-strand break repair and telomere maintenance." FEBS Lett 584(17): 3682-3695.

Larsen, C. N., J. S. Price and K. D. Wilkinson (1996). "Substrate binding and catalysis by ubiquitin C-terminal hydrolases: identification of two active site residues." Biochemistry 35(21): 6735-6744.

Leung, E., D. E. Weil, M. Raviglione and H. Nakatani (2011). "The WHO policy package to combat antimicrobial resistance." Bull World Health Organ 89(5): 390-392.

Lilley, D. M. (2008). "Analysis of branched nucleic acid structure using comparative gel electrophoresis." Q Rev Biophys 41(1): 1-39.

Lipinski, C. A. (2000). "Drug-like properties and the causes of poor solubility and poor permeability." J Pharmacol Toxicol Methods 44(1): 235-249.

Lipinski, C. A., F. Lombardo, B. W. Dominy and P. J. Feeney (2001). "Experimental and computational approaches to estimate solubility and permeability in drug discovery and development settings." Adv Drug Deliv Rev 46(1-3): 3-26.

Liu, Y., M. Tarsounas, P. O'Regan and S. C. West (2007). "Role of RAD51C and XRCC3 in genetic recombination and DNA repair." J Biol Chem 282(3): 1973-1979.

Lloyd, R. G. (1991). "Conjugational recombination in resolvase-deficient ruvC mutants of Escherichia coli K-12 depends on recG." J Bacteriol 173(17): 5414-5418.

Loughlin, M. F., F. M. Barnard, D. Jenkins, G. J. Sharples and P. J. Jenks (2003). "Helicobacter pylori mutants defective in RuvC Holliday junction resolvase display reduced macrophage survival and spontaneous clearance from the murine gastric mucosa." Infect Immun 71(4): 2022-2031.

Lu, T. K. and J. J. Collins (2009). "Engineered bacteriophage targeting gene networks as adjuvants for antibiotic therapy." Proc Natl Acad Sci U S A 106(12): 4629-4634.

Maxmen, A. (2010). "Beyond PARP inhibitors: agents in pipelines target DNA repair mechanisms." J Natl Cancer Inst 102(15): 1110-1111.

McGlynn, P. and R. G. Lloyd (2002). "Recombinational repair and restart of damaged replication forks." Nat Rev Mol Cell Biol 3(11): 859-870.

McKinney, S. A., A. C. Declais, D. M. Lilley and T. Ha (2003). "Structural dynamics of individual Holliday junctions." Nat Struct Biol 10(2): 93-97.

McKinney, S. A., A. D. Freeman, D. M. Lilley and T. Ha (2005). "Observing spontaneous branch migration of Holliday junctions one step at a time." Proc Natl Acad Sci U S A 102(16): 5715-5720.

Meddows, T. R., A. P. Savory and R. G. Lloyd (2004). "RecG helicase promotes DNA double-strand break repair." Mol Microbiol 52(1): 119-132.

Megnin-Chanet, F., M. A. Bollet and J. Hall (2010). "Targeting poly(ADP-ribose) polymerase activity for cancer therapy." Cell Mol Life Sci 67(21): 3649-3662.

Merrifield, R. B. (1964). "Solid-Phase Peptide Synthesis. 3. An Improved Synthesis of Bradykinin." Biochemistry 3: 1385-1390.

Michel, B., H. Boubakri, Z. Baharoglu, M. LeMasson and R. Lestini (2007). "Recombination proteins and rescue of arrested replication forks." DNA Repair (Amst) 6(7): 967-980.

Mosmann, T. (1983). "Rapid colorimetric assay for cellular growth and survival: application to proliferation and cytotoxicity assays." J Immunol Methods 65(1-2): 55-63.

Nabetani, A. and F. Ishikawa (2011). "Alternative lengthening of telomeres pathway: recombination-mediated telomere maintenance mechanism in human cells." J Biochem 149(1): 5-14.

Nefzi, A., J. M. Ostresh, J. R. Appel, J. Bidlack, C. T. Dooley and R. A. Houghten (2006). "Identification of potent and highly selective chiral tri-amine and tetra-amine mu opioid receptors ligands: an example of lead optimization using mixture-based libraries." Bioorg Med Chem Lett 16(16): 4331-4338.

Nefzi, Adel, John M. Ostresh, Marc Giulianotti and Richard A. Houghten (1999). "Solid-Phase Synthesis of Trisubstituted 2-Imidazolidones and 2-Imidazolidinethiones." Journal of Combinatorial Chemistry 1(3): 195-198.

Neidle, S. (2010). "Human telomeric G-quadruplex: the current status of telomeric G-quadruplexes as therapeutic targets in human cancer." FEBS J 277(5): 1118-1125.

Nguyen, L. T., E. F. Haney and H. J. Vogel (2011). "The expanding scope of antimicrobial

Ogawa, T., X. Yu, A. Shinohara and E. H. Egelman (1993). "Similarity of the yeast RAD51 filament to the bacterial RecA filament." Science 259(5103): 1896-1899.

Oleksy, A., A. G. Blanco, R. Boer, I. Uson, J. Aymami, A. Rodger, M. J. Hannon and M. Coll (2006). "Molecular recognition of a three-way DNA junction by a metallosupramolecular helicate." Angew Chem Int Ed Engl 45(8): 1227-1231.

Pan, P. S., F. A. Curtis, C. L. Carroll, I. Medina, L. A. Liotta, G. J. Sharples and S. R. McAlpine (2006). "Novel antibiotics: C-2 symmetrical macrocycles inhibiting Holliday junction DNA binding by *E. coli* RuvC." Bioorg Med Chem 14(14): 4731-4739.

Parsons, C. A., I. Tsaneva, R. G. Lloyd and S. C. West (1992). "Interaction of Escherichia coli RuvA and RuvB proteins with synthetic Holliday junctions." Proc Natl Acad Sci U S A 89(12): 5452-5456.

Pegg, A. E. (2000). "Repair of O(6)-alkylguanine by alkyltransferases." Mutat Res 462(2-3): 83-100.

Petermann, E. and T. Helleday (2010). "Pathways of mammalian replication fork restart." Nat Rev Mol Cell Biol 11(10): 683-687.

Pilon, A., P. Yost, T. E. Chase, G. Lohnas, T. Burkett, S. Roberts and W. E. Bentley (1997). "Ubiquitin fusion technology: bioprocessing of peptides." Biotechnol Prog 13(4): 374-379.

Pinilla, C., J. R. Appel, E. Borras and R. A. Houghten (2003). "Advances in the use of synthetic combinatorial chemistry: mixture-based libraries." Nat Med 9(1): 118-122.

Pinilla, C., J. R. Appel, P. Blanc and R. A. Houghten (1992). "Rapid identification of high affinity peptide ligands using positional scanning synthetic peptide combinatorial libraries." Biotechniques 13(6): 901-905.

Pitcher, R. S., N. C. Brissett and A. J. Doherty (2007). "Nonhomologous end-joining in bacteria: a microbial perspective." Annu Rev Microbiol 61: 259-282.

Raghavan, S., Z. Yang, R. T. Mosley, W. A. Schleif, L. Gabryelski, D. B. Olsen, M. Stahlhut, L. C. Kuo, E. A. Emini, K. T. Chapman and J. R. Tata (2002). "Combinatorial library of indinavir analogues: replacement for the aminoindanol at P2'." Bioorg Med Chem Lett 12(20): 2855-2858.

Rajeev, L., A. Segall and J. Gardner (2007). "The bacteroides NBU1 integrase performs a homology-independent strand exchange to form a holliday junction intermediate." J Biol Chem 282(43): 31228-31237.

Rajeev, L., A. Segall and J. Gardner (2007). "The bacteroides NBU1 integrase performs a homology-independent strand exchange to form a holliday junction intermediate." J Biol Chem 282(43): 31228-31237.

Ranjit, D. K. (2004). Small Molecules That Inhibit Recombination and Bacterial Growth. San Diego San Diego State University. Masters thesis.

Ranjit, D. K., M. C. Rideout, A. Nefzi, J. M. Ostresh, C. Pinilla and A. M. Segall (2010). "Small molecule functional analogs of peptides that inhibit lambda site-specific recombination and bind Holliday junctions." Bioorg Med Chem Lett 20(15): 4531-4534.

Rass, U., S. A. Compton, J. Matos, M. R. Singleton, S. C. Ip, M. G. Blanco, J. D. Griffith and S. C. West (2010). "Mechanism of Holliday junction resolution by the human GEN1 protein." Genes Dev 24(14): 1559-1569.

Reilley, K. J., M. Giulianotti, C. T. Dooley, A. Nefzi, J. P. McLaughlin and R. A. Houghten (2010). "Identification of two novel, potent, low-liability antinociceptive compounds from the direct *in vivo* screening of a large mixture-based combinatorial library." AAPS J 12(3): 318-329.

Rinnova, M., A. Nefzi and R. A. Houghten (2002). "Opioid activity of 4-imidazolidinone positional analogues of Leu-Enkephalin." Bioorg Med Chem Lett 12(21): 3175-3178.

Roberts, R. R., B. Hota, I. Ahmad, R. D. Scott, 2nd, S. D. Foster, F. Abbasi, S. Schabowski, L. M. Kampe, G. G. Ciavarella, M. Supino, J. Naples, R. Cordell, S. B. Levy and R. A. Weinstein (2009). "Hospital and societal costs of antimicrobial-resistant infections in a Chicago teaching hospital: implications for antibiotic stewardship." Clin Infect Dis 49(8): 1175-1184.

Rocha, E. P., E. Cornet and B. Michel (2005). "Comparative and evolutionary analysis of the bacterial homologous recombination systems." PLoS Genet 1(2): e15.

Rohwer, F. and F. Azam (2000). "Detection of DNA damage in prokaryotes by terminal deoxyribonucleotide transferase-mediated dUTP nick end labeling." Appl Environ Microbiol 66(3): 1001-1006.

Rudolph, C. J., A. L. Upton and R. G. Lloyd (2009). "Replication fork collisions cause pathological chromosomal amplification in cells lacking RecG DNA translocase." Mol Microbiol 74(4): 940-955.

Rudolph, C. J., A. L. Upton, G. S. Briggs and R. G. Lloyd (2010). "Is RecG a general guardian of the bacterial genome?" DNA Repair (Amst) 9(3): 210-223.

Sambrook, Joseph and David W. Russell (2001). Molecular cloning : a laboratory manual. Cold Spring Harbor, N.Y., Cold Spring Harbor Laboratory Press.

Scheel, C., K. L. Schaefer, A. Jauch, M. Keller, D. Wai, C. Brinkschmidt, F. van Valen, W. Boecker, B. Dockhorn-Dworniczak and C. Poremba (2001). "Alternative lengthening of telomeres is associated with chromosomal instability in osteosarcomas." Oncogene 20(29): 3835-3844.

Schimmer, A. D., K. Welsh, C. Pinilla, Z. Wang, M. Krajewska, M. J. Bonneau, I. M. Pedersen, S. Kitada, F. L. Scott, B. Bailly-Maitre, G. Glinsky, D. Scudiero, E. Sausville, G. Salvesen, A. Nefzi, J. M. Ostresh, R. A. Houghten and J. C. Reed (2004). "Small-molecule antagonists of apoptosis suppressor XIAP exhibit broad antitumor activity." Cancer Cell 5(1): 25-35.

Seeman, N. C. and N. R. Kallenbach (1983). "Design of immobile nucleic acid junctions." Biophys J 44(2): 201-209.

Segall, A. M. and H. A. Nash (1996). "Architectural flexibility in lambda site-specific recombination: three alternate conformations channel the attL site into three distinct pathways." Genes Cells 1(5): 453-463.

Sharples, G. J., S. M. Ingleston and R. G. Lloyd (1999). "Holliday junction processing in bacteria: insights from the evolutionary conservation of RuvABC, RecG, and RusA." J Bacteriol 181(18): 5543-5550.

Shinohara, A., H. Ogawa and T. Ogawa (1992). "Rad51 protein involved in repair and recombination in S. cerevisiae is a RecA-like protein." Cell 69(3): 457-470.

Singleton, M. R., M. S. Dillingham, M. Gaudier, S. C. Kowalczykowski and D. B. Wigley (2004). "Crystal structure of RecBCD enzyme reveals a machine for processing DNA breaks." Nature 432(7014): 187-193.

Slocum, S. L., J. A. Buss, Y. Kimura and P. R. Bianco (2007). "Characterization of the ATPase activity of the Escherichia coli RecG protein reveals that the preferred cofactor is negatively supercoiled DNA." J Mol Biol 367(3): 647-664.

Spellberg, B., M. Blaser, R. J. Guidos, H. W. Boucher, J. S. Bradley, B. I. Eisenstein, D. Gerding, R. Lynfield, L. B. Reller, J. Rex, D. Schwartz, E. Septimus, F. C. Tenover and D. N. Gilbert (2011). "Combating antimicrobial resistance: policy recommendations to save lives." Clin Infect Dis 52 Suppl 5: S397-428.

Spindler, E. C., J. D. Hale, T. H. Giddings, Jr., R. E. Hancock and R. T. Gill (2011). "Deciphering the mode of action of the synthetic antimicrobial peptide Bac8c." Antimicrob Agents Chemother 55(4): 1706-1716.

Stewart, E. J., F. Aslund and J. Beckwith (1998). "Disulfide bond formation in the Escherichia coli cytoplasm: an *in vivo* role reversal for the thioredoxins." EMBO J 17(19): 5543-5550.

Su, L. Y., D. L. Willner and A. M. Segall (2010). "An antimicrobial peptide that targets DNA repair intermediates *in vitro* inhibits Salmonella growth within murine macrophages." Antimicrob Agents Chemother 54(5): 1888-1899.

Sutherland, J. H. and Y. C. Tse-Dinh (2010). "Analysis of RuvABC and RecG involvement in the escherichia coli response to the covalent topoisomerase-DNA complex." J Bacteriol 192(17): 4445-4451.

Taubes, G. (2008). "The bacteria fight back." Science 321(5887): 356-361.

Ulrich, E. L., H. Akutsu, J. F. Doreleijers, Y. Harano, Y. E. Ioannidis, J. Lin, M. Livny, S. Mading, D. Maziuk, Z. Miller, E. Nakatani, C. F. Schulte, D. E. Tolmie, R. Kent Wenger, H. Yao and J. L. Markley (2008). "BioMagResBank." Nucleic Acids Res 36(Database issue): D402-408.

Walker, B., S. Barrett, S. Polasky, V. Galaz, C. Folke, G. Engstrom, F. Ackerman, K. Arrow, S. Carpenter, K. Chopra, G. Daily, P. Ehrlich, T. Hughes, N. Kautsky, S. Levin, K. G. Maler, J. Shogren, J. Vincent, T. Xepapadeas and A. de Zeeuw (2009). "Environment. Looming global-scale failures and missing institutions." Science 325(5946): 1345-1346.

Wardrope, L., E. Okely and D. Leach (2009). "Resolution of joint molecules by RuvABC and RecG following cleavage of the Escherichia coli chromosome by EcoKI." PLoS One 4(8): e6542.

West, S. C. (2003). "Molecular views of recombination proteins and their control." Nat Rev Mol Cell Biol 4(6): 435-445.

Whitby, M. C. and R. G. Lloyd (1998). "Targeting Holliday junctions by the RecG branch migration protein of Escherichia coli." J Biol Chem 273(31): 19729-19739.

Wyman, C., D. Ristic and R. Kanaar (2004). "Homologous recombination-mediated double-strand break repair." DNA Repair (Amst) 3(8-9): 827-833.

Zheng, M., F. Aslund and G. Storz (1998). "Activation of the OxyR transcription factor by reversible disulfide bond formation." Science 279(5357): 1718-1721.